CHALMERS

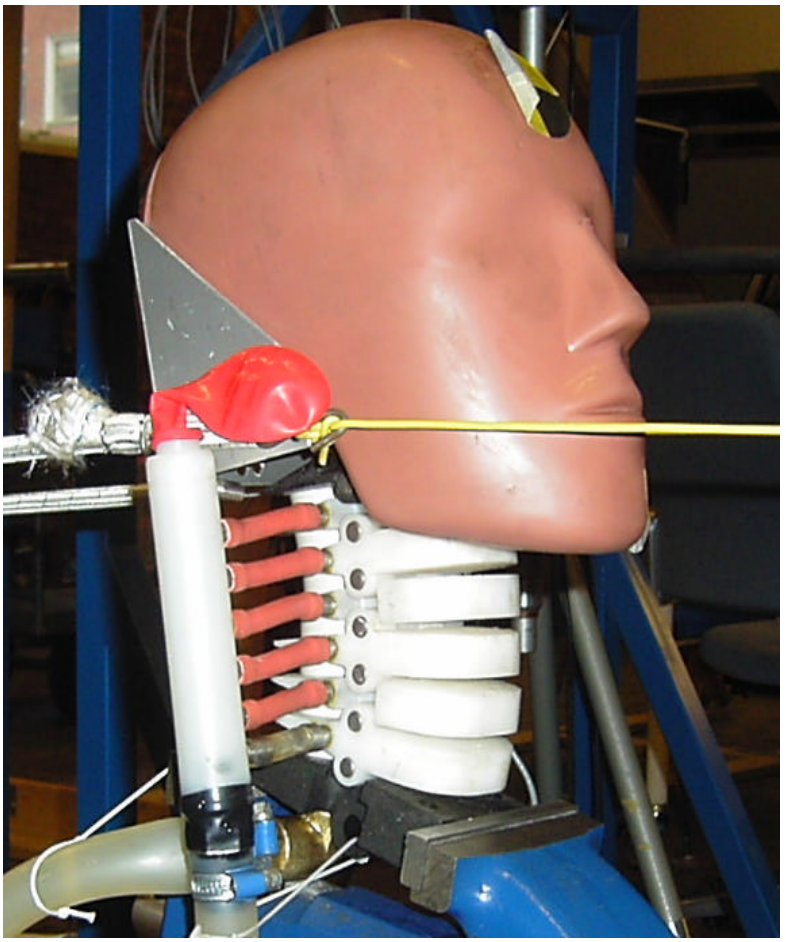

A Rear-End Collision Crash Dummy Neck for Spinal Canal Pressure Transient Simulation- Design upgrade and evaluation testing

GIANCARLO CANAVESE

Department of Machine and Vehicle Systems,
Crash Safety Division
CHALMERS UNIVERSITY OF TECHNOLOGY
Göteborg, Sweden 2004

Master Thesis 2004-04-29

MASTER'S THESIS 2004-04-29

A Rear-End Collision Crash Dummy Neck for Spinal Canal Pressure Transient Simulation- Design upgrade and evaluation testing

GIANCARLO CANAVESE

Department of Machine and Vehicle Systems, Crash Safety Division
CHALMERS UNIVERSITY OF TECHNOLOGY
Göteborg, Sweden 2004

A Rear-End Collision Crash Dummy Neck for Spinal Canal Pressure Transient Simulation – Design upgrade and evaluation testing
GIANCARLO CANAVESE

Master's Thesis 2004-04-29
Department of Machine and Vehicle Systems, Crash Safety Division
Chalmers University of Technology
SE-412 96 Göteborg
Sweden
Telephone:

Cover:
Photograph of the modified BioRID-neck incorporating a spinal canal fluid system for pressure transient simulation.

ABSTRACT

A number of accident studies and claims statistics coming from the insurance industry clearly indicates that low severity rear impact can lead to neck injuries causing long-term disability and discomfort. These injuries are usually classified as AIS 1 (Abbreviated Injury Scale) and often referred to as Whiplash injuries. The costs of such injuries are very high. The strategy of the neck-injury research carried out at Chalmers University of Technology, Göteborg, has been to address the problem of AIS 1 neck injuries in car collisions. The work, originated from a hypothesis by Aldman (1986), postulating that injury could be induced in the cervical spinal nerve root region as a result of transient pressure gradients during a swift extension-flexion motion of the cervical spine.

When the neck is flexed or extended in the sagittal plane the length of the cervical canal alters but the cross-sectional area remains almost the same. During flexion-extension motion of the neck, the size of the inner volume of the spinal canal will change. Since the tissues inside the spinal canal can be considered incompressible, an alteration will take place on the amount of fluids (cerebro spinal fluid and blood) in the veinplexa of the epidural space. This requires fluid transportation through the intervertebral foramina as well as along the spinal canal. During a whiplash motion a rise of the flow velocity far above the physiological levels can be expected and pressure gradients can thus be expected to occur. Anaesthetised pigs were exposed to whiplash motion while the pressure inside the spinal canal was measured (Svensson, 1993). Other animal tests and mathematical model confirmed the same pressure profiles obtained in the pig experiments. The aim of this thesis was to upgrade the design of an existing fluid system of a mechanical dummy neck to simulate and measure the pressure changes inside spinal canal during a traumatic flexion-extension motion. The prototype developed in this project was a modification of BioRID II neck and includes a model of the spinal canal with its outflows and outer vein system.

The efforts done in this work were directed to find a constructive solution to manufacture a monolithic spinal canal and to find an appropriate material. The new prototype was tested with a Hybrid III head and the test set-up was improved. High speed video camera, accelerometer and pressure transducers were trigged at the same time in order to know for each instant the corresponding head position and acceleration to the pressure curve.

The pressure curves in these experiments showed the expected negative pressure dip found in the animal experiments. The profiles and the amplitudes of these peaks were very similar to the reference curve. There were small differences in the timing pressure events between the curves obtained in this study and the reference one, but this was due to the different anatomy between pigs and dummy. The results of this work therefore represent a significant contribution to the development of mechanical models of the human neck, able to simulate the pressure transient phenomenon that was hypothesized to be the cause of injury at low severity rear impacts. This project can be considered to be a starting point in the development of a modified crash dummy that can reproduce these pressure transients.

Contents

ABSTRACT I

CONTENTS III

LIST OF ABBREVIATIONS V

ACKNOWLEDGEMENTS VII

1 BACKGROUND 1

1.1 Anatomy 1
1.1.1 The vertebrae of cervical spine 1
1.1.2 Ligaments 4
1.1.3 Muscles 4
1.1.4 The spinal cord 4
1.1.5 The vein system 5
1.1.6 Biomechanics of the cervical spine 7
1.1.7 Range of motion 8

1.2 Statistics and Scales 9
1.2.1 Injury scaling 9
1.2.2 Statistics 12

1.3 The whiplash motion 13

1.4 Injury hypotheses 15
1.4.1 The symptoms of injury 15
1.4.2 Parameters of injury 17
1.4.3 Injury criteria 23

1.5 Aldman's hypothesis 26
1.5.1 Theoretical injury mechanism model 27
1.5.2 The CNS from a hydro mechanical point of view 29
1.5.3 Volume change inside the spinal canal 31
1.5.4 Pressure and injury mechanisms 32

2 DUMMIES FOR REAR IMPACT PROTECTION EVALUATION 34

2.1 Brief description 34

2.2 Biofidelic rear impact dummy: Bio RID II 35

3 PREVIOUS RESEARCH 40

3.1 Introduction 40

3.2 Animal experiments 40
3.2.1 Pressure phenomena into the pig's neck during whiplash motion 40
3.2.2 Results of the injury mechanism 42
3.2.3 Discussion of the injury mechanism 45

3.3 Experiments with Post Mortem Human Subject 49

3.3.1 Methodology and test set conditions 49
3.3.2 Results and discussion 50
3.4 FEM of the cervical spine for pressure phenomena 51
3.4.1 Methodology 52
3.4.2 Results and discussion 53
3.5 Conclusions 55
4 NECK DUMMY TO SIMULATE PRESSURE PHENOMENA 57
4.1 Previous neck prototype 57
4.1.1 Components and design 57
4.1.2 Experiment and results 58
4.1.3 Possible causes of failure 59
4.2 Different designing solutions for the new neck prototype 60
4.2.1 Pipe with external rubber rings 61
4.2.2 "Vacuum pipe" solution 62
4.2.3 Metal-ring pipe 63
4.2.4 Pipe with one spring 64
4.2.5 Curved shaped pipe 66
4.2.6 Pipe moulded in loco – Final solution 67
4.2.7 Structural modifications of the neck dummy BioRID II 68
4.2.8 External pipe simulating the external venous plexus 70
4.3 Choice of the materials: theoretical approach 72
4.3.1 Stiffness calculation 72
4.3.2 Other parameters 78
4.4 Tested materials 80
4.5 Test set up 83
4.5.1 Components and their properties 83
4.5.2 Method 84
5 RESULTS AND DISCUSSION OF THE TESTS 88
6 CONCLUSIONS 95
7 REFERENCES 96
APPENDIX A 99
APPENDIX B 108
APPENDIX C 116

List of abbreviations

AIS	Abbreviated Injury Scale
C1 – C7, (C8)	Seven Cervical vertebrae (and levels of corresponding eight nerve roots) in descending order.
CG	Centre of Gravity
CNS	Central Nervous System
CSF	Cerebro Spinal Fluid
EBA	Evans Blue dye conjugated with Albumin
Extension (of the	Rearward bending of the neck
Flexion (of the neck)	Forward bending of the neck
FEM	Finite Element Method
g	Acceleration of gravity (1g= 9.841 m/s^2)
Hybrid III	Hibryd III crash test dummy
kyphosis	Rearward convex bending of the spine
lordosis	Rearward concave bending of the spine
BioRID	Biofedelic Rear Impact Dummy
sagittal	In the median longitudinal plane of the body
T1 – T12	Twelve Thoracic vertebrae in descending order
? v	Velocity range
whiplash	Swift extension-flexion motion of the neck caused by forward acceleration of the trunk
WAD	Whiplash Associated Disorders

Acknowledgements

I express my gratitude to all those who have participated in manufacturing the prototype, carrying out the tests and helping me to finish this report and in particular:

Professor Cristina Bignardi and Professor Pasquale Mario Calderale, my supervisors, to have given me the opportunity to realize this work in the Chalmers University of Technology and for advice their encouragement.

Professor Mats Svensson, my Chalmers relator, for his help and advice in the art of biomechanics and crash test dummies.

Anders Flogård researcher at Chalmers Crash Safety Division, for his valuable ideas, engineering knowledge, and patience in helping me.

Luisa, Luca, Marco and Massimiliano for the help in writing the report.

1 Background

1.1 Anatomy

In the process of developing a dummy neck, it is necessary to identify the essential parts of the neck and therefore, knowledge about the human anatomy is needed. The basic mechanical elements of the neck are the vertebrae, the intervertebral discs, the muscles, the ligaments, the vein system and the spinal cord. In this chapter the fundamentals of the human cervical spine will be presented.

1.1.1 The vertebrae of cervical spine

The human spine has 33 vertebrae and from the literature, it is divided in five sections. From up to down the sections are the cervical spine (C1-C7), thoracic spine (T1-T12), lumbar spine (L1-L5), sacrum (five fused vertebrae) and coccyx (four fused vertebrae). One important mechanical function of the spinal column is to provide protection to the spinal cord. This protective role is comparable to the function of the skull in protecting the brain. Injuries of the spinal cord can result in severe disability and death. Another important function of the neck is to act as the principal load-bearing structure of the head and to provide mobility between head and torso. Due to this multitude of functions, the cervical spine is a rather complex structure (Figure1.1).

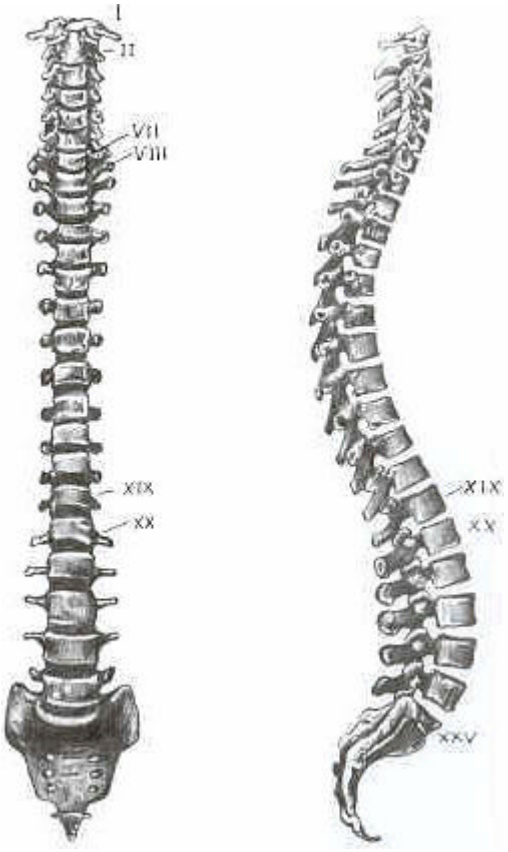

Figure 1.1 Anterior (left) and lateral (right) view of the vertebral column.

Except for C1 and C2 the vertebrae are quite identical in structure although the cervical vertebrae are smaller than the thoracic and lumbar vertebrae. A vertebra is made up of the "body" at the anterior side and the "neural arch" at the posterior side. The body consists of spongy bone surrounded by a layer of compact bone. The neural arch is a bony ring that ends posteriorly in the spinous process and lateral on each side in the transverse process. The processes are the attachment points for the ligaments and muscles. The spinous processes function as a lever. When the neck perform hyperextension the posterior spinous processes will come in contact with each other. The neural arch surrounds an open area called vertebral foramen, which forms together with the other vertebral foramina the vertebral canal through which the spinal cord passes.

The load-bearing function of the vertebral column is realized by two load paths: one at the posterior side and one at the anterior side. The first load path is through the bodies of the vertebrae, which are connected by intervertebral discs that work as dampers. The disc has a soft and elastic nucleus and a layer of collagen fibres, the annulus fibrosus that surrounds the nucleus (Figure 1.2). The strong fibres prevent the nucleus from too much bulging during compression and gives stability to the disc. The second load path is through the neural arch of a vertebra, which is provided for this purpose by four articulation surfaces, called facets: two at the superior side and two at the inferior side. These surfaces articulate with the facets of the vertebrae above and below, the so-called facet joints. The rakes of these facets vary in the cervical spine but the mean value is about 42° in the sagittal plane.

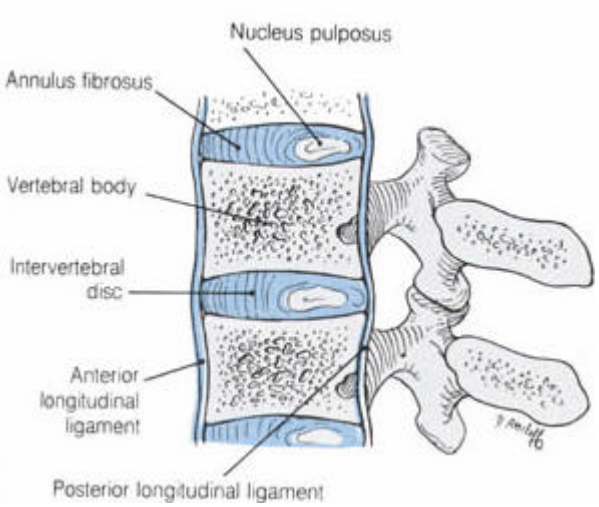

Figure 1.2 Intervertebral disc.

The seven cervical vertebrae can be divided into two parts, the upper one and the lower one (Figure 1.3). The upper part of the cervical spine consists of the two upper most vertebrae, C1 and C2. These two vertebrae differ in their structure compared to the five other vertebrae (C3-C7) in the lower cervical vertebrae column.

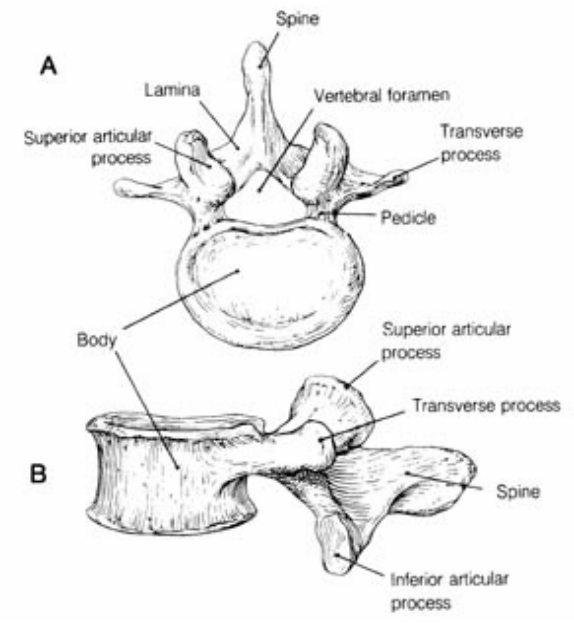

Figure 1.3 Upper view (a) and lateral view (b) of a cervical vertebra.

The first vertebra C1 is called "the atlas" (Figure 1.4) and can be considered as a ring of bone; it has no body and no spinous process. The atlas is provided at the superior side with a pair of facets, each covered with cartilage, which articulate with the bases of the skull, the atlanto-occipital joint. The skull part of this articulation is formed by the condyles of the occipital bone referred to as occipital condyles. This articulation allows a nodding motion of the head (flexion and extension motions). Its vertebral foramen is bigger than those of other vertebrae is.

C2 is called "the axis" (Figure 1.3) and has a knoblike dens, the odontoid process, projecting superior from its body. This dens fits into the vertebral foramen of the atlas. This atlanto-odontoid joint allows horizontal rotation in the upper part of the cervical spine, C1 rotates on top of C2 with the dens as the centre of rotation.

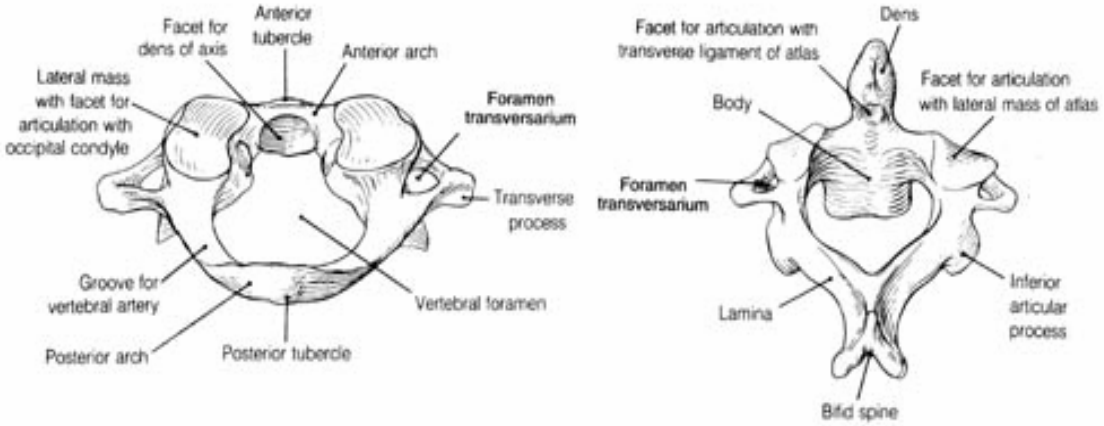

Figure 1.4 Atlas (left) and axis, from s superior view.

1.1.2 Ligaments

The ligaments give stabilities to the spine and connect the vertebrae to each other. Inside he vertebral canal is a series of ligaments called ligamentum flavum connecting adjacent vertebrae, these are the only stretchable ligaments. Ligamenta flava prevent an abrupt stop in motion when the head is bent forward. The ligamenta flava act as a buffer between the vertebral arches in dorsal extension and bulge slightly into the canal.

The ligaments which run along the whole spine, i.e. from skull to the tailbone, are the long longitudinal anterior ligament and the long longitudinal posterior ligament. The anterior ligament is thinner and runs closer to the anterior side of the spine, it limits the range of extension motion, while the posterior ligament is stronger and runs between and outside the process.

Shorter ligaments connect two, three, or four vertebrae to each other. The facet joints mentioned before are completely surrounded by ligamentous tissue: the capsular ligaments. Important ligaments at the posterior side of a vertebra are the interspinous ligaments and superspinous ligament. This last ligament also connects the entire spine. It is called ligamentum nuchae in the cervical area. Flexion motion of the head is partly controlled by this ligament.

The dentate ligaments in the upper cervical region are short and thick, and pass almost perpendicularly from their attachment in the pia to the dura midway between the root nerves. The lower cervical ligaments are somewhat longer and narrower, and follow an oblique course.

1.1.3 Muscles

Just like the ligaments the muscles give stability but also ability to move. Seen the neck in a cross-section the largest area is muscles. The muscles exist in several layers and just as with the ligaments, they come in different lengths. They can be divided into three groups. One of the group runs between close vertebrae. These short muscles (the deep muscles) control the movement of individual vertebra and attach the vertebrae to one another. The second group of muscles is longer and run from the head to vertebrae. These muscles belong to the superficial muscle group of the neck. The last group is the intermediate muscle group; it contains of those muscles that go from the head to the clavicle or the upper part of the thoracic spine

On the posterior and lateral side there is a larger number of muscles. The explanation for this is that the centre of gravity in the head is a bit in front of the geometrical centre. More muscles are needed on the posterior side of the neck to keep the head upright. Muscles are attached to the body and to the processes of the vertebrae.

1.1.4 The spinal cord

The spinal cord runs inside the spinal canal (Figure 1.4). It consists of the grey and white matter, which can be considered as semi-fluid cohesive masses. The grey matter is shaped like a butterfly and is surrounded by the white matter. It consists of a mixture of neurone cell bodies. The white matter consists of nerve fibres, which

allow communication between different parts of the spinal cord or between the spinal cord and the brain. It is covered by the pia matter, which is again surrounded by the arachnoid. The spinal cord cannot move up and down axially within the canal but it adapts itself to the changing of lengths during motions of the spine by plastic deformation.

Dorsal nerve roots are leading from the spinal cord to the spinal ganglion, which is situated in the intervertebral foramen.

Both spinal cord (covered by pia matter) and the spinal ganglions are surrounded by the Cerebro Spinal Fluid (CSF) and covered by dura matter.

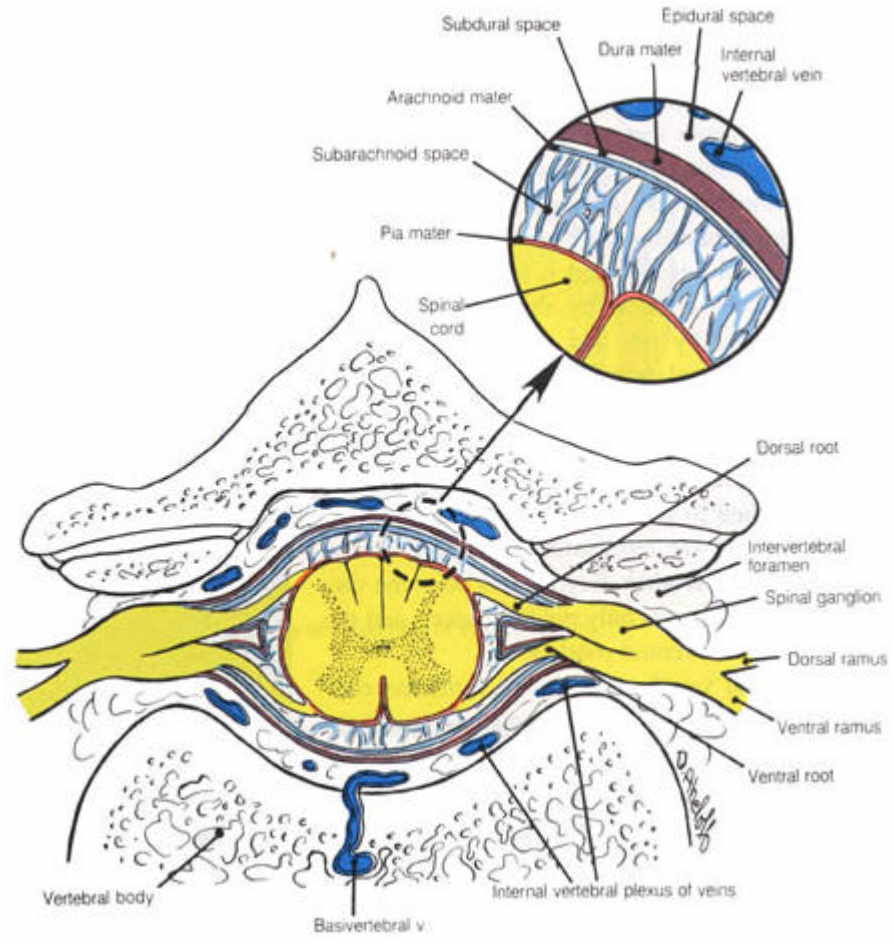

Figure 1.4 Horizontal cross- section of a cervical vertebra with soft tissues.

1.1.5 The vein system

The vertebral vein system is a low-pressure system. It is divided in three different parts, which intercommunicate with each other: the internal vein network, the in- and out- leading bridging veins and the external veins plexus. The internal vein network

is the largest one, surrounding the dura matter. It consists of two-vein network (plexus), which are situated posterior and anterior within the spinal canal. The two plexus (posterior and anterior) are joined through several vessels respective small networks. The volume capacity of these plexus is about 100 ml or even more. This is 20 times the arterial capacity; it is much larger than required to return the blood brought in by the arteries. It seems to be clear that bringing out blood is not the main job of these plexus. More probable they serve as regulator to balance the volume and pressure changes during movements of the cervical spine and to the storage of blood. Out of this reason, they do not have any valves. The blood is able to flow in any direction within the plexus.

A similar vein plexus is outside the cervical spine, the external vertebral venous plexus (anterior and posterior) The intervertebral veins (Venae Intervertebralis), which lead in groups through the intervertebral foramen on both sides of the vertebral body, and the basivertebral veins (Venae Basivertebralis), which lead in radial direction through the vertebral body (Figure 1.5 and Table 1.1).

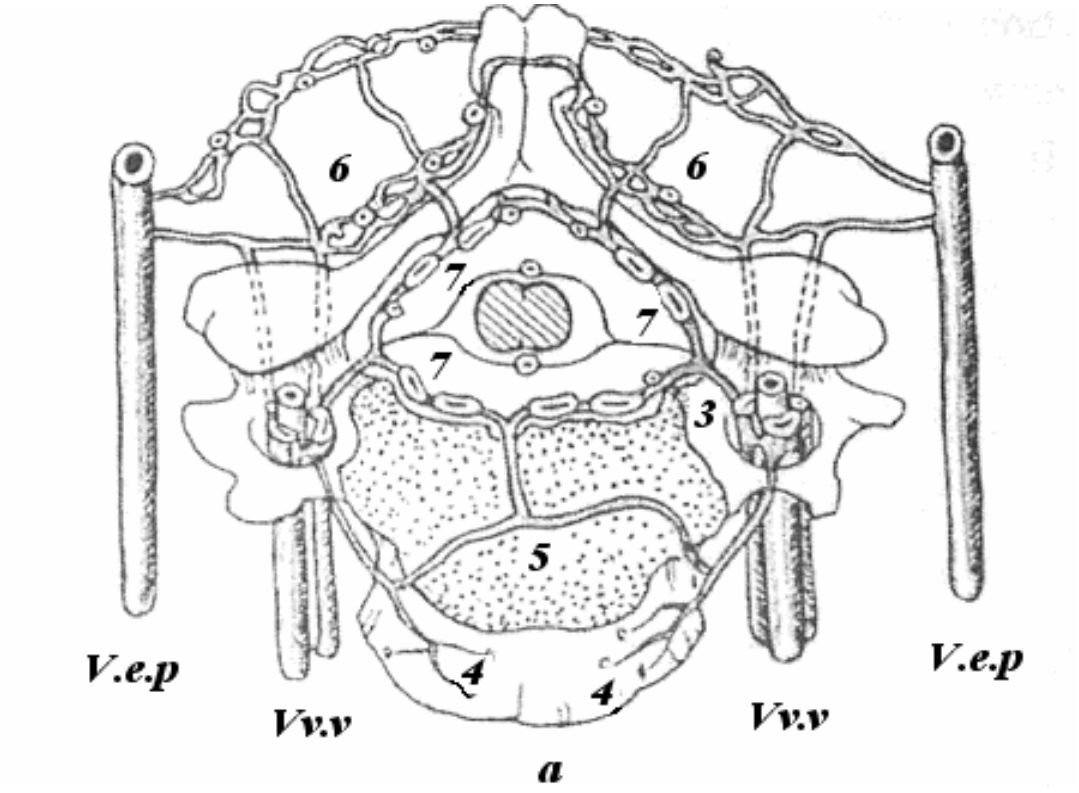

Figure 1.5 Charting of the internal and external cervical venous plexus: a= Cevical vertebrae; Vv.v=Venae vertebralis; V.e.p.=Venae cervicalis profunda; 3=Venae intervertebralis; 4=Anterior external cervical venous plexus; 5=Venae basiventralis; 6=Posterior external cervical venous plexus; 7=Internal cervical venous plexus

Vein	Diameter in mm
Internal vertebral cervical venous plexus, anterior	2.0-2.5
Internal vertebral cervical venous plexus, posterior	2.5-3.0
Intervertebral cervical veins	<5.0
Basivertebral cervical veins	1.0-2.0
External vertebral cervical venous plexus, anterior	0.1-0.5
External vertebral cervical venous plexus, posterior	0.2-0.5

Table 1.1 Diameters of cervical vertebral veins (Clemens, 1961)

1.1.6 Biomechanics of the cervical spine

According to O' Connell (1955) there is an angle of 90° between the position of the cervical spine axis in ventroflexion and dorsal extension. Bakke (1933) on radiographs of living subjects found the maximum mobility of the cervical spine is at the level C5-C6, with a range of flexibility of 20.4° in the sagittal plane. The total range for the cervical spine was 80.5°, of which dorsal extension accounted for 64.2° in the sagittal plane. In ventroflexion the cervical spine curves slightly forwards, each body being displaced about 2 mm in front of the subjacent one. In the erect position, the forward convexity of the cervical spine is determined by the intervertebral discs, the sum of their thicknesses being some 8mm greater anteriorly than posteriorly (Fick, 1904). In ventroflexion, the discs are compressed anteriorly and the annulus fibrosus is stretched posteriorly.

In ventroflexion the cervical canal is lengthened, the posterior contour more than the anterior, while in dorsal extension the canal is shortened, the posterior contour more than the anterior. (Mean values for female's neck; length of the central axis of cervical canal, ventroflexion: 13.4mm, dorsal extension: 10.5mm; difference: 2.9mm).

In ventroflexion, the axis of curvature is located anterior to the cervical spine. The fulcrum is in the ventral part of the disc and at the anterior margins of the two vertebrae, and the canal is in the convex side of the bodies. In dorsal extension, the axis of curvature is located posterior to the cervical spine, as a result of which the cervical canal lies on the concave side of the bodies of the vertebrae, with the fulcrum in the dorsal part of the disc and at the posterior margins of the vertebrae. The inferior articular surfaces of the upper vertebrae than glide backwards and downwards on the superior surface of the lower vertebrae. This causes the cervical canal to shorten, both anteriorly and posteriorly. In lateral flexion, the axis of curvature is lateral to the cervical spine, and the fulcrum is in the lateral side of the disc and at the lateral margins of the vertebrae; there is then an extension on the convex side and a compression on the concave side of the vertebrae.

In ventroflexion, the length of the dura matter corresponds to that of the spinal canal. Only in maximum ventroflexion are the dura and the roots sleeves completely unfolded, so that they assume their optimal straightened form. Whit the shortening of the spinal canal in dorsal extension the dura folds like an according along the whole of its length, but more distinctly on the dorsal than on the ventral aspect, especially in those parts of the spinal column subjected to a greater degree of backward flexion. In maximum ventroflexion, the dura is under a slight physiologic tension. Straightening of the root sleeve then brings its superior surface into contact with the inferior and medial margin of the pedicle. In dorsal extension when the dura is folded owing to simultaneous slackening of the sleeve its superior surfaces separate from the margin of the pedicle. Are these deformations that give the impression that the dura ascends and descends in the canal during flexion and extension of the column.

The dentate ligaments consist of a rhomboid mesh of fibres. In ventroflexion, the lateral bands and the pairs of the dentate attachments of ligaments are straightened axially and transversely and a slight elastic tension is set up in them. As a result of this there is an uniform distribution of the physiologic tensile forces over the length and cross-section of the spinal cord. The function of the dentate ligaments would seem to lie in governing this distribution. Only in the supine position and by ventroflexion of the cervical spine in the cadaver is the cervical cord raised from the dorsal surface of the canal. Owing to stretching of the ligaments in ventroflexion and to the fact that they will not yield in the dorsal direction, a protrusion of the ventral l wall of the canal tending to displace the cord further dorsal will set up a pathologic axial tension in it. In dorsal extension of the spine, the dentate ligaments are slack in any position of the body and the cord can be moved to the dorsal, ventral or lateral aspect of the dura without setting up tension in it. This is true also in living subject.

1.1.7 Range of motion

The range of motion in the cervical spine depends on several factors and differs from person to person. Age and individual elasticity influence on the flexibility in the spine and determine the maximal range of motion for the neck. In *Table1.1* the range of motion (according to White and Panjabi, 1978) can be seen. The values have to be considered as averages that represent a range of motion. The objects of the study were both in vivo and vitro and the angles were detected with radiographic technique. The values of the upper cervical spine differ from the lower cervical spine that has somewhat similar values. The coupling occiput-C1 has no rotation while the coupling C1-C2 has a high degree of rotation (47° to each side) but no lateral flexion. In *Table1.2*, Kapandij's values for the range for motion are presented. These values were found using oblique radiographs in the extreme positions (for flexion and extension). They differ from Panjabi and White's values in the range for extension-flexion between C2-C7, rotational motion between occiput-C2 and C2-C7. The differences can be due to the selected samples and measurement method.

Coupling	Flexion-Extension (total)	Lateral bending (one side)	Rotation (one side)
Occiput-C1	13°	8°	0°
C1-C2	10°	0°	47°
C2-C3	8°	10°	9°
C3-C4	13°	11°	11°
C4-C5	12°	11°	12°
C5-C6	17°	8°	10°
C6-C7	16°	7°	9°
C7-T1	9°	4°	8°

Table 1.2 Average of range of motion for flexion-extension, lateral bending and rotation (White and Panjabi, 1978)

Coupling	Flexion-Extension	Lateral bending	Rotation
Occiput-C2	20-30°	8°	24°
C2-C7	100-110°	45°	80-90°

Table 1.3 Average of range of motion for flexion-extension, lateral bending and rotation (Kapandji)

1.2 Statistics and Scales

1.2.1 Injury scaling

Injury scaling is defined as the numerical classification of the type and severity of an injury. Many schemes have been proposed for ranking and quantifying injures. They can be grouped into three main types:

Anatomic scales which describe the injury in terms of its anatomical location, the type of injury and its relative severity. These scales rate the injuries itself rather than the consequences of injuries. The most well-known scale, which is accepted worldwide, is the Abbreviated Injury Scale (AIS).

Physiological scales, which describe the physiological status of the patients, based on the functional change due to injury. This status and consequently its numerical

assignment may change over the duration of the injury's treatment period, in contrast to anatomical scales where a single numerical values is assigned to a certain injury. A well-known example is the Glasgow Coma Scale (GCS), which was specifically developed for head injuries. It is a way of quickly assessing the nature and severity of brain injuries based on three indicators: eye opening, verbal response and motor response. These kinds of scales are important in a clinical environment.

Impairment, disability and societal loss scales. Here not the injury itself or the functional changes due to the injury are rated, but the long term consequences and in relation to this the "quality of life". Examples are the Injury Cost Scale (ICS), and the HARM concept, which all are attempts to assign an economic value to the various injures.

Note that above types of injury scales basically relate to the living human body. Anatomical scales like the AIS however also can be applied to rate the injury severity in human cadavers after dissection of the body.

1.2.1.1 The abbreviated injury scale (AIS)

The need for a standardized system for injury severity rating arose in the mid nineteen-sixties in the USA with the first generation of multidisciplinary motor vehicle crash investigation teams. In 1971 the first AIS was published and has since then been revised four time. The last update (in 1990) will be referred to as "AIS 90". Although originally intended for impact injuries in motor vehicle accidents, the several updates of the AIS allow its application now also for other injuries like burns and penetrating injuries (gun shots). The AIS distinguishes between the following severities of injury (Table 1.4).

AIS	SEVERITY CODE
0	No injury
1	Minor
2	Moderate
3	Serious
4	Severe
5	Critical
6	Maximum injury (virtually unsurvivable)
9	Unknown

Table 1.4 The abbreviated injury scale AIS

The information for AIS scaling is contained in the AIS manual, which is organized into nine sections dealing with several body regions. Within each section, injury descriptions are provided by specific anatomical part. For each specific injury the

manual provides a 7-digit coding, where the digit right of the decimal point is the AIS score. Other digits are used to specify body region, anatomic structure, type of injury etc.

The AIS is a so-called "threat of life" ranking. Higher AIS levels indicate an increasing threat to life. The numerical values have no significance other than to designate order. They do not indicate relative magnitudes, in other words an AIS 2 level is not twice as severe as an AIS 1 level. Several attempts have been made to establish a quantitative relationship between the various AIS levels. One attempt is the calculation of fatality rate for each AIS value. Table 1.5 summarizes the range of results of several studies (Pike 1990).

Another attempt is the HARM concept, which assigns an average economic value to each of the AIS injuries.

Injury severity AIS	Fatality rate (range %)	Costs (HARM $1000)
1	0.0	0.4
2	0.1-0.4	2.7
3	0.8-2.1	7.1
4	7.9-10.6	38.8
5	53.1-58.4	186.6
6	--	165

Table 1.5 AIS vs. fatality rate and vs. Economic Costs (HARM)

1.2.1.2 Injury severity score (ISS)

The AIS does not asse the effect of multiple injures in patients. One possibility is to take the highest AIS score for a certain body region as a measure for the overall injury severity the M(aximum)AIS. The value of the MAIS in trauma research is considered limited due to its nonlinear relationship whit the probability of death.

A more general accepted approach for rating multiple injures is the ISS that distinguishes 6 body regions: head and neck, face, chest, pelvic contents, extremities and external (lacerations, abrasions and burns independent of their location on the body surface). For each of these regions the most severe injury on the basis of the AIS code is determined. The ISS is the sum of the squares of the three largest AIS values. The maximum value for the ISS is 75 (three AIS 5 injures). The ISS is correlated quite well with the probability of death.

1.2.1.3 Injury cost scale

In case of injury severity scale which rates the long term consequences of injury, numerical values are much more difficult to determine and the status of the accident victim has to be monitored during a long time. The interest in, and importance of these scales is growing since they provide a much better means of establishing

priorities for injury prevention measures than the anatomical based scales since much more factors are taken into account and since injury severities usually are expressed in term of economic costs. Examples of these scales are the Injury Priority Rating (IPR) the HARM concept and the Injury Costs Scale (ICS), which are all attempts to assign an economic value to the various injuries.

The HARM concept is an attempt to assign an average economic cost to an AIS value. Since the AIS rates the injury severity itself and not the long term consequences a large variation in actual economic costs per injury within an AIS level will exist and therefore useful application of the average costs for each AIS level as rated by HARM is rather limited.

1.2.2 Statistics

Neck injuries frequently occur in rear-end car accidents. Nygren (1984) found that 18% of all accidents in Sweden involving injured drivers were rear end collisions and similar findings have been reported by others (States et al., 1972; James et al., 1991). Data published by Langwieder et al. (1981) and Kahane (1982) indicate that 80%-90% of those injured in rear impacts sustained neck injuries. According to Foret- Bruno et al. (1991) and James et al. (1991) this type of injury is nearly always classified as ”minor injury” (AIS=1) in the abbreviated injury scale (AIS). In spite of this low AIS rating, these neck injuries lead to permanent disability (disability degree ≥10%) in about 10% of the cases, which should be compared with 0.1 % of the cases for all other AIS 1 injuries (Nygren, 1984). Neck injuries in rear impacts mostly occur at very low impact-velocities, typically less than 20 km/h (Kahane, 1982; Romilly et al., 1989; Olsson et al., 1990). Glasko et al. (1993) presented data which indicate that 52% of all cervical spine disorders claimed were sustained in rear-end collisions, 27% in frontal collisions, and 16% in side impacts. Langwieder and Hell (1996) founded that occupants of 81% of the accidents included in their database (total number: 1500) complained about neck injuries rated AIS1. Rear-end collisions contributed the majority of 61%, side impact 28% and frontal collisions 11%.

A Swedish study by Von Koch et al. (1995) shows that 23% of all injury cases resulted from frontal impact, while 64% resulted from rear-end impact. Therefore, it is clear that also in frontal impact there is a need for improvement of whiplash protection. In the first European Whiplash (Cappon et al., 2001) project the rear impact loading phase was the main focus but some of the mechanisms of whiplash injury are suggested to originate from the rebound phase of rear impact (Von Koch et al, 1995).

Each year about 150 people get severe neck injuries and a number get slight neck injuries in Sweden, most of them are from car accidents (Folksam). In USA the number of whiplash injured are approximately 4 per 1.000 citizens per year. According to Ono and Kanno (1993), 50% of all car-to-car accidents in Japan lead to neck-injuries and the number of neck injuries are on the increase. In the Netherlands, the annual number of neck injuries increased by 54% during the period 1983 to 1991 (Kampen, 1993).

Rear-end impacts have the largest risk of whiplash injury (Temming and Zobel, 2000) and therefore much effort is being spent on decreasing this injury risk. The total number of frontal whiplash cases may be higher, despite the smaller risk. According to German accident data (Temming and Zobel, 2000) 38% of the injury cases are single impact frontal accidents (589 of 1558), with an injury risk of 12% (100% are all belted occupants), while 15% of the injury cases are single impact rear-end accidents (233 of 1558), with an injury risk of 26%. From the German Motor insurers shows that the incidence of whiplash injuries (also denoted cervical spine distortion injuries, CSD; or whiplash associated disorders, WAD) in Motor Vehicle Accidents has almost doubled in the last 20 years (Hell 1999). Morris and Thomas (1996) also show similar figures from UK. Swedish insurance data show that the risk of whiplash injuries leading to long-term disability is found to have doubled comparing recent car models with car models introduced 20 years ago (Folksam, 2001), and do to date account for nearly 60% of injuries leading to long-term disability (Krafft 1998).

The assumed socio-economic losses for rear-end collisions in Germany (calculated after German Injury Cost Scale) would amount up to 2 Billion € only for rear-end collision cases. For 2000 estimations of annual costs from other countries regarding whiplash injuries were also very high: USA 10 Billion US$, UK 800 Million Pounds, NL 1 billion Dutch Guilders (Dutch Transport Ministry), European Union, roughly at least 10 Billion Euro (Whiplash 1).

In 2002 a study over 21031 cases conducted by ANIA and ACI Italy resulted to be the first in Europe in road injuries that terminated with a request of compensation. The most claimant case is the whiplash injury. In Italy 18% of the accidents involves to money indemnity (11% Germany, 10% Spain, 8.7%, France, 8% UK). 66% of the injuries are imputable to the whiplash (40% Germany, 38% Holland, 15% Spain, 6% France). In 83% of cases, the Italian legal medics identify a injury with permanent infirmity (40%Germany, 35% Holland, 15% France, 5% Norway, 4.8% Denmark). In Italy in the year 2002, the amount of money compensation for whiplash injury has been about 2.44 billions of Euro.

1.3 The whiplash motion

In a rear end car collision the struck car is accelerated. This means that the car occupant is pushed forward by the seat back. If the seat is equipped with a head-rest there is usually space between the skull and the head-rest. This means that the skull, due to its inertia, tends to lag behind when the trunk is accelerated forward. An extension motion of the neck will follow. This motion is abruptly interrupted either when the head is reached by the heat-restraint or when the head and neck reach the maximum extension angle (Figure 1.6). The motion scenario described above is in the literature called whiplash motion.

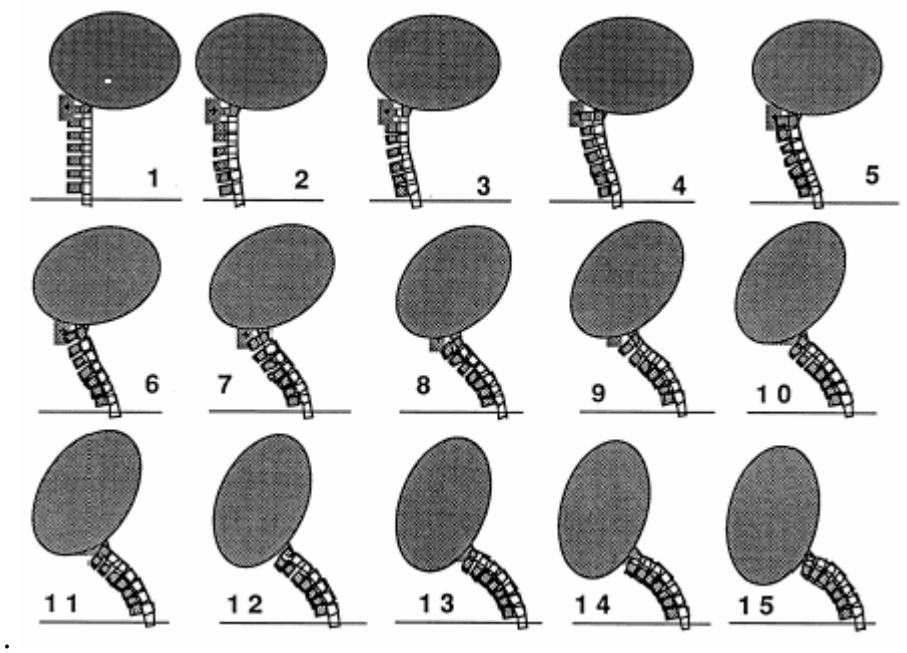

Figure 1.6 Schematic representation of whiplash motion (Svensson, 1989).

The common whiplash extension-flexion motion can be divided in three phases (Figure 1.7).

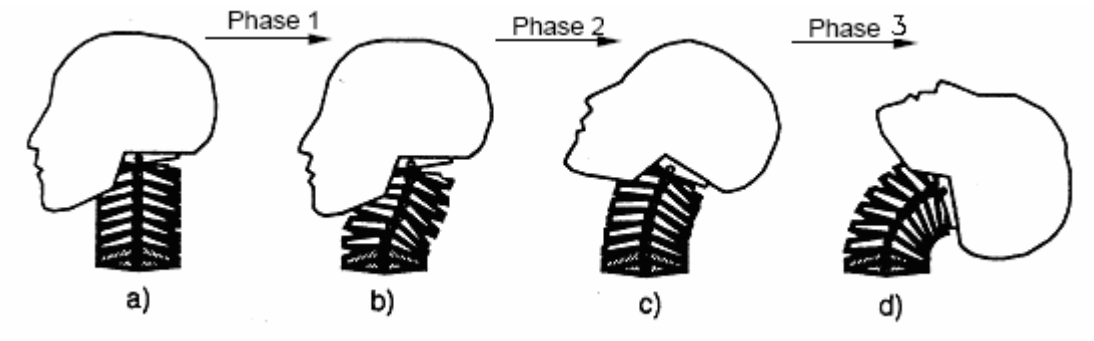

Figure 1.7 The three phases of a whiplash motion: 1) Linear rearward motion from the initial posture; 2) The head starts rotating rearward; 3) Rearward rotation until fully extended position.

The first phase lasts up to circa 100 ms. The seatback pushed the torso forward while the head stays still. This can be considered as a linear reward motion of the head relative to the torso. There is no angular motion of the head occurring. Hence, the spine adopts an S-shape. In this motion, the upper part of the cervical spine goes into flexion and the lover one into extension. When both parts reach their limits for maximum flexion respective extension the linear reward motion will stop and the head starts rotating rearward.

At the end of the Phase 1 the linear rearward motion of the head is abruptly decelerated at the same time as the head starts rotating backwards. This is explained

by the fact that the upper cervical spine reaches its limit for maximum flexion while the lower cervical spine reaches the limit for full extension. In the second phase (circa 100 ms to 150 ms), the extension motion of the upper cervical spine still accelerates, but the lower part of the cervical spine goes into a less extended position.

In the third phase (circa 150ms to 250ms), the whole cervical spine goes into full extension until it is stopped by the structures of the neck.

Following this extension motion, the whole cervical spine returns towards its initial posture by means of the elastic energy that is stored in the neck structures at the fully extended posture. This flexion part is normally much less violent than flexion motions that are seen in frontal collisions and it is much lower than the initial extension motion.

In frontal and side impacts, the neck usually experiences the same type of inertial loading from the head as in rear end collisions. During the initial phase of these neck loading situations, the head normally undergoes a horizontal translational displacement relative to the torso. This is particularly evident in frontal and rear end collisions. This translational motion is called protraction for forward motion and retraction for rearward motion. The neck is exposed to very significant mechanical loads when the end of the normal range of protraction or retraction of the neck is reached, and neck injuries may well occur at this point. This may be one explanation for the fact that modern head restraints do not provide better protection. They may simply come into play too late, after the neck has exceeded the maximum range of retraction motion and gone into extension. Another possible explanation, involving transient pressure gradients in the central nervous system causing cervical nerve root ganglion injuries at the point of maximum retraction or protraction, will be presented later in the next chapter.

1.4 Injury hypotheses

1.4.1 The symptoms of injury

The symptoms of injury following neck trauma in rear-end collisions include pain, weakness or abnormal responses in the parts of the body (mainly the neck, shoulders and upper back) that are connected to the central nervous system via the cervical nerve-roots. Vision disorder, dizziness, headaches, unconsciousness, and neurological symptoms in the upper extremities are other symptoms that have been reported (Deans et al., 1987; Hildingsson, 1991; Nygren et al., 1985; Spitzer et al., 1995; Sturzenegger et al., 1995; Watkinson et al., 1991). The neck injury symptoms appear to be very similar for all impact directions (Minton et al., 2000). It is important to distinguish between initial symptoms and long term symptoms (Krafft, 2000). Long term (chronic) whiplash symptoms appear to be associated with central pain sensitisation (Sheather- Reid and Cohen, 1998; Johansen et al., 1999). The exact origin of this pain sensitisation has not been established. Successful treatment methods could possibly provide a clue. Byrn et al. (1993) reported significantly

reduced symptoms during a time period after sub-cutanious sterile water injections on the back of the neck. Bogduk (2000) reported pain relief in about 50 percent of the patients after coagulation of the small nerves that innervate the facet joint that is associated with the painful dermatome.

Soft tissue injuries have been found in several different structures and locations in the neck region in experimental studies and autopsy studies. In a recent study Yoganandan et al. (2000) reported injuries to several ligaments, the intervertebral discs and the facet joint structures. Siegmund and Brault (2000) and Brault et al. (2000) presented indications of muscle injury due to eccentric muscle loading in the early phase of the neck motion in rear impacts. Taylor et al. (1998) reported interstitial haemorrhage in cervical dorsal root ganglia in an autopsy study of victims who had sustained severe inertial neck loading during impacts to the torso or to the head. The structures around the ganglia were mostly uninjured. These findings correlate to experimental findings in pigs of nerve cell membrane dysfunction in cervical spinal root ganglia reported by Svensson et al. (2000).

It appears likely that several types of neck injury may appear as a result of a whiplash trauma (muscles, ligaments, facet joint, discs, nerve tissue etc.). Several injury types may be present in the same patient at the same time. The relation between these possible injuries and the large set of known whiplash symptoms (neck pain, headache, shoulder pain, neurological symptoms etc.) is unclear. It would be of particular interest to know which one (ones) of these injuries that would result in long term symptoms and central pain sensitisation. It would then also be of interest to know which injury mechanism is responsible for this particular injury. At the initial symptom stage, arm pain and high symptom intensity seem to correlate to an increased risk of long term consequences (Sturzenegger, 1995; Karlsson et al., 2000). The apparent influence of the crash pulse on the risk of long term consequences in patients with initial symptoms (Krafft, 2000) indicates that there could be a separate injury and a separate injury mechanism behind the long term symptoms. This particular injury could in the acute stage often co-exist with other injuries that normally heal without causing residual pain. Sturzenegger et al. (1995) found a higher risk of long term symptoms in those patients that were injured in a rear end collision and this may indicate that one particular injury (which may cause long term symptoms) is more likely to occur in a rear impact. In more peripheral parts of the body most of these injury types (tissue types) normally recover without long term pain and central pain sensitisation. There is may be, something special about the neck region that makes one or several of these injuries result in long term pain. Cavanaugh (2000) for instance, explained that the facet joint capsules are particularly rich in nerve endings why an injury at this point would be a likely reason for long lasting pain. This pain may cause referred pain in e.g. the shoulder region. Facet joint capsule strain and pinching has been shown in post mortem human subjects in rear impact testing (Yoganandan and Pintar, 2000b; Deng et al., 2000). It is however not known whether the same type of mechanisms may occur also in side impacts and frontal impacts. There is some type of structure that is unique for the neck. The spinal nerve root ganglia would be an example of such a structure. Cavanaugh (2000) explained that injury to the dorsal root ganglia is likely to cause radiating pain to dermatomes of for instance the shoulders and the arms. These symptoms are, as mentioned earlier, known to correlate to increased risk of long

term consequences. Cervical dorsal root ganglion injuries have been observed in various impact directions (Svensson et al., 2000, Taylor et al., 1998) and this explain the similarity in symptoms between different impact directions.

The risk of neck injury to rear seat occupants was only about 50% of the risk of neck injury for front seat occupants in rear-end collisions (Kihlberg, 1969; States et al., 1972; Carlsson et al., 1985; Lövsund et al., 1988; Otremski et al., 1989). The injury symptoms following neck trauma in rear-end collisions include pain, weakness or abnormal response in the neck, shoulders and upper back as well as vision disorders, dizziness, headaches, unconsciousness, and neurological symptoms in the upper (States et al., 1972; Nygren et al., 1985; Hildingsson, 1991; Watkinson et al., 1991; Spitzer et al., 1995). Spangfort (1985) used Figure 1.8 to describe the stages of the symptoms. Findings similar to those of Spangfort (1985) were reported by Deans et al. (1987).

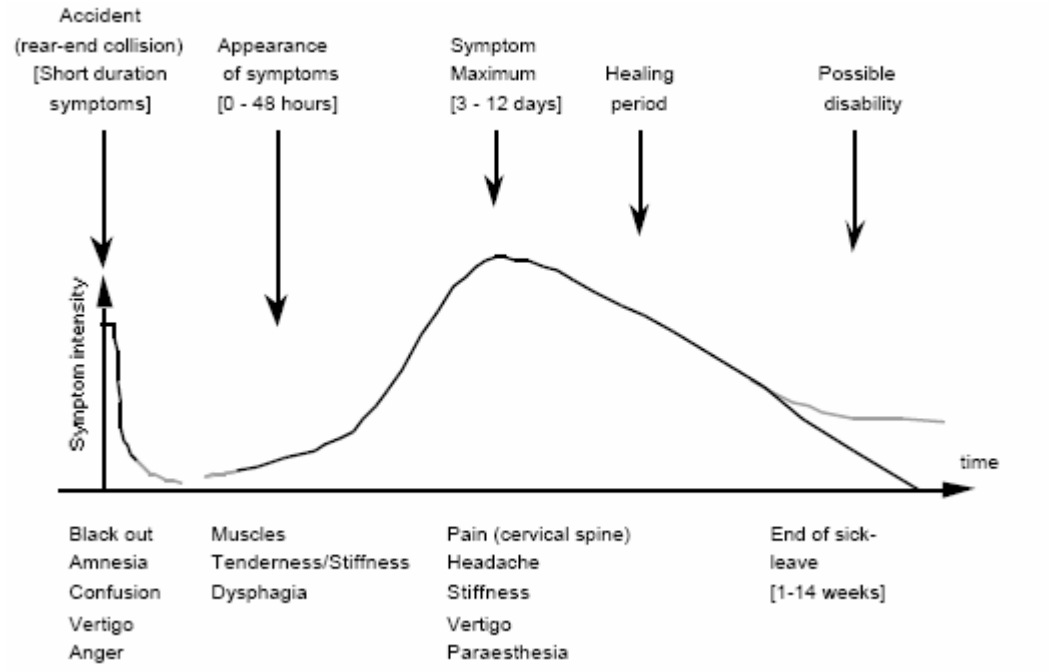

Figure 1.8 The stages of the neck injury symptoms sustained in a rear end collision (Spangfort, 1985).

1.4.2 Parameters of injury

Accident data have been collected in a number of studies and this section shows a view of the injury incidence as a function of various parameters. The main aim of accident statistics is to determine the parameters of a crash, which have an influence on whiplash injury risk. Parameters like impact speed, deceleration, gender and seat structure may have influence on injury occurrence and injury severity.

Neck injuries in rear-end collisions mostly occur at very low impact-velocities, typically less than 20 km/h (Kahane, 1982; Olsson et al., 1990) and are mostly

classified as ”minor injury” (AIS 1) on the abbreviated injury scale (AIS) (Foret-Bruno et al., 1991; James et al., 1991; Ono and Kanno, 1993). In spite of this low AIS rating, these injuries lead to permanent disability (disability-degree ≥10%) in some 10% of the cases (Nygren, 1984). This can be compared with other AIS 1 injuries where the risk of permanent disability is 0.1% (Nygren et al., 1985).

1.4.2.1 Influence of gender and age

In each of the studies published by Folksam Research, ETH Zurich and Volkswagen, a significant higher risk for women to suffer a whiplash injury was found. VW found an almost double whiplash injury risk throughout the entire age range of women compared with men. The same study found that the risk for females increases from the age of approximately 18-27 years. After reaching this peak, no further increase could be observed. The risk for male occupants increased to its highest level in the same age group (18-27 years). VW found that in the whole range of body height the risk for male occupants to get whiplash was nearly constant and significant lower than the female risk. The taller the women were, the higher was their risk to suffer a whiplash injury.

McConnell W. Howard R. et al. observed a higher head x-acceleration for females.Taller drivers have an increased injury risk in rear impacts (Jakobsson, 2000) and the injury risk increases if the vehicle occupant is unaware of the impending accident (Ryan et al., 1994).

Women were found to be up to twice as vulnerable as men in rear-end accidents (Kihlberg, 1969; States et al., 1972; Kahane, 1982; Otremski et al., 1989; Foret-Bruno et al., 1991; vKoch et al., 1995; Spitzer et al., 1995) (Figure 1.9).

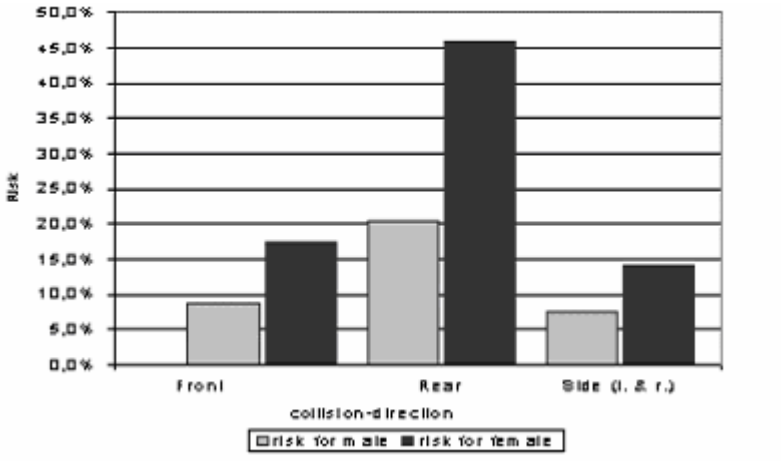

Figure 1.9 Injury risk related to gender and impact direction.

1.4.2.2 Accident severity

Accident severity is often described with velocity change (Delta V) or acceleration (peak or mean impact acceleration).

Results from Folksam have been presented where crash severity, recorded with crash pulse recorders, have been correlated to injury risk (Krafft et al. 2001 and 2002).. Crash severity was found to have a large influence on the duration of symptoms. Also grades of WAD were directly correlated to crash severity. Acceleration was found to be more important in explaining the risk of whiplash injury than change of velocity, indicating that when designing a crash test, focus should also be set on acceleration. It was also found that no one in the sample had WAD symptoms for more than 1 month as long as the mean acceleration was below 3g (figure 1.10). This finding is also supported from several volunteer tests (Mc Connell et al. 1995, Ono and Kaneoka 1997, Siegmund et al. 1997).

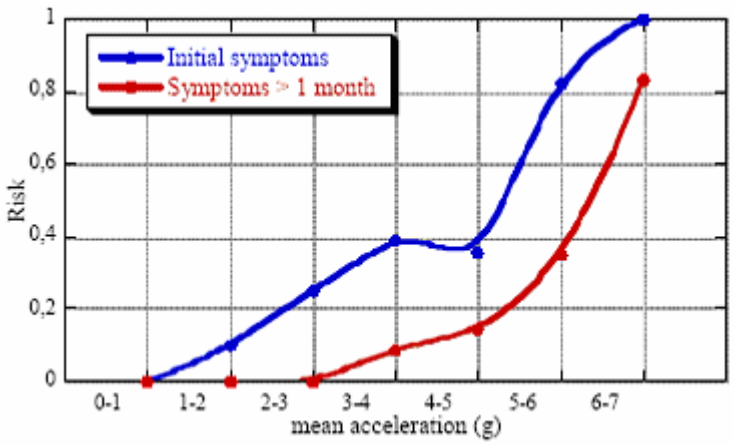

Figure 1.10 Injury risk as a function of mean impact acceleration in rear-end impacts.

In rear-end impacts the average change of velocity and mean acceleration for occupants with symptoms for more than one month were 20 km/h and 5.3g, respectively, and for occupants recovering within a month 10.3 km/h and 3.9g. In frontal impacts, the average change of velocity and mean acceleration for occupants with symptoms for more than one month were 30.5 km/h and 7.9 g, respectively, for occupants recovering within a month this was 19.6 km/h and 5.4 g.

Concerning the injury risk and the direction of impact VW showed that the risk of whiplash was more than twice as high in rear-end collisions than in frontal and side impacts. Also here the risk for women was twice as high as for males in all collision types.

In the study by Krafft et al (2002) the average change of velocity and the mean acceleration for those occupants with symptoms more than 1 month, were found to be 20 km/h and 5.3 g respectively. The average peak acceleration was approximately 11g. The risk of initial neck symptoms increases with velocity change (delta-v) but among those initially injured the acceleration pulse appears to be more important

than the delta-v as a predictor of risk of long term consequences (Krafft, Kullgren et al.,) (Table 1.6).

Injury classification	Category	Number of occup.	Delta-V (km/h)	Mean acc. (g)	Peak acc. (g)
All		94	10,4 +/- 2,0	3,6 +/- 0,3	7,9 +/- 0,7
Reporting	No reported neck injury	53	7,7 +/- 1,2	3,0 +/- 0,3	6,7 +/- 0,7
	Reported neck injury	41	13,9 +/- 2,6	4,4 +/- 0,4	9,5 +/- 1,0
Duration of symptoms	Symptoms < 1 month	26	10,3 +/- 2,1	3,9 +/- 0,5	8,7 +/- 1,3
	Symptoms > 1 month	15	20,0 +/- 4,8	5,3 +/- 0,6	10,8 +/- 1,4
Grade of WAD (Quebec Task Force)	WAD Grade 0	53	7,7 +/- 1,2	3,0 +/- 0,3	6,7 +/- 0,8
	WAD Grade 1	20	10,1 +/- 2,3	3,9 +/- 0,6	8,6 +/- 1,5
	WAD Grades 2 and 3	18(13+5)	16,2 +/- 3,8	4,8 +/- 0,6	10,1 +/- 1,5

Table 1.6 Average values in crash severity for different injury classifications and categories for rear end collisions (from Krafft 2002).

1.4.2.3 Influence of car and seat characteristics

Different factors influence the risk of sustaining neck injuries in rear impacts. These include the distance between the head and the head restraint, the stiffness properties of the seat and of the car rear structure. Differences in mass reflect differences in change of velocity. A correlation between change of velocity and risk of both long-term and reported WAD has been shown (Krafft et al. 2001). Furthermore it has been shown that cars with similar weights may have large differences in risk of WAD (Krafft 1998), indicating that other factors than mass, such as car structure and seat stiffness, are strongly influencing the risk of WAD

Most cars in the study were equipped with head restraints in the front seats but not in the rear seats. The risk of neck injury to rear seat occupants was only about 50% of the risk of neck injury for front seat occupants in rear-end collisions (Kihlberg, 1969; States et al., 1972; Carlsson et al., 1985; Lövsund et al., 1988; Otremski et al., 1989). Generally, there is a difference in design between front-seats and rear-seats. The seat back of the rear seat is usually firmly attached to the sides of the car body and yields very little when loaded during a rear-impact. In contrast, the front-seat seat back is relatively loosely attached at its bottom joints. This difference in seat design could explain the difference in injury risk between the front-seat and the rear seat.

McConnell W. and Howard R. studied neck kinematics after low velocity rear-and impacts and observed a not significant difference between using a restraint system or not. They concluded that restraint system might not play an important role in low speed impacts.

Instead, Nygren et al. (1985) found that the use of head restraints decreased the risk of neck injury in a rear-end collision by about 20% on average. Fixed head-restraints gave a 24% reduction and adjustable ones gave a 14% reduction. Similar findings have been presented by O'Neill et al. (1972) and by Huelke and O'Day (1975).

However, Nygren et al. (1985) also found that the risk of whiplash injury was not reduced in newer cars. The study disclosed great differences in protective performance between different designs of seats and headrests.

.States et al. (1969) suggested that the elastic rebound of the seat back could be an aggravating factor for the whiplash extension motion. The rebound of the seat back can push the torso forward relative to the vehicle at an early stage of the whiplash extension motion when the head begins rotating rearward. This in turn increases the relative linear and angular velocity of the head relative to the upper torso at the same time as it delays contact between the head and the head restraint. This hypothesis was corroborated by Svensson et al. (1996) and others. If the seat back of the front seat collapses or yields plastically during a rear-end collision, the elastic seat-back rebound is likely to be reduced. In fact, Foret-Bruno et al. (1991) reported that seatback collapse decreased the risk of neck injury in rear-end collisions.

In a study involving 33 occupants in Volvo cars in Sweden, Olsson at al. (1990) reported that the neck symptoms lasted longer whit increasing horizontal distance between the head and the head restraint. These observations were supported by another study (Jakobsson, 1994). This latter study also showed that impact involving stiff structures of the car increased the risk of neck injury compared to impacts involving softer structures. None of the occupants who were aware of the impending impact and had pushed themselves against the seat back and head restraint was injured.

Merz and Patrick (1967) carried out rear and impact sled tests on a volunteer in a seat with a high rigid seat back. In this study, the volunteer's head was always in contact with the seat back during impact. Tests were done at velocity changes up to 30 km/h without signs of injury symptoms occurring.. McConnell et al. (1993) undertook staged rear-end collisions at low impact-velocities. In these tests, volunteers were seated in car seats with head restraints. The maximum extension angle of the neck never exceeded 45° during the tests. The volunteers were thus not exposed to hyperextension of the complete cervical spine and yet symptoms of minor neck injuries in the form of pain in the neck region were experienced.

The result of these two studies indicates that in rear-end impacts it is not enough to avoid hyperextension of the complete cervical spine to prevent neck injury but injuries can be prevented assuming that no head-neck motion occurs during the impact.

The literature about the head restraint is huge and, as previously shown, it presents several discrepancies about the importance of its function. Those contradictions suggest the idea that the parameter decisive for its effectiveness is the distance from the head in the normal position before the impact. Mats Svensson came to the same conclusions in "The influence of seat back and head restraint on the head-neck motion"(1993). A production car seat was modified and minor changes might radically improve the protection against neck injuries: this is a clear indication of the need for further research in this area.

In his study an adequately high head-restraint with a flat vertical front surface was attached to the seat-back. Two different head to head-restraint gaps were tested

combined with different stiffness of the seat-back frame and the lower seat-back cushion as well as different depths of the upper seat-back cushion. Rear-impacts on a sled were staged at Δv of 5 km/h and 12.5 km/h using a Hybrid III-dummy equipped with a RID-neck. Of the parameters tested in this study, the horizontal head to head-restraint gap proved to have the largest influence on the head-neck motion during rear-impact.

The initial horizontal and vertical distance between the head and the head restraint has a significant influence on the maximum allowable head-neck displacement. Deformation or displacement of the head restraint relative to the seat back during contact whit the head probably has a similar influence on the head neck motion as an increased initial distance between the head and the head restraint would have. If the upper torso can compress the upper seat back cushion early on the crash event, without deforming the seat back frame, this will decrease the horizontal distance between the head and the headrest before any larger displacements between the head and the torso take place. If the rebound of the torso starts before the head has reached its rearmost position, the relative velocity between the head and the torso will increase. The stiffness of the seat back frame is another important factor. When the seat back frame yields backwards, the head restraint will follow, thereby increasing the distance and delaying the contact between the head and the head restraint. The difference in stiffness between the top and the lower part of the seat back could cause the upper torso to rebound earlier than the lower torso. The pelvic area is loaded by the mass of the legs and might penetrate deeper and rebound later than the middle and upper torso would. This might in turn induce a forward angular motion of the torso aggravating the head neck motion relative to the torso.

It can be assumed, though, that the risk of neck injury in a rear-end collision is related to the linear and angular rearward motion of the head relative to the torso and that these injuries can be prevented by preventing this motion from occurring. Based on this assumption the results of the Svensson's study indicate that it should be possible to radically increase the protective performance of modern car seats. There is probably no incompatibility between making the seat back strong enough to prevent seat-back collapse during high-speed rear-impacts and improving the neck protection at low-speed rear-impacts, provided that the head-restraint is placed close to the head and that the stiffness of the seat-back frame and the seat-back cushion are properly chosen.

Mats Svensson found also that in the 5km/h tests the head neck motion appeared to be somewhat smoother, with lower initial head angular acceleration in the rear seats compared to the front seats. This indicated lower angular velocities between adjacent vertebrae in the rear seats compared to the front seats.

Those results accredit the hypothesis of Aldman, which is described in the next chapter. According to this hypothesis in the low velocity accidents, the injury is provoked in the first stage of the movement by hydrodynamic causes that occur before reaching the kinematical limits. The magnitudes of the pressures in the central nervous system (CNS) most probably increase with increasing the angular velocity between adjacent vertebrae.

1.4.3 Injury criteria

Dependent on the time duration of the load, static and dynamic load is distinguished. Generally, a load is considered static if it lasts longer than 200ms although this distinction is rather arbitrary. Dynamic load, the most frequently occurring type of mechanical load to the human body in accidents, usually lasts in the order of a few ms to 50 ms. The dynamic load may result from contact of the head with its environment or from a force transmitted to the head through the neck. These cases are referred to as contact load and inertial load respectively. In case of translational acceleration of the skull, the brain is compressed at one side of the skull. At this side, the brain experiences compressive strains, resulting in a positive pressure. At the opposite side, the brain will experience tensile strains, either through direct connections between brain and skull, or through a pressure decrease in the subdural space. These tensile strains are reflected in a negative pressure. This pressure distribution is known as the coup contre-coup effect. In the case of a rotational acceleration, there is a tendency of the skull to rotate around the brain. The absence of spherical symmetry and the presence of falx and tentorium limit the rotational freedom of the brain within the skull. These factors have a protective function for the bridging veins. Moreover, in the human head the centre of rotation is located in the neck, rather than in the centre of gravity of the head. The resulting combination of rotational and translational acceleration is also called angular acceleration.

Already in the 1950's it was indicated that rotational acceleration could develop tensile and shear stress in the brain resulting in concussive brain injuries. Later studies have postulated that especially rotational acceleration is the most important cause for severe head injury: subdural hematoma (SDH) and shearing injury. The injuries, induced by rotational acceleration, depend on the duration of the loading. Short duration loading is considered to cause of SDH, disruption of the bridge veins between skull and brain. The explanation for this lies in the fact that the veins are particularly sensitive to high strain rate loading. If the rotational loading lasts longer, with lower magnitude, the bridging veins remain intact, and the loading is transferred to the brain.

For several years, research has been undertaken to assess the mechanisms causing head injury in impact conditions and to establish associated tolerance levels of the human head. The firs extensive quantification of head tolerance to impact was the Wayne State Tolerance Curve (WSTC). The WSTC gives a relationship between a linear acceleration level and pulse duration that give similar head injury severity in head contact impact. Figure 1.11 shows the now accepted form of the WSTC. The ordinate represents the effective or average acceleration (measured at the rear of the head) and the abscissa represents the time duration of this acceleration. Combinations of acceleration and time, which lie above the curve, are likely to result in considerable brain damage (AIS 3 or higher) and combinations that lie below this curve stay below human tolerance.

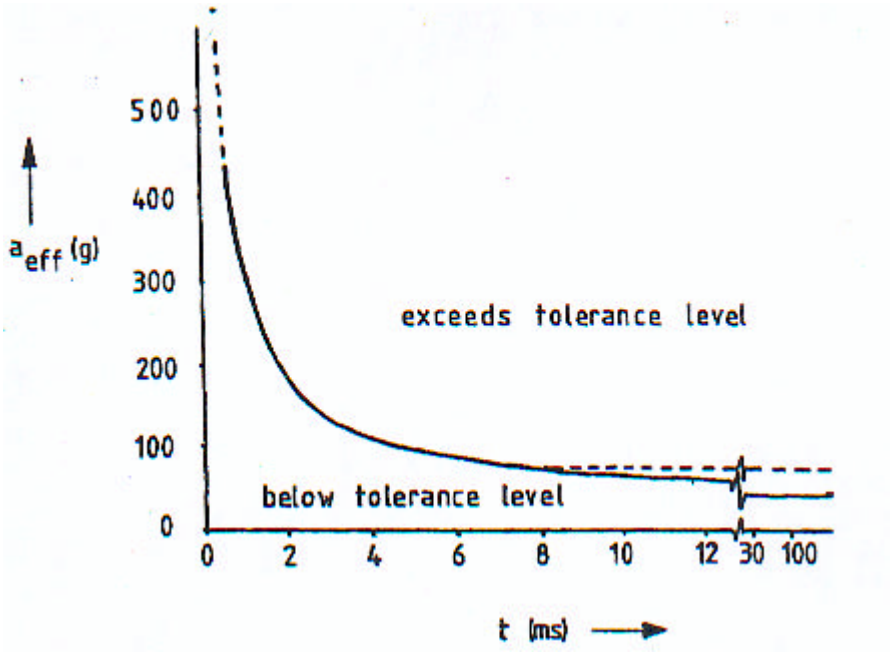

Figure 1.11 The Wayne State Tolerance Curve

For evaluating complex acceleration-time pulses to the WSTC, difficulties arise in the determining the affective acceleration. To overcome this problem Gadd developed a weighted impulse criterion for establishing a Severity Index (SI), which for the head is:

$$SI = \int_T^0 a^{2.5}(t)dt \tag{1.1}$$

Were *a(t)* represents the acceleration in *g*'s, *T* the pulse duration and *t* the time in seconds. The weighting factor 2.5 only applies to the head and is primarily based on a straight-line approximation of the WSTC plotted on log-log paper between 2.5 and 50 ms. The tolerance level proposed by Gadd of concusion for frontal impact is 1000. He also used the uniaxial acceleration of the head, measured at the occipital joint in the direction of impact. For non-contact impact, Gadd proposed a tolerance of 1500 for concussion.

In response to a study by Versace on comparison of the WSTC and the SI a new injury criterion for the head was defined by the U.S. government, the Head Injury Criterion (HIC):

$$HIC = \left\{ (t_2 - t_1)\left[\frac{1}{t_2 - t_1} \int_{t_1}^{t_2} a(t)dt \right]^{2.5} \right\}_{\max} \tag{1.2}$$

Where *a(t)* is the resultant head acceleration in *g*'s (measured at the head's centre of gravity), t_1 and t_2 are the initial and final times (in seconds) of the interval during which the HIC attains a maximum value. As for the SI, a value of 1000 is specified for the HIC as concussion tolerance level in frontal impact. For practical reasons, the

maximum time interval $(t_2 - t_1)$ which is considered to give appropriate HIC values was set to 36 ms. This time interval greatly affects HIC calculation and recently, this time interval has been proposed to be reduced to 15 ms in order to restrict the use of HIC to hard contact impacts.

Mainly because of human variability, no precise separation between a non-injurous and an injurous load condition can be defined. This raises the problem of injury probability. HIC value obtained in reconstructed accidents using dummies, cadavers and mathematical, have been gathered by Newman and he concluded from these data that HIC and AIS do not correlate. Most important drawbacks and human surrogate head acceleration-time response and that HIC only takes into account the linear aspects of head motion. Despite its drawbacks, HIC is the most commonly used criterion for head injury in automotive research. There are important conclusions that can be drawn from HIC vs. injury severity analyses. HIC only considers linear acceleration, while biomechanical response of the head also includes angular motion which is believed to cause head injury. It is only valid if hard contact occurs thus the time duration of impact is limited. HIC is based on the WSTC, which is derived from subjects loaded in anterio-posterior direction.

The WSTC and HIC, concern linear head impact response. An attempt to combine translational and rotational head acceleration response was made by Newman. Considering these accelerations as the cause for stresses generated in the brain and resulting in brain injury, a Generalized Acceleration Model for Brain Injury Threshold (GAMBIT) is proposed. Newman assumed that the tolerances derived from experiments with only translational or only rotational head motion are also valid for combined head response. However, thus far the GAMBIT lacks extensive validation.

Several neck injury mechanisms and neck injury criteria have been proposed during recent years. Two criteria, Nij (Kleinberger et al., 1998; Kleinberger et al. 1999) and Nkm (Muser et al., 2000), use combinations of neck loads to predict the risk of injury to the skeletal spine. The IV-NIC (Panjabi et al., 1999) uses the angular displacement between adjacent vertebrae to estimate the risk of injury to various structures of the intervertebral joints. Viano and Davidsson (2001) introduced the Neck Displacement Criterion (NDC), a new injury criterion based on neck displacement. Occipital rotation was plotted against occipital x-displacement and occipital z-displacement and envelopes for different degrees of injury risk were proposed. The correlation between these three injury criteria and the risk of long term soft tissue neck injury has not yet been established. The Neck Injury Criterion (NIC) (Boström et al., 2000) uses differential horizontal acceleration between the head and the T1 vertebra to assess the neck injury risk. The NIC was initially based on experimental injury findings summarised by Svensson et al. (2000). NIC would also function as a predictor of other types of injury mechanisms and indications of correlation between NIC and long term neck injury risk have been presented (Boström et al., 2000). The lower neck moment is sensitive to seat design parameters (Prasad et al., 1997; Song et al., 1996). Lower neck loads are also consistent with the facet-based injury mechanism supported by the works of Yoganandan et al, Ono et al., Deng et al. In rebound, the rebound velocity or the seat belt load may be used as injury criteria. The Nij, Nkm, NIC, NDC and lower neck moment can be applied to

current rear impact dummies. Reference values have to be adapted to the chosen dummy. The validity of all these criteria, in predicting the injury risk, needs to be established.

The injury symptoms are well known both regarding type and duration. However, injuries causing the acute symptoms are not known though several possibilities have been suggested in the literature. Several injuries may coexist and cause very similar symptoms. It is unknown if one or several of these injuries could cause chronic neck symptoms. The relation between acute injury and chronic pain is not fully understood and the origin of the chronic pain is not known. Strong indications however exist for central nervous system pain sensitisation in the chronic stage. The head and neck kinematics during whiplash trauma is relatively well known.

Several injury criteria have been suggested but all of them would have to be better validated with respect to possible injuries before they could become commonly accepted. Three principle ways of verifying injury criteria were identified. It is possible by identification, in the clinic, of the actual acute injury that causes chronic pain. This would probably tell which injury mechanism is the cause and give an indication as to which injury criterion to use.

An alternative would be to evaluate proposed criteria against experimental data where certain injuries have been caused and where injury threshold levels can be identified (this will however leave an uncertainty about the relation between the observed injuries and the symptoms experienced by living patients). Another way is by high quality evaluation of injury criteria against field accident data. Reconstruction crash tests and computer modelling may be used in parallel.

Current neck injury criteria are acceleration based, like NIC, velocity based (T1 rebound velocity), displacement based (IV-NIC and NDC) or load based, like Nkm. An injury criterion that correlates to injury risk is a requirement for a future test procedure. It would however be possible to identify such a criterion even if the injury and injury mechanism is not fully known. (Medical symptoms can often be treated even if the origin of the symptom is not fully understood). From a regulatory perspective, it is essential that there is a good correlation between criteria and risk. Any given injury criterion should be accompanied by an injury risk function. Several promising candidates have been presented. It is not clear when such a criterion will be available.

1.5 Aldman's hypothesis

The phenomenon of soft tissue injuries of the human cervical spine following rear end impact has been investigated by a large number of researchers and Institutes but, up to now neither the injury mechanism has been identified nor a injury criterion has been established.

In earlier effort to explain whiplash injuries, for instance by Merz and Patrick (1971), the main interest has been directed towards the vertebra, discs and ligaments and their response and tolerance to injury. The predominant theory of the injury mechanisms for the nervous tissue of the central nervous system (CNS) has been mechanical stretching and compression of cervical nerve root (McMillan and Silver,

1987). Other studies indicate that neck flexion during rebound (Koch et al, 1995) in a later phase of the motion could be responsible and explain the fact by increased seat belt usage, that may in turn increases neck loads. Also shear forces in a rather early phase of the typical whiplash motion were taken into account as a possible injury inducing mechanism (Walz, 1995). Onto et al. (1998) have proposed a theory that relates soft tissue neck injuries to lesions of facet joints of cervical vertebrae.

Even at low rear end collisions, the car occupants often loose consciousness immediately after the collision even when no signs of impact to the head can be found. The typical symptoms of whiplash motion are probably caused by damage to nervous tissue. The symptoms often occur even though no signs of skeletal injury or injury to the vertebral disks or ligaments can be diagnosed (Maimaris et al. 1988). The mechanisms causing damage to the nervous tissue but leaving the surrounding tissues virtually unaffected have not yet been given a satisfactory explanation.

A new model for explaining these injuries was presented by Aldman (1986). He claimed that the pressure gradients, caused by fluid motion under the shortening of the spinal canal at extension movement, give rise to damage to the nervous tissue of the CNS.

1.5.1 Theoretical injury mechanism model

The length of the cervical spinal canal alters when the neck is flexed or extended, it increases at flexion and decreases at extension (Breig, 1978) (Figure 1). In one case where the cervical spine of a human cadaver was moved from maximal flexion to maximal extension, the length of the spinal canal decreased by about 30 mm (Breig,1978). The cross-sectional area of the cervical spinal canal decreases during neck extension since the ligamenta flava protrude into the canal (Breig, 1978) (Figure 1.12).

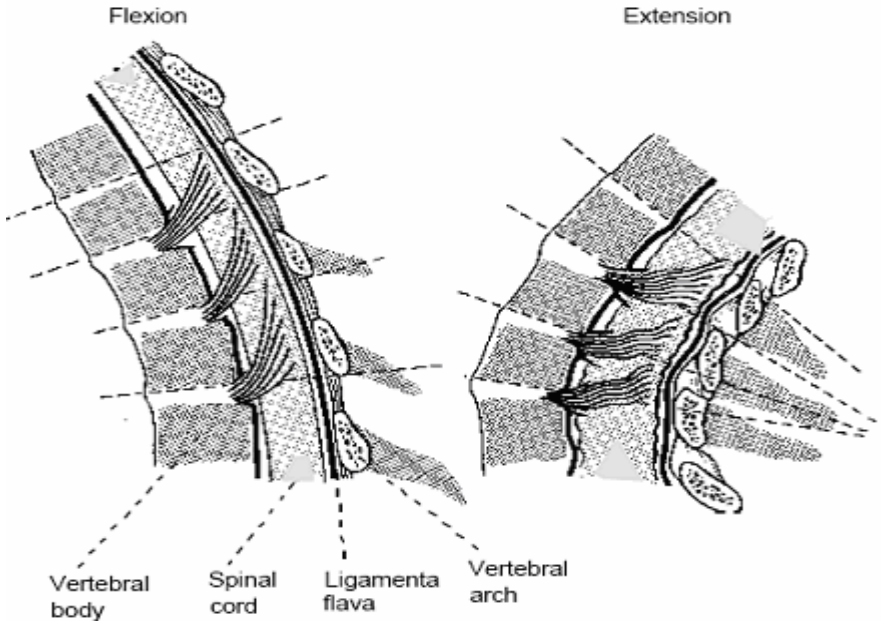

Figure 1.12 Sagittal cross-section of the lower cervical spine (C7-C3) in flexion and extension.

This means that the inner volume of the spinal canal decreases during neck extension and increases during flexion of the neck. However, all the tissues and fluids inside the spinal canal are virtually incompressible (Estes and McElhaney, 1971). This means that fluid transportation, to and from the cervical spinal canal, must take place during the flexion-extension motion of the cervical spine. The fluid moving to and from the cervical spinal canal during this motion could be either blood in the vein-plexa of the epidural space or cerebrospinal fluid (CSF) (Figure 1.13).

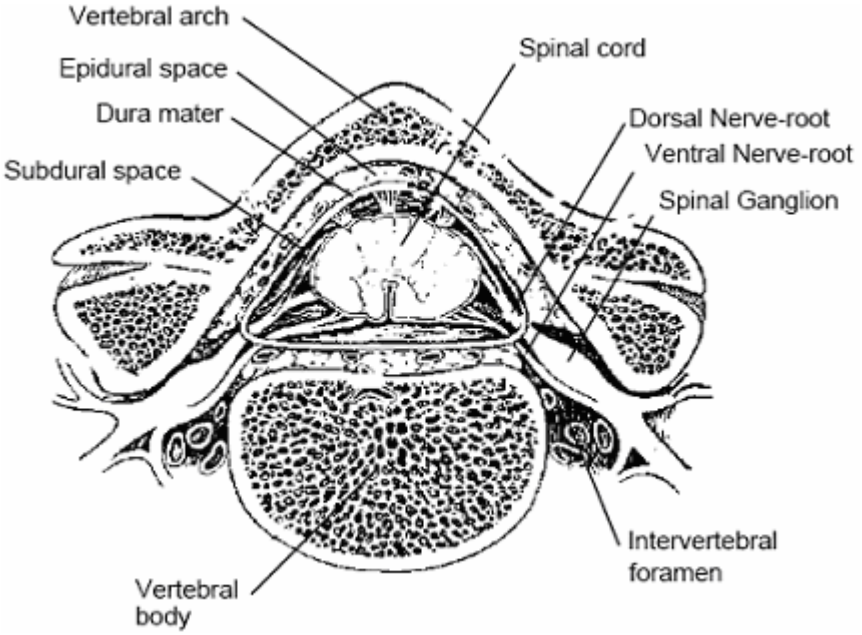

Figure 1.13 A horizontal cross-section of cervical vertebra with the soft tissues of the spinal canal and intervertebral foramina .

According to Batson (1957) both the internal and the external vertebral venous plexa that communicate via vein bridges through the intervertebral foramina have a capacity by far exceeding that of the arteries supplying the tissues of the same region. Since these vein-plexa do not have any valves, the blood can easily move in any direction within the plexa, and also back and forth between the inner plexus and the outer plexus. This means that blood volumes can move along the inside of the spinal canal as well as between the inside and outside of the spinal canal and thus compensate for the change in inner volume of the spinal canal during the flexion-extension motion.

CSF can move up and down the spinal canal and the amounts of CSF in the nerve-root sleeves can alter to compensate for the change in inner volume in the cervical spinal canal during the extension-flexion of the neck. Results by Löfgren et al. (1973) indicate that the flow resistance of CSF in the subdural space of the spinal canal is relatively high. Thus, the flow of CSF may in this context be of minor importance compared with the motion of the blood in the vein-plexa.

During the extension-flexion motion, particularly when the motion is rapid like for instance during a whiplash extension motion, the flow velocity can be expected to rise far above physiologically normal levels and pressure gradients along the spinal canal as well as across the intervertebral foramina can be expected. There are two

separate superimposed effects that will cause this gradient. The first effect is the pressure gradient that occurs when a column of fluid accelerates and the pressure difference is proportional to the height of the fluid column as well as the magnitude of the acceleration. The second effect is the pressure gradient caused by the flow resistance in the vessels. Inside the spinal canal, both higher and lower pressures relative to the soft tissues surrounding the spine could be expected to occur during an extension-flexion motion of the cervical spine. The pressure gradients mentioned above can be expected to generate injurious stresses and strains to the exposed tissues particularly in the intervertebral foramina (Svensson et al., 1993).

1.5.2 The CNS from a hydro mechanical point of view

In this section is reported a resume of the study "A theoretical model for a pilot study regarding transient pressure changes in the spinal canal under whiplash motion" (M. Svensson and B. Aldman, 1989). The CNS, i.e. the brain and the spinal cord, is situated in a container consisting of the cranial cavity and the spinal canal. The CNS is floating in the cerebro spinal fluid (CSF) inside this container (Figure 1.14). To get an understanding of the hydromechanical behaviour of the CNS and its ambient tissues, when involved in dynamic processes with short duration (tenths of a second), the following approach is made.

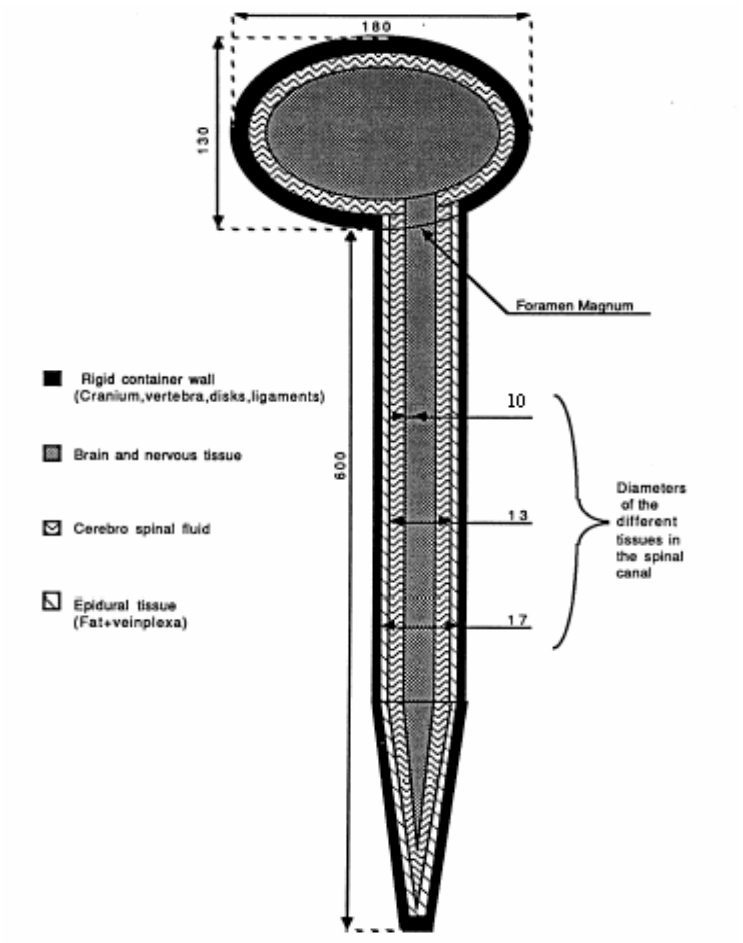

Figure 1.14 Schematic picture of the CNS.

A simplified model of cranial cavity and its contents can be described as follow: the cranial cavity is considered a rigid and impermeable container whit one large opening, the foramen magnum. All other openings in the cranial vault are relatively much smaller than the foramen magnum and almost no fluid is expected to penetrate these small openings under the very short duration of the whiplash motion.

The brain and CSF are of almost identical density (Margaria, 1953) so they will act as one homogenous medium. We consider this medium to be incompressible (Estes and McElhaney, 1971), thus no net fluid flow will take place through the foramen magnum.

Pressure gradients inside the container only occur due to acceleration forces since we consider velocities far below the velocity of sound in body tissues. Unless the head is submitted to rotational acceleration, there will be no fluid flow inside the cranial cavity. It must be emphasized that the simplified assumptions above only consider processes taking place under the short duration of whiplash motion. (This is a model with considerable simplifications. Its purpose is to make the theoretical analysis of the flow-pressure phenomena of the cervical spinal canal less complex. The model is unlikely to be fully applicable in a analysis of the injury mechanisms inside the skull when, for instance, impact to the skull is studied).

A simplified model of the spinal canal and its contents can be described as follows: the spinal canal consists of the vertebral foramina with intervertebral disks and ligaments filling the interspaces forming a tube, which is radically rigid but axially flexible. The inside of the canal is filled with different coaxially oriented tissues (Figures 1.14 and 1.15). The spinal cord in the centre of the spinal canal mainly consists of nervous tissue. It is surrounded by the CSF. The epidural tissue is situated peripherally. Between the epidural tissue and the CSF lies a flexible impermeable wall, the dura mater. The epidural tissue consists of fat with a lattice of inter connected veins, the veinplexa (Parke, 1982). The epidural tissue can easily change its volume within a certain range by changing the volume of blood in the vein vessels (Lofgren, 1973). The veinplexa have cross connections with veins outside the spinal canal in the interspace between every pair of vertebra (Crosby at al. 1962). Blood can also easily move along the spinal canal in the veinplexa.

Nerve roots spring out from the spinal cord and pass through each interspace between the vertebrae. The dura matter is forming a meningeal tube around every nerve root. Outside the spinal canal the maningeal tube is attached to the nerve root at its intervertebral passage. The nerve root is floating in CSF inside this sack (Figure 1.15).

It is possible that the volume of CSF inside the spinal canal can be altered if the CSF flows through the meningeal tubes and alters the size of the tube at its end outside the intervertebral passage.

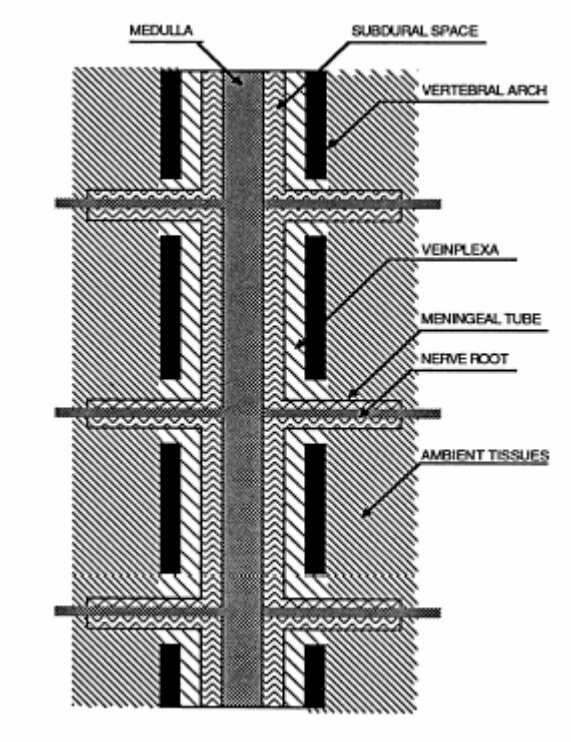

Figure 1.15 Schematic view of the tissues of the spinal canal.

1.5.3 Volume change inside the spinal canal

The length of the spinal canal will increase at flexion of the neck and decrease at extension. This occurs since every vertebra is pivoting around a virtual axis in the vertebral body of the closest inferiority laying vertebra (Kapandji 1974) and the spinal canal passes through the vertebral foramina posteriorly to the column of vertebral bodies (Figure 1.16). Breig (1978) describes one case where the cervical spine of a human cadaver was moved from maximal flexion to maximal extension, resulting in a change of the length of the canal of about 30mm.

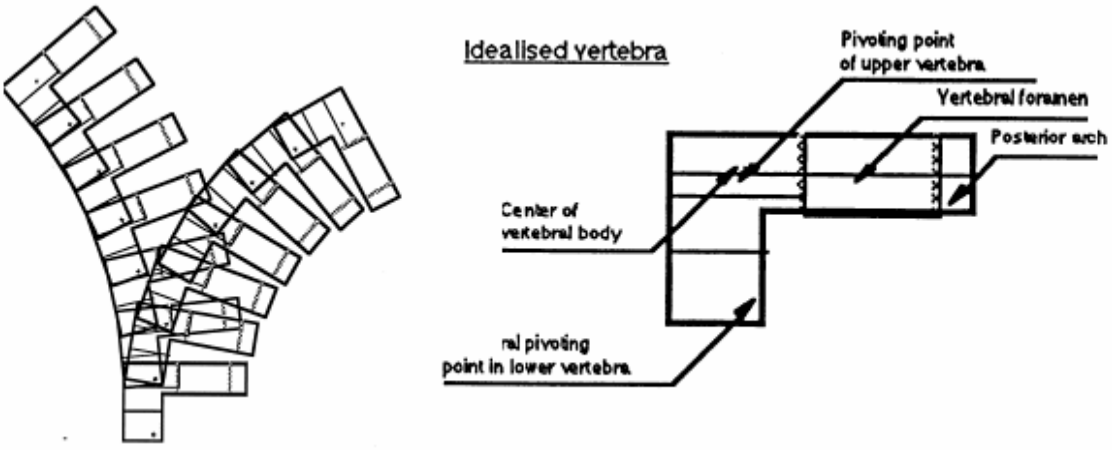

Figure 1.16 Schematic view of cervical spine in full flexion and full extension respectively.

The cross sectional area of the vertebral foramen in the lower neck can be estimated to 200-250 mm^2. Thus, the maximal volume change inside the canal in this case would be 7ml. Since the spine consists only of tissues and fluid that can be considered incompressible, the change of volume in the spinal canal ought to correspond to a fluid exchange between the inside and outside of the canal. This means a change of the volume of either the CSF or of the blood in the veinplexa, or both.

1.5.4 Pressure and injury mechanisms

The whiplash motion is swift compared to the maximal physiological speed of motion of the neck. Both flow speeds and flow accelerations in the spinal canal must be higher under the whiplash motion than under physiological conditions. It is expected that this induces markedly higher pressure gradients in the spinal canal under whiplash motion compared to physiological conditions.

To make a simple analysis of the possible flow-pressure mechanisms in the spinal canal the following simplified approach is made.

No distinction between blood and CSF is made. The bending of the canal is omitted and the cross sectional area is considered to be circular. The influence of gravitational forces is omitted.

With the model of the cranial cavity and its contents as described above, the net fluid flow through the cavity is zero. Thus, at the cranial end of the spinal canal the foramen magnum can be considered a rigid wall.

In other words, the spinal canal is considered to be a straight circular pipe, radially rigid but axially flexible. Both ends of the pipe have rigid walls. Fluid exchange between the inside and outside of the pipe can take place through holes in the pipe wall at levels along the pipe that correspond to the intervertebral vein connections and meningeal tubes. In the following approach, the first part of the whiplash motion where the neck is moved from an upright position to full extension is considered. The motion corresponds to a caudal movement of the wall at the cranial end of the pipe. Pressure phenomena according to the following three points are possible:

1) Consider a short moment of the whiplash motion under which the cranial and moves caudally with constant velocity so that the inner volume of the pipe decreases. When fluid is forced to flow out through the holes in the pipe wall a relative pressure increase inside the pipe arises due to flow resistance in the holes.

2) Consider a short moment of the whiplash motion during which the cranial and moves caudally with constant velocity. A fluid flow in a caudal direction is induced with caudally decreasing flow velocity due to successive outflows along the pipe through the holes. Due to flow resistance, a flow velocity dependent pressure gradient along the pipe is induced. Thus, this gradient decreases successively caudally.

3) When, the cranial end of the pipe is accelerated caudally the fluid column in the pipe will be accelerated caudally. Due to the successive outflows along the pipe, the

acceleration will decrease caudally and at the caudal end it will be zero. The acceleration will induce a pressure gradient along the pipe that is decreasing caudally. In the later part of the whiplash motion the cranial end of the pipe will be decreased, which means that this pressure gradient will change sign.

In a real rear end car collision, these three pressure phenomena will be added the initial natural pressure inside the spinal canal of a sitting car occupant. A pressure gradient due to the horizontal acceleration of the whole body will also be added. When considering the pressure gradient from the whole acceleration, the bending of the spine should not be omitted.

The skull: According to the previously presented simplified model of the skull, the pressure inside the cranial vault will be constant and equal to the pressure in the spinal canal at the foramen magnum, when the body is at rest and if gravity is omitted. This pressure will be added a pressure gradient inside the skull due to gravitation and acceleration.

On the bases of the model presented, the following possible injury mechanisms can be deduced.

a) The pressure gradient directly influences the spinal cord and nerve roots in the spinal canal.
b) The pressure gradient influences on the nerve roots in the meningeal tubes caused by swift pressure changes at expedited cerebro spinal fluid flow through the tubes
c) Ruptures at the end of the meningeal tube, where the dura matter connects to the epidermium. Spinal fluid is forced to flow through the tube due to the increased pressure in the spinal canal during the whiplash motion and the outer end of the maningeal tube is filled up. The dura matter as well as the epidermium and the nerve itself might rupture.
d) The unconsciousness that often follows immediately after a rear end collision might be induced by the rapid pressure change at foramen magnum that momentarily spreads through the hole of the skull cavity and might affect the function of the brain.

2 Dummies for rear impact protection evaluation

For car seat evaluations or ratings there are two basic methods available: a static evaluation and a dynamic evaluation. The static measurement estimates the quality of the head restraint position of which ratings are documented by RCAR (Research Council for Automobile Repairs), while the dynamic method relates the quality of the entire seat to measurements in rear impact dummies. During the past few years, several dummies have been evaluated for the use in rear impact testing. Some of these have been designed specifically for rear impact. The evaluation of biofidelity has its main focus on kinematic behaviour and does not specifically focus on loads measured in dummies as compared to those calculated in human testing. The reason is that there are assumptions made for the calculations of the human neck loads, which are not easily comparable to dummy load measurements. For instance, the Occipital Condyle joint in a dummy is a hinge joint, while in the human the OC is surrounded by other load bearing tissue

2.1 Brief description

The static measurement procedure defined by RCAR uses an extended H-point machine. The question of this method is, whether the quality assessment reflects the safety of a seat in dynamic rear impact. Furthermore, the Head Restraint Measuring Device is based on an H-point machine, designed to find the H-point of a seat. The back geometry of this machine may not reflect the human back geometry and therefore the HRMD head may end up in a different position than found in the average human. This is of concern for the design process, since a different head restraint distance will be found in dynamic testing using a rear impact crash dummy.

Based on the findings in dynamic rear impact testing, the dummies that are most likely to be useful for rear impact testing are the BioRID II and the RID2. The BioRID II has the advantage of being more established and accepted in automotive industry. The advantage of the RID2 is the wider instrumentation capabilities, like the lower neck and lumbar load cells and its capabilities to handle oblique impacts. Currently, the BioRID II is being changed to allow lower neck load measurements.

Hybrid III dummy (and TRID neck)

This is the most commonly used dummy for both frontal and rear impacts, although it was originally designed for frontal impact. The performance at high severity rear impact seems rather good (Prasad, 1997), but the performance in low severity (whiplash) cases is rather poor (Scott 1993, Davidsson 2000, Cappon 2001a). The main problems in low severity impact relate to the rigidity of the spine, the limited flexibility of the hip joints and the stiff neck, showing no head lag. Even the addition of a more flexible 2D TRID neck (Thunnissen, 1996), does not result in a biofidelic response.

BioRID II dummy

This dummy was designed by Chalmers University of Technology (Davidsson, 1999). The BioRID I was updated to the prototype BioRID P3, which is being manufactured by R.A. Denton Inc. under the name BioRID II. The dummy has a multi-segment spine, representing all the vertebrae in the human body. The dummy shows biofidelic behaviour in most responses, compared to volunteer experiments performed earlier at a low delta V (7-9 km/h). Also the typical s-shape in the neck, causing head lag, is present in the BioRID II. The only differences found relate to the spine straightening and the head rotation, but these are rather minor. The dummy was shown to be very repeatable, but also sensitive to ringing of the spinal structure (Kim, 2001).

RID2 dummy

The RID2 prototype dummy was originally designed and built within the European Whiplash Project (Cappon, 2001b). The dummy was later updated to a commercial version, called RID2, by FTSS (Cappon, 2001a). The RID2 is a 2½ D dummy, which means that it is not meant for 3D use, but yet can handle oblique rear impacts. The back shape of the dummy is based on the UMTRI data and reflects the 50th percentile male human back shape, ensuring human like seating. The dummy was evaluated against low severity volunteer tests (5g) and higher severity PMHS tests (12g). Most of the responses are biofidelic and the RID2 shows the typical s-shape in the neck. However, the dummy showed limited ramping up and lower neck rotations. Furthermore, the dummy was found to be repeatable and reproducible.

THOR dummy (and THOR Beta neck)

The THOR dummy is commercially available at GESAC. It is a frontal impact dummy with a more biofidelic frontal response than the Hybrid III, which has been evaluated for rear impacts as well. There is also a THOR Beta neck, which is a retrofit to the Hybrid III dummy. Also this neck has been tested in rear impact. No papers or reports have been published on the THOR dummy and THOR Beta neck performance in rear impact. The rear impact performance of the THOR shows enough flexibility in the neck, but no head lag. There is very little flexibility in the spine and thus limited T1 rotation, neither is there any ramping up of the pelvis. Repeatability in rear impact is nevertheless very good.

2.2 Biofidelic rear impact dummy: Bio RID II

Seemann et al. (1986) found the Hybrid III neck far too stiff to respond in a humanlike manner in the sagittal plane. Deng (1989) reported that results from a mathematical model of the Hybrid III neck indicated that the neck has a torque response similar to that of the human neck but has a higher shear response. Foret-Bruno et al. (1991) compared the Hybrid III dummy with a cadaver in simulated rear-end impact using a headrest closely fitted to the head, to minimise the relative movement between head and torso. The cadaver showed no sign of injury. In spite of this, very large shear forces at occipital level were registered in the Hybrid III test. The authors concluded that the human head can be moved relative to the torso with no stresses in the neck, but this is not the case for the dummy. In volunteer tests,

McConnell et al. (1993) found that during the acceleration phase of a rear-impact, when the occupants body was pressed against the seat-back, the spinal curvature straightened. This in turn caused an upward motion of the head and thus an elevated head contact point on the head-restraint. In a comparative study using volunteers and a Hybrid III-dummy, Scott et al. (1993) found that the dummy was less prone to ramp up along the seat-back than were the volunteers. Svensson and Lövsund (1992) developed and validated a Rear Impact Dummy-neck (RID-neck) that can be used on the Hybrid III dummy. The new neck was meant to be used in rear-end collision testing at low impact-velocities. It consisted of seven cervical and two thoracic vertebrae. It was designed to resemble the human anatomy to enable a trajectory, and angular range of motion similar to that of the human in the sagittal plane.

A dummy for rear-end collision testing at low velocity changes was developed (Davidsson et al., 1998a) (Figure 2.1) in a joint project involving Chalmers, Autoliv, Saab Automobile and Volvo Car Corporation. The dummy has been given the name Biofidelic Rear Impact Dummy (BioRID). It has a new torso, arm attachments, articulated spine, neck muscle substitutes and pelvis, to be used with Hybrid III legs, arms and head. Three dummy prototypes (BioRID P1, P2 and P3) for rear-end collision testing at low velocity changes were developed to resemble the human being in seated posture and to replicate the human motion in a rear end impact.

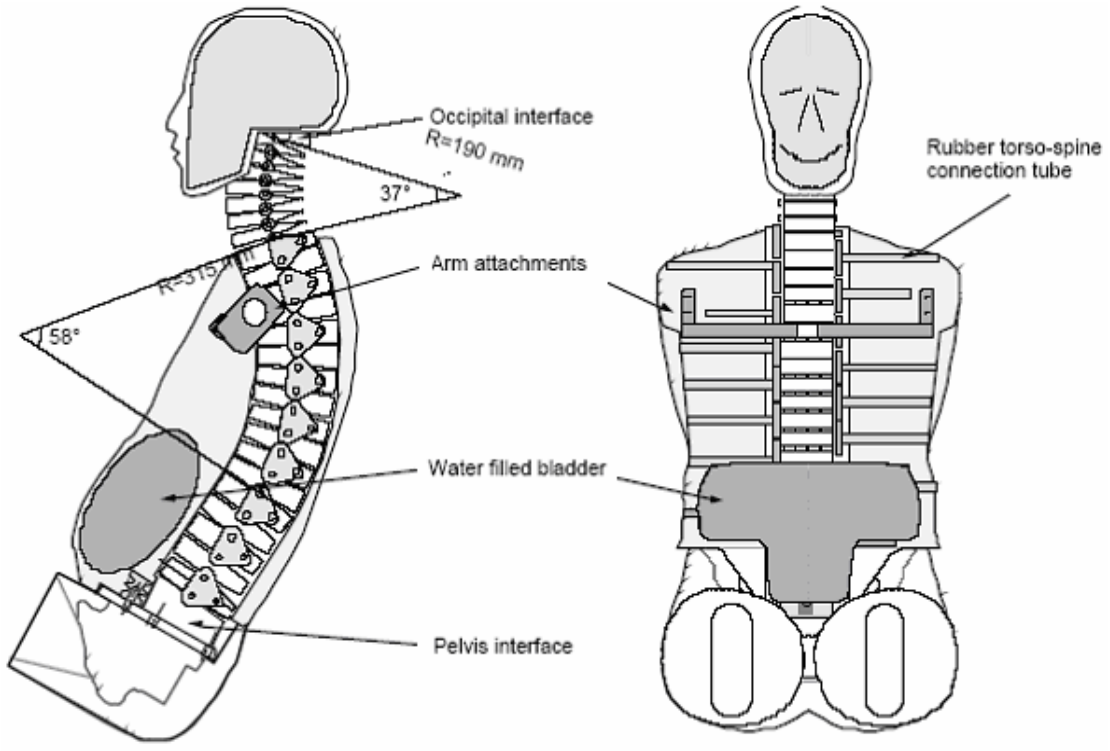

Figure 2.1 Schematic drawing of the BioRID dummy torso, arm attachments, spine, neck and modified pelvis with Hybrid III head (Davidsson et al., 1998a).

The BioRID spine consists of the same number of vertebrae as that of a human, i.e. 7 cervical, 12 thoracic and 5 lumbar vertebrae. The head and the top cervical vertebra is connected to each other by means of occipital interface. The occipital interface is rigidly mounted to a modified version of Denton type 2564 or 4037 Eng Hybrid III upper neck load cell. The top cervical vertebra and the occipital interface have special designs that allow the head to be horizontal while maintaining the same joint characteristics as the rest of the neck joints. The top thoracic vertebra is a hybrid; its upper side designed like a cervical vertebra and the bottom surface as a thoracic vertebra. The T1 upper face is also tilted rearward relative to the lower face. The upper surface of the top lumbar vertebrae matches the thoracic vertebra design and is tilted slightly rearward. The bottom lumbar vertebra is connected to a pelvis interface which, in turn, is mounted to the pelvis.

The BioRID P1 vertebrae are made of aluminium and the BioRID P2/I and P3/II are made in durable plastic (Acetal). The vertebrae are connected with pin joints that only allow for angular motion in the sagittal plane. All occipital interfaces and pelvis interfaces are made of aluminium. The cervical, thoracic and lumbar vertebrae are of the same height: 17.5 mm, 26.5 mm and 30.5 mm respectively (Figure 2.2)

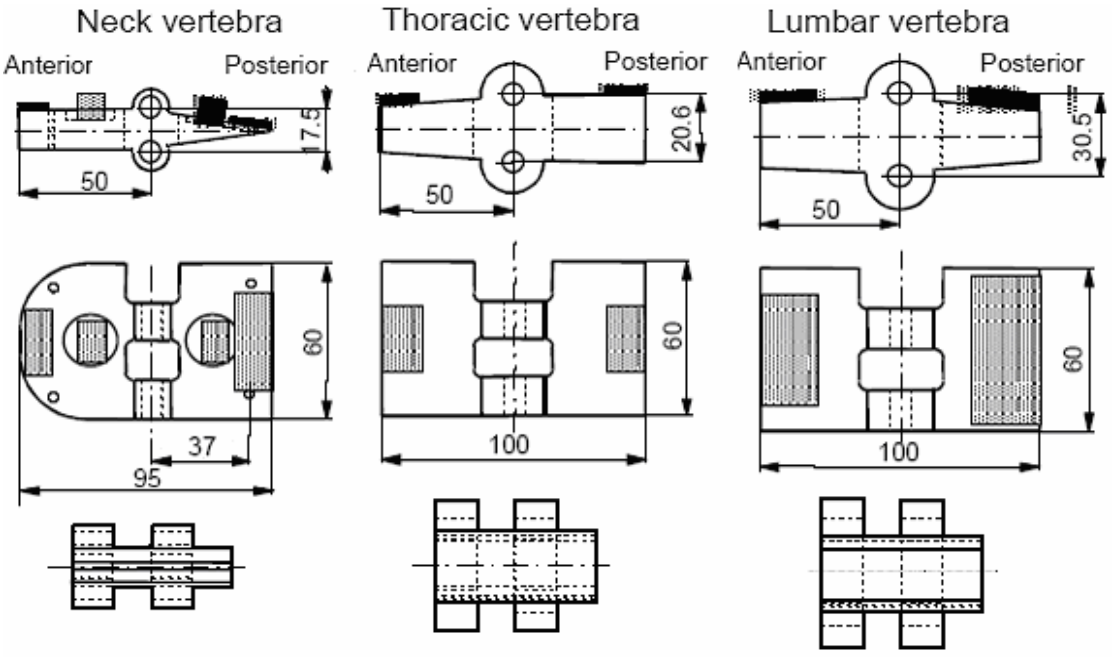

Figure2.2 Schematic of the BioRID cervical thoracic and lumbar vertebrae (side, top and frontal view).

In the inter-spaces between all vertebrae, there are blocks of polyurethane rubber glued to the nearest inferior vertebra. Two blocks are in the neck: the first contributes to the overall joint characteristics while the second is activated only when the spine is hyper-extended or hyper-flexed.The thoracic and lumbar spine are only equipped with blocks of the latter type. In the thoracic and lumbar spine, the steel pin joints constitute linear torsion springs (Figure 2.3). The ends of the pins are

connected on each side respectively to the superior and to the inferior pin by means of steel washers.

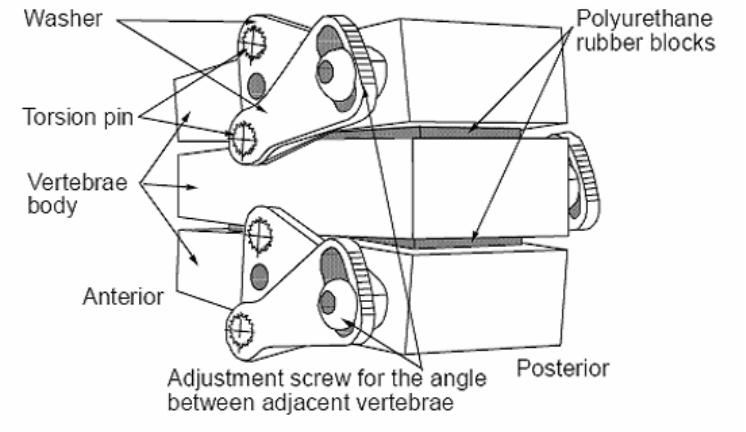

Figure2.3 Schematic of three thoracic vertebrae with torsion springs/pin-joints (oblique rear view).

For all BioRID prototypes, the cervical vertebrae and the occipital interface, thoracic and lumbar vertebrae have the same angular range of motion relative to the nearest inferior vertebra. The chosen range of motion of the lumbar, thoracic and cervical spine were based on data from the literature and adjusted for seated posture. Schneider et al. (1983) established a set of co-ordinates for the joint centers of the human bones, center of gravity of various body parts of an average midsize male in seated posture. The spinal joint center co-ordinates could relatively precise be represented by two arches, one arc for the thoracic kyphosis and one arc for the neck, and one line for the lumbar spine. The spine curvature can be changed thereby, enabling different initial seating postures. The choice of static joint characteristics in the cervical, thoracic and lumbar spine was based on MADYMO simulations (Davidsson et al., 1998a; Linder et al., 1998a). For the human cervical spine, White and Panjabi (1978) reported total range of motion of 8-17° (average 12.3°) per mobile unit (see Table 1.2 and 1.3). In the BioRID, this range of motion was increased with 2° per unit for all 8 joints in booth flexion and extension to allow for some hyperextension, hyper-flexion and sufficient retraction (s-shape motion)of the head.

In order to better replicate the human head and neck retraction motion (head lag), and thus more precisely injury risk, the necks was equipped with muscle substitutes. In all dummy prototypes, these consist of cables originating from the head, in the front and in the back of the occipital joint, guided through the cervical vertebrae and terminating at either T1 or T3. In the P3 prototype the left and right neck muscle substitute were connected to a rotational damper and coil springs, respectively. The damping constant was approximately 310 Ns/m. The anterior and posterior muscle substitute spring constants were 12.1 kN/m and 9.8 kN/m respectively. The springs and damper was fitted inside the torso.

The torso consists of chest and abdomen and is moulded in a soft silicon rubber. The torso surface contour resembles a seated 50% male.The spine is contained in a curved rectangular container inside the torso. A total of 15 steel tubes with a diameter of 10 mm connect the rubber torso to the spine (Figure 2.1). In order to reduce the bending resistance of the rubber torso, a water filled bladder (volume 2.05 litres) is enclosed in the abdominal region of the torso (Figure 2.1). The bottom of the rubber torso is attached to the pelvis. In the BioRID, the original Hybrid III pelvis anterior-superior iliac spine height is decreased to conform with the modifications to the Advanced Anthropometric Test Dummy prototype (Schneider et al., 1992). The original pelvis front flesh is removed to allow the abdomen to bulge forward. The pelvis flesh was modified to reduce femur joint flexion/extension resistance.

The BioRID was dressed in two layers of elastic nylon/Lycra shirt and pants to mimic the low friction observed between the human skin and normal clothing. The BioRID P1 and P2/I are equipped with standard Hybrid III legs, arms and heads. The P3 is fitted with a modified Hybrid III head and with standard Hybrid III legs and arms. The BioRID P3 had a somewhat modified spine stiffness and rubber-torso stiffness compared to the BioRID I

The validation data used for test the prototypes were from 5 volunteer tests, a subset of a larger series of rear-end impact volunteer tests (Davidsson et al., 1998b). The angular displacements of the dummy head, T1 and head relative to T1 were compared to volunteer data. The T1 angular displacement and angular velocity for the BioRID were similar to those of the volunteers for the first 250 ms. The BioRID maximum T1 rearward angular displacement was well within the volunteer corridor. The head relative to T1 angle for the BioRID P3 stayed within the volunteer corridor, and had a significantly improved time history compared to the Hybrid III.

3 Previous research

3.1 Introduction

In the last few years, some effort has been done to explore the injury mechanism of traumatic neck motion. In this chapter, three studies that are of relevance for this thesis are mentioned. One study about experiments with pig (Svensson,1993); one about test with post-mortem human subjects and one about the development of a Finite Element model to calculate the pressure phenomena inside the spinal canal. Those experiments work as experimental guidelines and as terms of comparison with the results obtained in tests made with the prototypes realized in this thesis work. In particular, the curves of pressure measured in the prototype described in chapter 4 will be compared to the ones obtained in the experiments described below.

3.2 Animal experiments

The overall anatomy of the cervical spine of the pig is similar to that of the human being even though the dimensions and the detailed shape of different tissues differ somewhat between the two species. The spine and head of the pigs serve as a qualitative substitute of the corresponding parts of the human body and serve as guidance in terms of what kinetic and kinematical parameters are related to the risk of injury. The following section is an abstract from the publication: "Pressure Effect in the spinal Canal during Whiplash Extension Motion: A possible Cause of injury to the Cervical Spinal Ganglia" Mats Svensson et al. 1993).

3.2.1 Pressure phenomena into the pig's neck during whiplash motion

The pig was chosen as a model of the human body for the study of the neck trauma. Fourteen male and female pigs of Swedish landrace strain (body weight about 20-25 kg) were used in the experiments (Svensson et al., 1993). The animals were anaesthetised throughout the experiments approved by the local animal experimentation and ethics committee.

A first group of two animals was used to measure pressure in the CNS during simulated rapid neck extension motion or neck flexion motion. A second group was used for histopathological examination. In the second group, some animals were exposed to simulated rapid neck motion and others served as sham-exposed controls. The animals that were exposed to whiplash extension motion were placed laterally on an operating-table with the right side of the body down. The table was equipped with a backrest to which the animals were strapped. In order to provide as good reproducibility of the test set-up as possible the backrest was made rigid. The upper (superior) end of the backrest was placed in level with the T1 spinous process. Acceleration and displacement were measured during the experiments.

A schematic view of the test set-up for the experimental neck extension/flexion trauma is shown in Figure 3.1

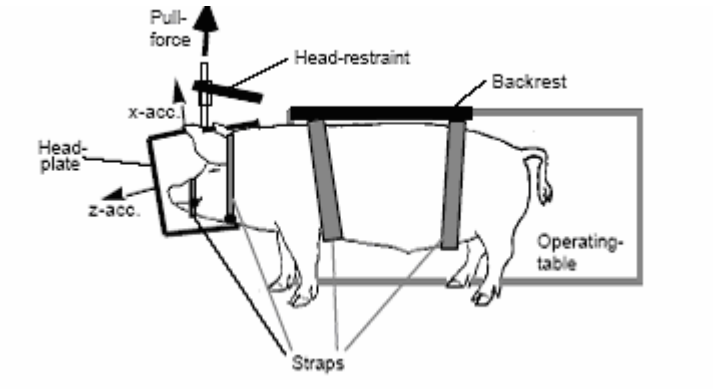

Figure 3.1 AThe test set-up seen from above. The head is strapped to the bolts in horizontally moveable head plate. During the experiment, a pre-tensed rubber strap pulls the head-plate by the pull-rod. The pull rod is active until the pull-rod is disconnected, and thereafter the head moves in the sagittal plane due to its inertianter.

The two animals used for the pressure measurement experiments were equipped with three pressure transducers, one transducer mounted in the frontal bone of the cranium measuring the CSF pressure inside the cranium and two transducers placed subdurally in the spinal canal (Figure 3.2).

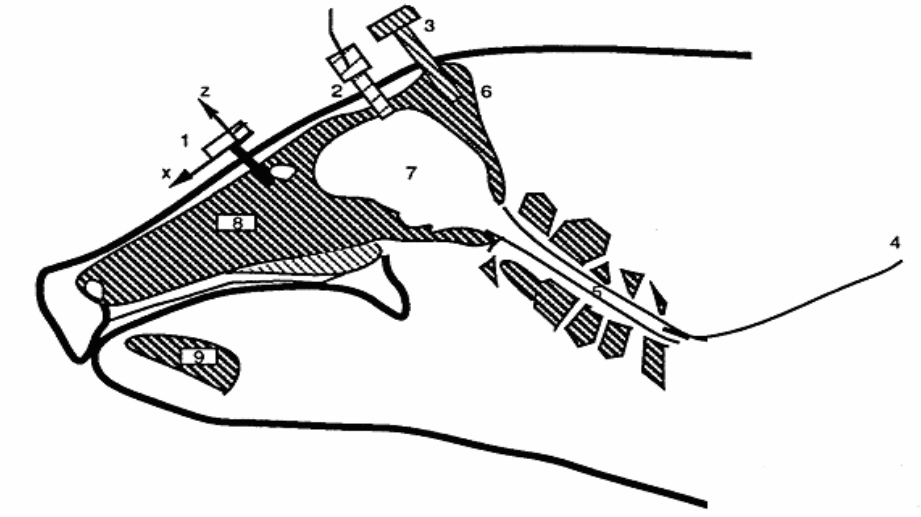

Figure 3.2 Schematic sagittal cross-section of the pig: 1) accelerometer; 2) Pressure transducer; 3) Screw for attachment of pulling device; 4) Pressure sensor; 5) Spinal canal; 6) Nuchal crest; 7) Cranial cavity; 8) Skull; 9) Mandible.

A hole was drilled through the frontal bone and through the dura mater at eye level about 20 mm to the side of the sagittal line. Saline was poured into the hole to prevent air entry while the pressure transducer was fastened into the hole. Laminectomy was done on one of the lowest thoracic vertebra, a small hole was cut in the dura mater and the two catheter-tip pressure transducers were operated into the subdural space and pushed into place, one at cervical level and the other in level with the upper thoracic region.

Each of the two animals used for the pressure measurements were exposed to several whiplash extension motions with various degrees of pulling force (from 150 N to 900 N) and with various positions for the pressure transducers along the spinal canal. The state of the animal was observed after each run.

The twelve animals were used to investigate by histopathological examination whether whiplash extension motion could cause dysfunction of the membranes of neural spinal ganglia cells. These animals were given an injection of the Evans Blue dye, conjugated to Albumin (EBA). The animals were anaesthetized for an additional two hours and were thereafter sacrified by transcardial perfusion with buffered formalin solution for fixation of the body. The brain and the spinal cord to about the T4 level were dissected. The spinal ganglia and proximal parts of corresponding nerves were identified and isolated. Cryostate microtome sections were prepared and examined in a fluorescence microscope according to e procedure described by Suneson (1987). EBA functions as an indicator of the damage sustained to the blood-brain barrier in the CNS. If, at microscopical examination, EBA can be detected outside the blood system, this shows that the blood vessels have been damaged. Due to the fenestration of the capillaries in the spinal ganglia, however, EBA will normally pass into the intercellular space, but not the nerve cells. Thus, EBA inside the nerve cells indicate damage to the nerve cell membranes and satellite calls.

3.2.2 Results of the injury mechanism

Pressure measurement results from one whiplash extension run is shown in Figure 2.3 a, b , c

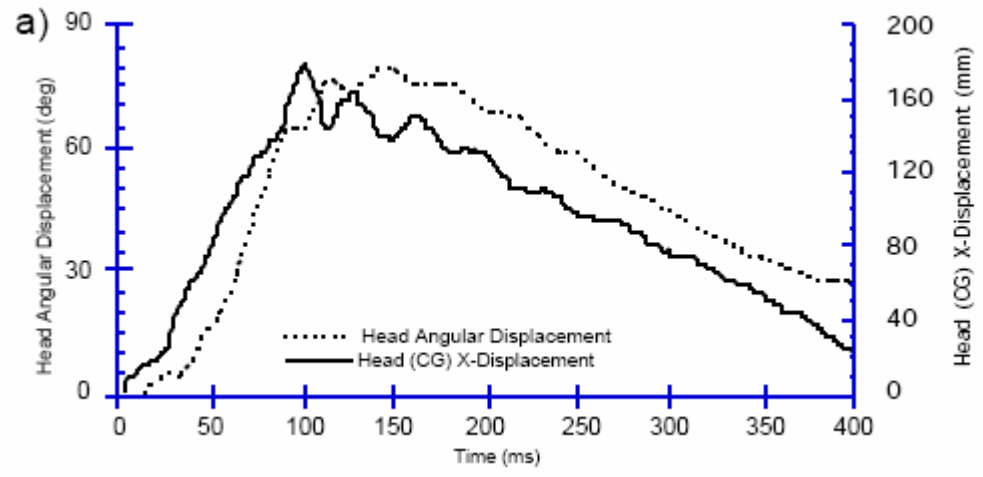

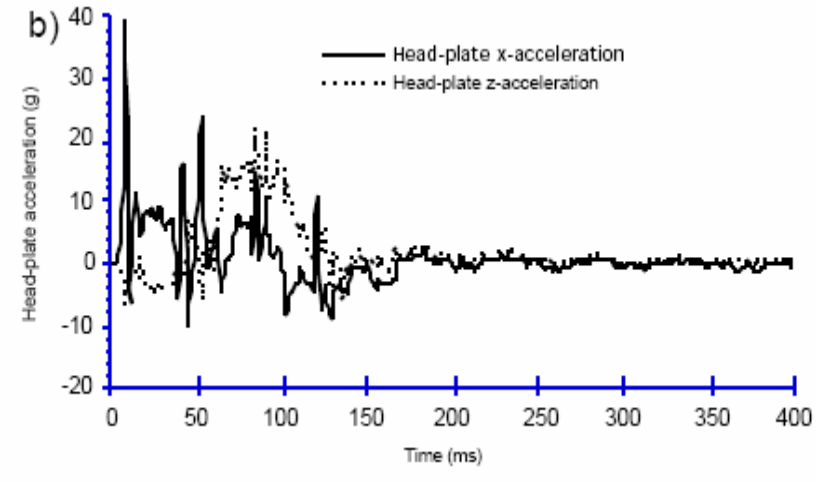

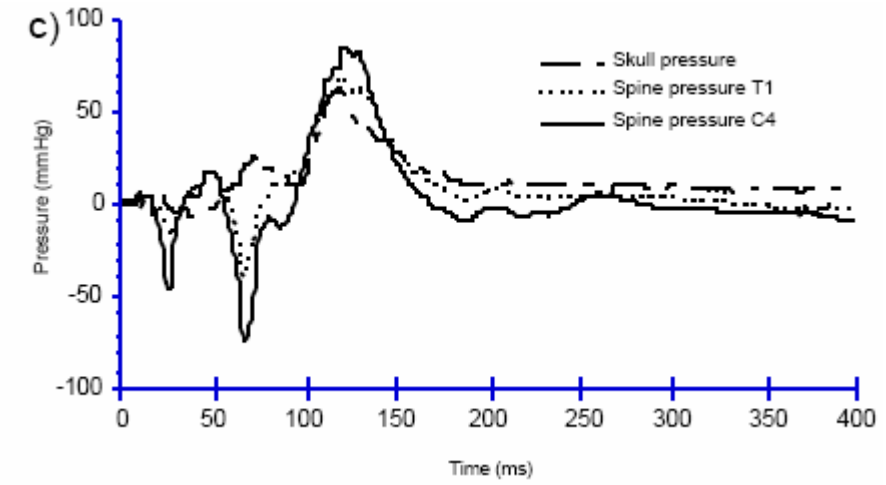

Figure 3.3 The results from one whiplash extension run with pressure measurements (pull force 600 N). a) Angular displacement and linear x-displacement of the head CG (centre of gravity) versus time. b)Accelerations of the head-plate versus time.c)The pressure versus timein the CNS at three levels: skull, C4, and T1.

The pulling force was 600 N, which is the same as that for the animals in the histopathological examination. The angular displacements and linear X-displacements of the head, and the readings from the three pressure transducers in the CNS are shown in the figure. The onset of the angular motion of the head is delayed about 30 ms compared to the linear X-displacement, indicating that the head moves mainly translationally during the first 30 ms. After about 60 ms the transformation from retraction motion to extension motion is completed and the head has reached its maximum rearward angular velocity (Figure 3.3a). The general pattern of the pressure pulse in the spinal canal is the same for all degrees of pulling force, but the duration of the pulse becomes shorter and its magnitude higher with increasing pulling force. The maximum angular head displacement occurs earlier and increases in magnitude with increasing pulling-force. The peak values for the pressure in the spinal canal at C4 level are about -70 mmHg and +85 mmHg (-9.3 kPa and +11.3 kPa) in this test. The general pattern of the pressure pulse at C4 level in the spinal canal is the same for all degrees of pulling force but

the pulse becomes shorter in duration and higher in magnitude with increased pulling force (Figure 2.4). Pressure peak values of down to -110 mmHg (-14.6 kPa) and up to +145 mmHg (+19.3 kPa) relative to the mean pressure at rest were measured

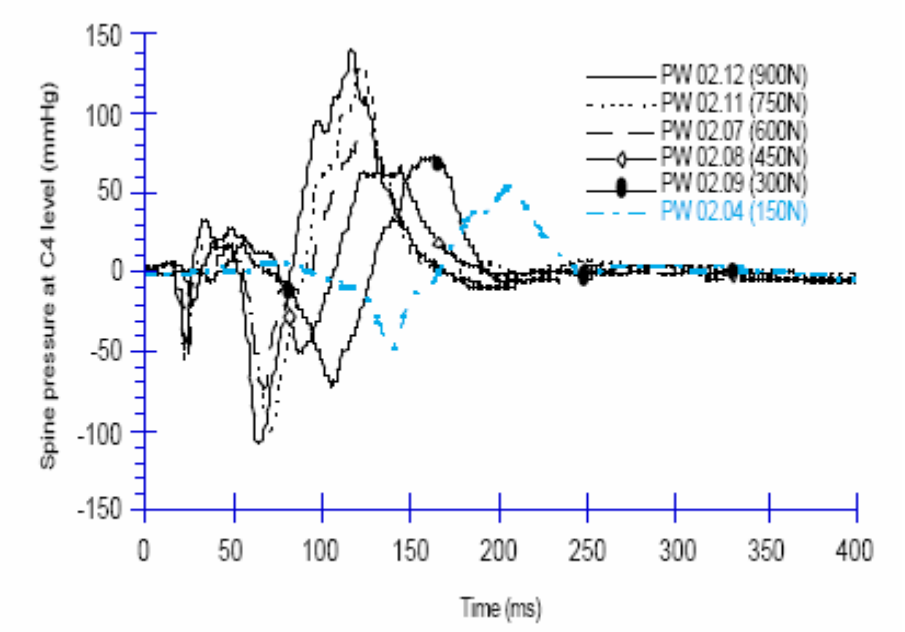

Figure 3.4 The pressure versus time in the spinal canal C4 level in a pig for various pulling forces.

A comparison of the pressure readings in the spinal canal at C4 level between a test without a head restraint and a test with a head restraint positioned 100 mm behind the head are shown in Figure 3.5. The pressure pulse is drastically reduced after head to head restraint contact at about 60 ms in the test showed in figure 2.5. With a 130 mm head restraint gap the contact would occur at about 80 ms, which means that the deep pressure dip at about 70 ms would not be avoided.

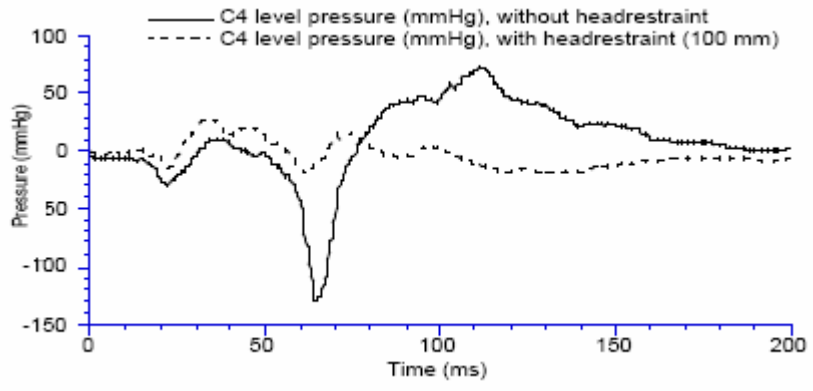

Figure 3.5 The pressure inside the spinal canal at the C4 level, with and with out head-restraint, during swift extension motion at pull force of 600N.

The macroscopical inspection of the nervous tissue from the 8 and 4 pigs revealed no abnormalities. There were no bleedings, fractures of vertebral structures or ruptures of ligaments. Fluorescence microscopic examination disclosed that satellite cells and nerve cells in the spinal ganglia contained red fluorescent material, indicating EBA leakage of the protein-dye complex and thus membrane dysfunction. These findings were most obvious at the C6 - C8 levels and diminished in both cranial and caudal direction. There were no signs of EBA leakage into the satellite cells or the nerve cells in the spinal ganglia from the sham-exposed animals.

In the tests with a head restraint in place, there was no sign of EBA leakage at a 100 mm head restraint gap, but for tests with 130 mm head-restraint gap, the frequency of leakage was the same as in the animals where no head restraint was used (Boström et al., 1996). Static loading of the cervical spine under loading conditions resembling those caused by a posterior pull force of 600 N did not result in any pressure gradients or nerve cell membrane dysfunction (Boström et al., 1996).

3.2.3 Discussion of the injury mechanism

A key finding for the group of animals used in the histopathological examination was the observation that the spinal ganglia from whiplash-exposed animals showed an increased frequency of EBA-stained nerve cells as compared to the sham-exposed controls. Further, the uptake of EBA-complex within the nerve cell cytoplasm and nucleus was distinct and striking in the whiplash-exposed animals in contrast to the controls.

It is tempting to presume that the pressure gradients induced during the whiplash extension motion (Figure 3.3) constitute an important factor in the pathogenesis of the observed change. To verify the relationship between the pressure gradients and the observed change, an experimental set-up would be needed in which a stationary animal is exposed to pressure gradients of the same type as in this whiplash experiments. Olmarker et al. (1989), using a different loading condition, demonstrated that nerve roots can be damaged by pressures of less than 50 mm Hg, particularly when the onset rate is high. The loading conditions in their study were, however, somewhat different to those of the Svensson's study.

Crushing or transaction of a peripheral nerve, e.g. the sciatic nerve, results in reactive changes in corresponding spinal ganglia nerve cells (Sunderland, 1991) with an initial loss and subsequent restoration of their afferent input (Woolf et al., 1992). Adaptive as well as aberrant patterns of synaptic connections are established in the deeper laminae in the dorsal horn of the spinal cord concomitant with the regeneration of the injured peripheral nerve. Tentatively, the whiplash-related changes observed in the spinal ganglion neurones could be sufficient to cause similar loss and rebuilding of the afferent synaptic connections within the laminae in the posterior horn of the spinal cord. That could contribute to the exacerbated clinical symptoms reported by patients even weeks post whiplash injury. This working hypothesis, however, requires further investigation.

Symptoms similar to those incurred during rear-end collisions also occur in patients that have been involved in frontal impacts (Hildingsson, 1991; Larder et al., 1985; Maimaris et al., 1988) though the relative injury risk appears to be smaller in the latter circumstance (Temming and Zobel, 1998). The lower risk in frontal impacts could possibly be explained by the fact that car occupants in frontal collisions usually are aware of the impending impact and brace their neck muscles. This will in turn mitigate the relative motion between the head and the torso thereby reducing the transient pressure gradients in the spinal canal. The posterior neck muscles that resist forward head motion are also stronger compared to the anterior neck muscles and this will further increase the difference in injury risk between frontal and rear-end collisions. Pressure measurements in the CNS during swift experimental flexion motion of the neck revealed only negative pressures, but these were of similar magnitudes as in the extension motion experiments (Svensson et al., 1993). The positive histopathological findings from experimental swift flexion motion indicate that the negative portion of the pressure readings corresponds to the occurrence of nerve cell membrane dysfunction.

The data presented in Figure 3.3 clearly indicates that pressure pulses occur in the pig during this type of motion. Such pressures are not likely to be induced by other mechanisms or to be due to a measurement artefact (Svensson et al., 1993).

In the neck-extension trauma experiments, the negative part of the pressure readings was avoided only when the head restraint was at the closest distance, 100 mm behind the head. Only at this narrow head-restraint gap were the injuries to the spinal ganglia avoided. This is another indication that the negative part of the pressure readings is responsible for the nerve-cell membrane dysfunction. The findings also indicate that a head restraint, in order to be effective, must interact with the head motion early on, before the point of maximum neck retraction has been reached.

The test set-up for the animal experiments offered a good reproducibility of the head neck motion between the different pigs in the critical interval from 0 ms until 150 ms. The reproducibility of the pressure pulses in the CNS between the different animals in the study is acceptable. The repeatability when the same animal is used under identical conditions is also acceptable. It was difficult to control the exact initial angular position of the animals head in the test set-up of this study. This may explain the spread in the pressure measurement results between identical repeated test runs. The fact that the animals' neck structures may have been affected by each whiplash extension exposure and thus gradually changed their mechanical properties is another possible cause of spread in the results.

In the experiments, the shape of the pig spine altered during the simulated whiplash extension motion in a way similar to that seen in experiments with the RID-neck (Svensson and Lövsund, 1992). At the start time the neck is straight (Figure 1.7 a) and during the first phase (Phase 1) of the motion the head is moving rearwards relative to the torso without any angular motion which means that the spine is formed into an "s-shape" (Figure. 1.7b). Thus the upper cervical spine is undergoing a flexion motion and the lower cervical spine is undergoing an extension motion. This phase resembles the time period 0 ms to about 100 ms in (Figure 3.6) where the pressure curves show a small pressure rise at the C4 level below which the spinal

canal becomes shorter and a pressure decrease at C1 where the spinal canal becomes longer.

At the end of Phase 1 the linear rearward motion of the head is abruptly decelerated at the same time as the head starts rotating backwards. This is explained by the fact that the upper cervical spine reaches its limit for maximum flexion while the lower cervical spine reaches the limit for full extension. In the next phase (Phase 2) the angular head motion is accelerated while the upper cervical spine goes from full flexion into extension and at the same time the lower cervical spine goes from full extension to a less extended posture. This phase resembles the time period 100-150 ms in Figure 2.6. During this period there is a clear dip in the C4 pressure since the lower cervical spinal canal is lengthening from its initially fully compressed position. The C1 curve also displays a small pressure dip although the spinal canal is shortening at this level. This might be explained by the fact that the effect of the volume expansion in the lower cervical spine dominates the compression of the upper cervical spine and superimposes on the pressure at C1 level. In the last sequence (Phase 3 in Figure 1.7), the whole cervical spine goes into full extension and the motion stops and turns. During this phase the spinal canal shortens and a clear pressure peak is seen in Figure 3.6

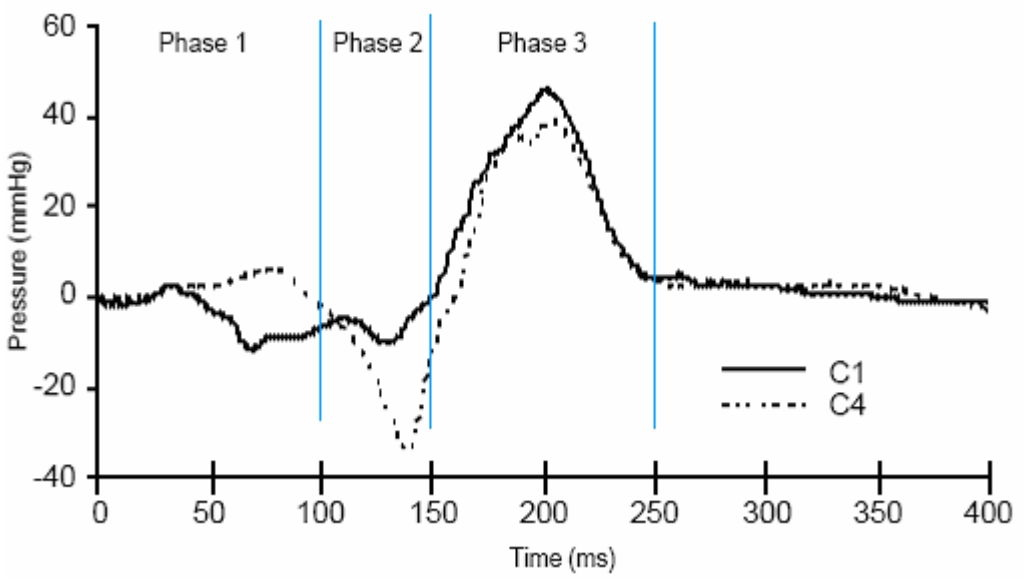

Figure 3.6 Average pressures of six pigs at C4 and C1 level versus time.

Following this extension motion, the whole cervical spine returns towards its initial posture by means of the elastic energy that is stored in the neck structures at the fully extended posture. It should be emphasised that there are no clear and exact borders between the different phases described above. The upper thoracic vertebrae probably follow the motion of the lower cervical vertebrae during all the five phases though they have a more restricted range of motion than the cervical vertebrae have.

There is a time-history correlation between the head-neck motion and the pressure profiles at the three different pressure transducers. This clearly indicates that the

pressure pulses measured in this study during extension and flexion motions of the neck are caused by the hydro-dynamic effects that result from the change in inner volume in the spinal canal according to Aldman's (1986) hypothesis.

Pressure gradients could also arise in the CNS due to the accelerations of the head and the individual segments of the neck during the whiplash extension motion. This pressure effect though, would give rise to pressures that are proportional to the acceleration of the individual body segment. Since this type of correlation was not found in the pressure measurements of this study the acceleration of the different body segments probably only contributed mildly to the pressures measured.

The soft tissue of the neck is virtually incompressible and has viscous properties. As a result of the swift deformation of the tissue during a whiplash extension motion, pressure changes inside the tissue can thus be expected to occur. Since the spinal canal is situated close to the centre of the neck where these soft tissue deformations are small, this soft tissue deformation is probably not an important factor in this context.

The pressure in the CNS when the animal is at rest is independent of the posture in the sagittal plane of the head and neck. This was shown in a pilot study (Svensson et al., 1989) where the pressure inside the skull and in the spinal canal at the upper thoracic spine was monitored during extension-flexion motions of the neck done by hand.

A typical mean level of the CSF pressure in a dog would be in the range 5-15 mmHg (0.7-2.0 kPa), (Löfgren et al., 1973) and it was assumed to be of the same order of magnitude in the pig. The magnitudes of the pressures measured in the CNS reached about 150 mmHg (20 kPa) which is about 10 times higher than the normal pressure.

The results from the pressure measurements indicate that the pressure gradients generated during the simulated whiplash extension motions are of greater magnitude across the inter-vertebral foramina than along the spinal canal. The pressures had the largest values in the lower half of the cervical spine. This correlates with the findings of the histopathological examination, where tissue damage was found in the spinal ganglia that are situated in the inter-vertebral foramina, and the injuries to the ganglia were most severe at the lower half of the cervical spine.

The injuries to the cervical spinal ganglia are also corroborated by many of the known whiplash extension symptoms. Pain and sensory disturbances to the parts of the body that are associated with the cervical dorsal nerve-roots are common and vision disorders could be caused by injury to the upper cervical spinal ganglia (Hildingsson et al., 1991).

The EBA complex must be present in the intercellular space to enable cell membrane dysfunction to be displayed curing histopatological examination. Except for the ganglia, the EBA did not enter the intercellular space surrounding the nerve cells in the brain, spinal cord and nerve roots since the blood-brain barrier remained intact.

The injuries to the spinal ganglia found in this study are probably caused by mechanical stresses and strains to the ganglia and surrounding tissues. These

mechanical loads to the ganglia could be caused by deformation of the intervertebral foramina in turn caused by motions between adjacent vertebrae exceeding the normal range of motion. The deformations of the intervertebral foramina could be of compressive, tensile or shearing type. The loads to the ganglia could also be caused by the pressure gradients between the inside and outside of the spinal canal according to the hypothesis by Aldmans (1986). The fact that no signs of injury to vertebrae, discs or ligaments could be detected during the excision of the CNS specimens indicates that displacements between adjacent vertebrae only marginally exceeded the normal range of motion. This in turn also supports the hypothesis by Aldmans. It is also possible that the injuries to the ganglia were caused by a combination of pressure pulse and the motion and mechanical loading of the cervical vertebrae column.

If the typical symptoms found in patients whit AIS 1 neck injuries are caused by the pressure phenomena observed in the pig experiments, this could in turn indicate that the negative portion of the pressure may cause the injuries to the spinal ganglia.

The pressure magnitudes measured in the CNS are relatively moderated (-100 to +150mmHg) and the question is whether they could actually be capable of causing damage to the spinal ganglia. Surely, the ganglia should be able to withstand much higher isotropic pressure increases, but under pressure loading conditions, other than isotropic, different results could be expected.

3.3 Experiments with Post Mortem Human Subject

Arno Eichberger and Mario Darok (University of technology Graz, Austria, 1999) conduced pressure measurements in the spinal canal in post mortem humans subjects (PMHS) during rear end impact. The aim of that study was to validate the pressure effect theory on human beings and to correlate the Neck Injury Criterion to pressure in the spinal canal. Sled experiments were performed using a test setup similar to real rear-end collisions

3.3.1 Methodology and test set conditions

The tests were setup to that realistic condition for rear car crashes were replicated as good as possible. Impact velocities of the sled of approximately 9 and 15 km/h were chosen. Taken into account the rebound velocity of the sled, this resulted into velocity changes of the sled of approximately 10 and 16 km/h. Basis of the sled pulses were recordings of crashes at these velocity changes. Velocity change, acceleration level and head restraint position were varied in order to study their effect on the pressure in the spinal column.

A total number of 28 tests wee performed and 5 subjects. Only four were equipped with pressure transducers. Age was between 30 and 87 years (mean 62 years). In all subjects a relevant trauma prior to death could be excluded according to the case history.

Pressure measurements in the cerebrospinal fluid were performed using catheter-tip pressure transducers placed bubdurally in the spinal canal, similar to the tests in pigs performed by Svensson. Due to the difference in anatomy between pigs and humans,

a new technique for operating the transducers into the spinal canal had to be developed. The transducers were fixed to a metal wire in a given distance estimated from the length of the subject's neck (the upper transducer would be at the level of C1-C2 and the lower one at C6-C7). The metal wire with the fixed transducers on it, was then placed through the small opening in the cranium, through the dura and the brain into the spinal canal. This special technique for positioning the pressure transducers was used to avoid any damage to the soft tissues of the neck, which probably would cause an unwanted alteration in neck mobility. Position of the pressure transducers was revealed during autopsy, which was performed in all subjects after the test series.

Due to the equipment available for these experiments, the vascular system of the subjects could not be pressurized. In addition, it was not possible to take X-rays. The subjects were instrumented with two triaxial accelerometers on the head and on the chest; one biaxial accelerometer at the height of T1.

3.3.2 Results and discussion

Positioning of the pressure transducers was successful in only one subject. The upper transducer was at the level of C2 and the lower one at C7, both of them inside the CSF space. In one subject, the upper transducer was situated inside the cerebellum, the lover one at C1. In two subjects the pressure transducers were lying at C1 and at the level of C6. In one subject (very old woman), the pressure curves differ significantly from the other subject curves. The autopsy revealed that there was almost no CSF in the spinal canal and the in the skull, therefore the results of the pressure measurement are not valid for this subject.

During autopsy, each subject was checked for lesions of the neck. A lesion was only diagnosed in one subject, which consisted of a rupture of the ligamentum longitudinal anterior between C5 and C6. All of the other subjects showed no signs of neck lesions. Of course, rupture of small vessels, leading to local haemorrhage when blood circulation is active, or damage to nerve fibres could not be detected in autopsy. Results of pressure measurement of the CSF in the subject with the pressure transducer in position C2 and C7 are illustrated in Figure 3.7

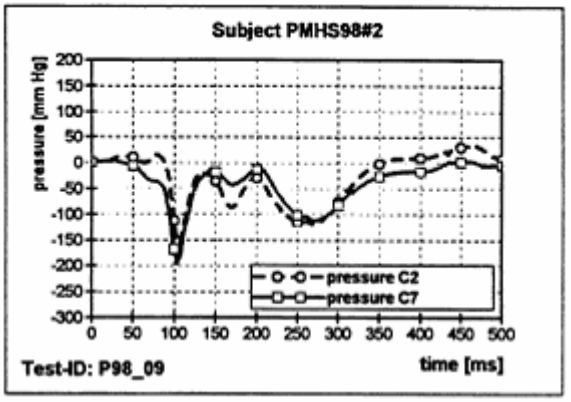

Figure 3.7 Pressure of CSF in one subject at level of C2 and C7 in function of time during rear impact.

When comparing the pressure time histories of the PMHS tests (Figure 3.7) to results of the pig experiments (Figure 3.6) a similar pattern can be observed. Within the spinal canal, a pressure minimum occurs at the maximum retraction phase of the cervical spine after approximately 100ms. In tests where transducers were positioned in the skull, positive pressure amplitudes could be found in PMHS tests as well as in pig experiments. The magnitude of negative pressure amplitudes in pig experiments have been found between 20 and 90 mmHg in the PMHS tests between 0 and 220 mmHg. This difference in the magnitude could have two reasons: on the one hand differences in anatomy of pigs and humans and on the other hand differences in the experimental setup and test conditions. One disadvantage of the pigs study was that the subjects were not human and therefore anatomic differences should result in different results. Another disadvantage was that the motion was not a real head-neck motion during a rear-end collision but a simulated swift head motion induced by a pulling force on the head.

The absence of normal arterial blood pressure is certainly one of the main limitations of this study. The pig experiments have been conducted with living animals and it is not possible to comment on the influence of blood and intra cranial pressure to the pressure effects of CSF during rear impact motion. This influence could be of interest in future research. Another limitation was the lack of X-Rays. By taking images before the tests, it would be possible to see the location of the transducers and correct them.

Four human subjects were instrumented with accelerometers and pressure transducers in the spinal canal. In contrast to the pig experiments, a test setup was chosen that reproduced realistic conditions for a rear impact car crash. Conditions from accident investigations and statistics were used for this purpose.

Due to the fact that the autopsy could not investigate damage to nerve cells, as it was demonstrated by Ortengren *et al* (1996), no clear answer can be given if and which level of pressure amplitudes can induce damage to the nerve cells of spinal ganglions. First indications for threshold levels for soft tissue neck injuries concerning the NIC are given by Bostrom *et al.* (1996), Eichberger *et al*, (1998) and Wheeler *et al.* (1998).

3.4 FEM of the cervical spine for pressure phenomena

A theoretical analysis has been undertaken in order to investigate the pressure and flow pulse emerging in a cervical fluid compartment under conditions representing rear-end impacts with a ?v of 15 km/h. Using the finite element method, a three-dimensional model of the cervical spine was developed in the Institute of Biomedical Engineering (ETH) Zurich. The model consists of eight vertebrae (C1-T1), the intervertebral discs, the intervertebral joints, all the major ligaments, most of the neck muscles and the head. Additionally, a typical venous blood vessel was included. To determine the pressure behaviour inside the blood vessel, fluid-structure interaction was taken into account.

3.4.1 Methodology

K. Schmitt, M. Muser, P. Niederer and F. Walz developed a theoretical model which allows to analyse the pressure phenomena occurring during the extension-flexion motion of the neck which is induced by a rear impact. For this purpose, the kinematics of the solid neck structures, obtained from a motion simulation have to be combined with a fluid model. Of particular interest thereby is the fluid-solid interaction developing during the critical S-shape of the cervical spine.

A theoretical approach using the Final Element (FE) technique was developed which allows analyze the flow of blood inside a characteristic vessel undergoing the critical S-shape deformation. The FE model in this study was a complex model of the cervical spine which can for practical purpose was thought of consisting of two separate parts: a solid model and a fluid model. The basis of the solid model was a three dimensional FE model of the cervical spine and the first thoracic vertebra developed previously (Yang et Al. 1998). The geometry of the model was derived from a man volunteer using MRI scan. Thus it exhibits a high anatomical accuracy, represents however an individual case. The volunteer (height: 1.74 m, weight: 75 kg) was chosen such as to replicate a 50^{th} percentile hybrid III dummy as closely as possible.

As shown in Figure 3.8 the model consists in eight vertebrae (CI – TI), the intervertebral discs, the intervertebral joints, all major ligaments and the head. Most of the neck muscle believed to be relevant in rear-end collisions were also included into the model. The muscle was implemented as bar elements using a hill-type formulation and thus take into account active and passive muscle characteristic.

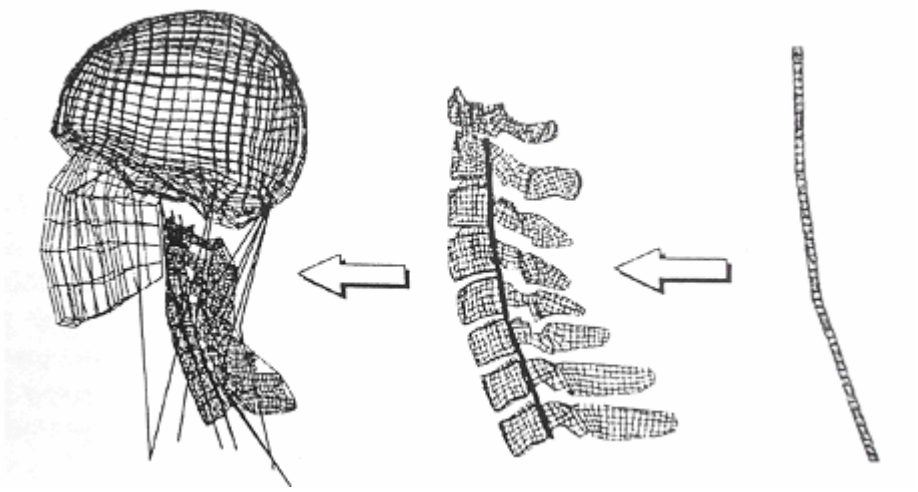

Figure 3.8 3D FE model of the cervical spine including a venous blood vessel situated in the spinal canal

In order to simulate curving of long extensor muscles around the vertebrae during neck bending some muscles (e.g. M. longus capitis) were modelled by chains of connected Hill-type bars. The intermediate nodes of these chains were attached to

the respective vertebrae. A reflex time of 50 ms for all muscles was used according to electomyography (EMG) measurements.

Additionally, the outer bounds of a fluid compartment situated inside the spinal canal was added to the model. Shell elements were used to model the wall of the fluid compartment whose dimension represent a typical blood vessel of the plexus venosus vertebralis with a diameter of 2,5 mm and a length of 118 mm. To connect the vessel to the spinal model, it was attached to the posterior side of the ligamentum longitudinale posterior. Thus, the vessel was deformed according to the ligament. For the 530 shell elements that were assumed to be elastic, homogenous, and isotropic, mechanical properties was chosen such as to represent a typical venous wall. Ring-shaped rigid body definitions were introduced to stabilize the vessel and to prevent the cross section from collapsing.

In order to take into account the fluid-structure interaction, the fluid-filled volume inside the venous blood vessel was modelled separately. The volume was automatically meshed by 5634 tetrahedral elements. An initial flow velocity of 0,2 m/s in vertical directions from cranial to caudal was assumed. The inlet velocity profile was flat (plug flow) and steady. The fluid representing blood was assumed incompressible, homogenous, and Newtonian. Materials parameters describing the fluid were taken to be 0,0035 kg/ms for the viscosity and 1050 kg/m^3 per density. For the entire calculation, laminar flow was assumed.

For the FE calculations the following procedure was used: prior to the coupled fluid-structure analysis a steady state solution for the fluid model was gained, i.e. , a CFD (computation fluid dynamic) calculation was performed without moving the fluid compartment. This step was included to ensure a fully developed and uniform flow field inside the vessel at the beginning of the fluid-structure interaction computation.

Then the CFD-CSD (computational structure dynamics) calculation was started and the solid model was subjected to a crash pulse, resulting in the deformation of the model, and thus allowing to record the deformation of the fluid compartment. In a next step, this deformation was imposed to the fluid model and the interaction with the fluid herein was calculated. Finally, the reaction of the fluid in terms of load of the vessel walls was taken as boundary conditions for the solid model.

The crash pulse used in the deformation process represents a pulse with a peak acceleration of 4 G. the translation crash pulse leading to a linear velocity of approximately 15 km/h was applied on the TI vertebra in x-direction.

3.4.2 Results and discussion

To analyse the pressure inside the blood vessel, the velocity flow fields and the shear stress on the vessel wall were determined as functions of time. The pressure values reported represent the results at the centre of the cross section. Due to the continuous remeshing it was not possible to ensure that for all time steps suitable nodes were exactly at the mid cross section, in such cases time history points as close as possible to it were taken instead. Since the pressure exhibits small variations over the cross

sections only in case of a primarily one-dimensional flow, this aspect is of minor significance. The pressure was analysed at three different levels of the cervical spine: at C2, C4 and C6 level (see Figure 3.8). For both the C4 and C6 level a significant drop of the amplitude followed by an increase was observed in the interval calculated. The negative peak of the pressure coincided with the maximal S-shape deformation of the spine model. For C4 level an amplitude of 87mmHg (=11571 kPa) was obtained, while for C6 level the amplitude was about 35% smaller. At C2 level no characteristic pressure peak was determined.

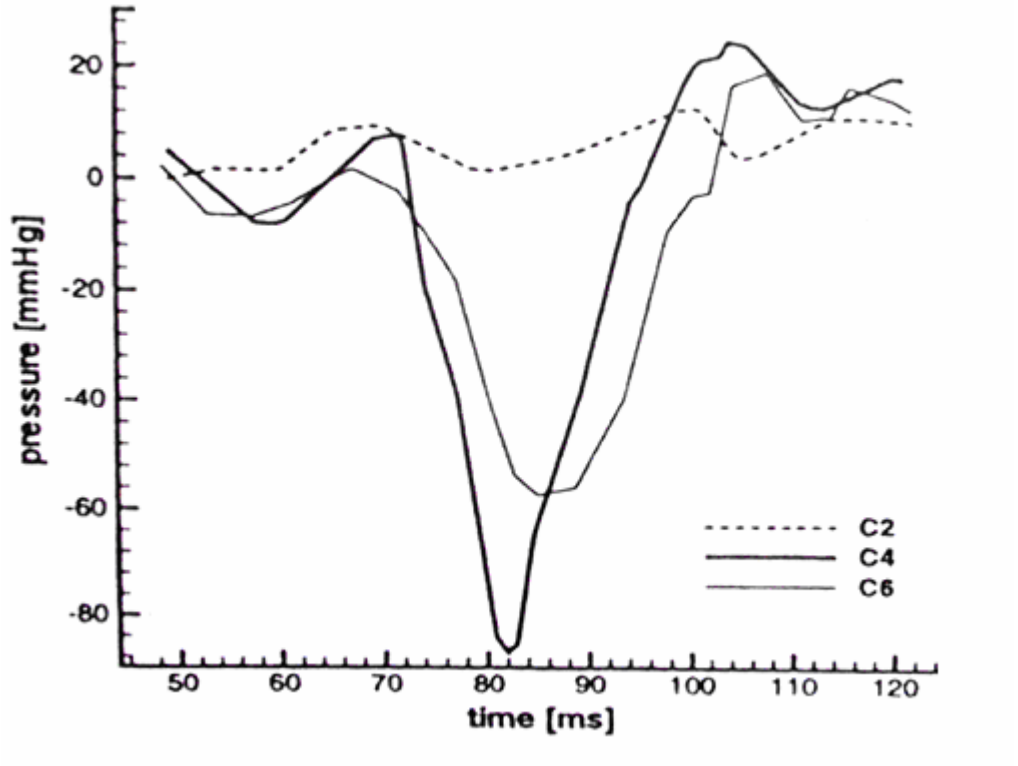

Figure 3.9 Pressure computed at C2, C4 and C6 level. The calculation of the fluid-structure interaction was started at time =50ms of the total FE simulation.

Furthermore, the flow pattern within the vessel was analysed. As initial condition, a plug profile was used. This type of velocity profile prevailed in the beginning of the deformation phase. However as the deformation reaches the maximum S-shape a change in the flow direction occurring at the same time as the peak of the pressure amplitude can be seen in the part of the vessel cranial to C4 level. The shear stress on the vessel wall was also computed. Maximal values in order of 0,76 N/m2 have been calculated which were mainly situated at the anterior side of the vessel.

The pressure amplitude determined varied for different levels: at C4 and C6 level a distinct drop followed by an increase was calculated. This result is qualitatively in agreement with the measurements by Svensson et Al (1993) and those by Eicchberger et Al (2000). The magnitude computed is slightly lower compared to the experimental results given, though closer to the animal experiments. Considering the fact that the fluid is incompressible, those differences can be attributed to differences

in the anatomy modelled and thus are due to the details of the shape changes of the fluid volume during deformation. Furthermore, also the experiments, in particular those performed with the PMHS, exhibit a large variability in the measurements. Because the anatomical data are not available, the FE model could not be designed to simulate one of experiments with which it is compared. The essentially one-dimension flow patter has also to be considered a simplification of the highly tortuous venous plexus. Thus, especially the time at which the S-shape developed is different. These results as well in a different timing for the pressure drop as can be seen from Figure 3.10.

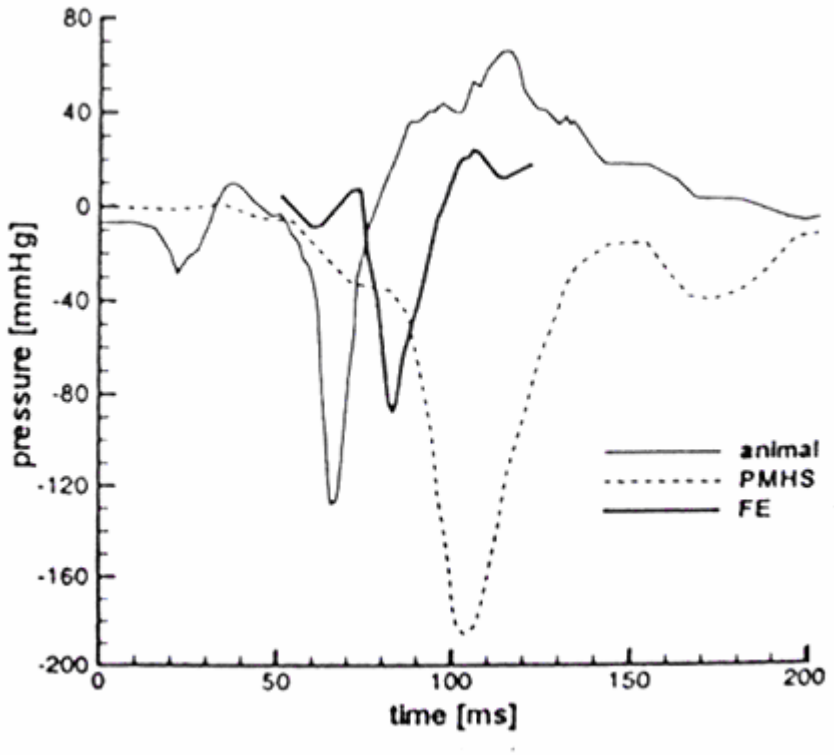

Figure 3.10 Comparison at C4 level of the pressure computed with results from pig experiments (600 N pull force) and from PMHS experiments.

For the pressure results at C2 level, no characteristic pressure aberration was found. The amplitude was relatively small; a fact that can also be found in the experimental results..

3.5 Conclusions

In conclusion the Aldman-hypothesis (Aldman, 1986) regarding transient pressure gradient during swift neck-bending motion is supported by the pressure recordings during experimental whiplash motion. Spinal ganglion nerve-cell membrane dysfunction was revealed after experimental whiplash trauma. These findings could very well explain many of the symptoms that are connected to whiplash associated disorders and that are related to afferent nerves passing through the cervical spinal ganglia. It seems possible that the negative pressure readings observed during experimental whiplash trauma could be the cause of the ganglion injuries. Should

this assumption turn out to be correct, the pressure gradient injury mechanism could explain the similarity in symptoms for different crash directions as well as the reason for the poor effectiveness of current head restraints that are usually placed too far behind the head to prevent the neck from reaching maximum retraction.

In following chapter, in order to reproduce directly in a dummy the cause of injury during rear end impact, basing on the hypothesis above, the design of a new neck prototype is updated.

A future possible employment of this new neck for dummy will be in evaluating the protective performance of car seat-systems in rear-end collisions at low impact-velocities.

4 Neck dummy to simulate pressure phenomena

4.1 Previous neck prototype

4.1.1 Components and design

L. Olofsson and I. Persson (2001) developed a first neck prototype and after C. Keiser (2002) afforded a little improvement to the design. The base was an extent of a BioRID-neck, including the seven cervical vertebrae and the basement to fix it on a table. The first vertebra is the connecting piece between the dummy head and the neck. The cables, which were used in the original BioRID-neck have been removed and instead of the foam blocs between the vertebrae, silicone discs were used to give the neck its stability. These silicone discs were wedge-shaped, so the neck will assume a slight lordosis.

To build the spinal canal, a hole was drilled with diameter 20mm vertically through the centres of the faces on the posterior side of the vertebrae C2 to C6 and also through the centre of all silicone discs. The discs were fixed with glue between the vertebrae; the canal was tight and it leads along the whole neck. As the discs were soft, they could be compressed and stretched. Therefore, the volume change inside the spinal canal during flexion-extension motion could be simulated. To represent the spinal cord, which can be considered as a elastic semi-liquid substance, a silicon tube with diameter 15 mm was leading through the centre of the canal. It consisted of the same material of the discs and it was able to move freely inside the spinal canal. The tube was fixed on one end at the first vertebra and on the other at the basement. On the right side of the neck, horizontal, lateral holes were drilled in the vertebrae C2 to C6 leading into the canal. Some plastic tubes with inner diameter 2 mm, which represent the veins connecting internal with external venous plexus, were plugged in those holes (see Figure 4.1).

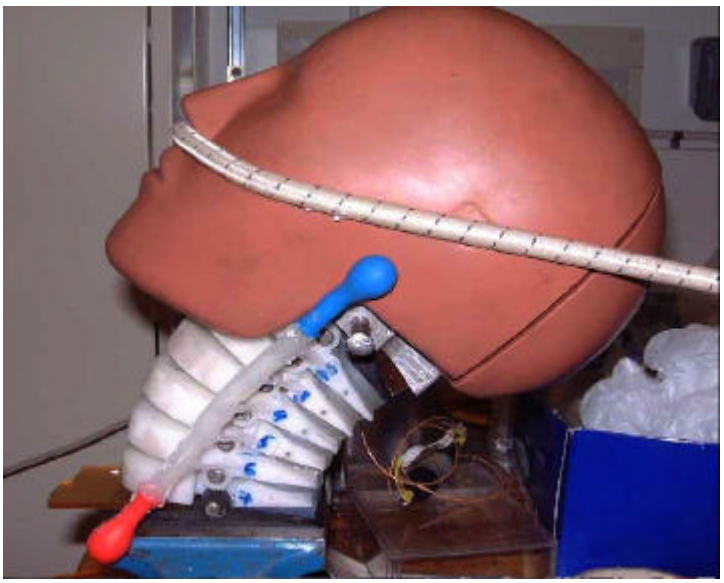

Figure 4.1 Previous neck prototype in fully extended position during the Olofsson's experiment.

To simulate the external venous plexus a silicone tube with inner diameter 6 mm, in which all the connection tubes led, was used. On both end of the tube there was a balloon fixed. These balloons cushion the volume changes of the spinal canal during the swift extension motion of the spine.

The system was filled with tap water representing the vein blood inside the spinal canal and on the left side of the vertebra C2 was drilled a hole used as inlet for the fluid and plugged during the experiments.

C. Keiser used the same system which had been used in the previous prototype, but the dimension of the holes drilled in the transversal plane of the vertebrae was changed (diameter 8mm). Inside these holes there was a thread. Outlet screws with different sizes of drilled centre holes can be screwed in. The external venous plexus was represented by a plastic tube with inner diameter 17mm and the upper end was plugged; on the bottom there was a balloon fixed, which serves as water reservoir. Along the tube there were five metallic outlets, on which the rubber tube could be connected.

4.1.2 Experiment and results

A standard Hybrid III head was used for the experiments. The neck was clamped on a table. To simulate the traumatic neck motion a pre-stressed rubber cord was spanned around the head to the posterior side. The head was turned by hand (manually)to its original position and then disengaged.

During the experiment, the pressure inside the spinal canal was measured as a function of time (see Figure 4.2)

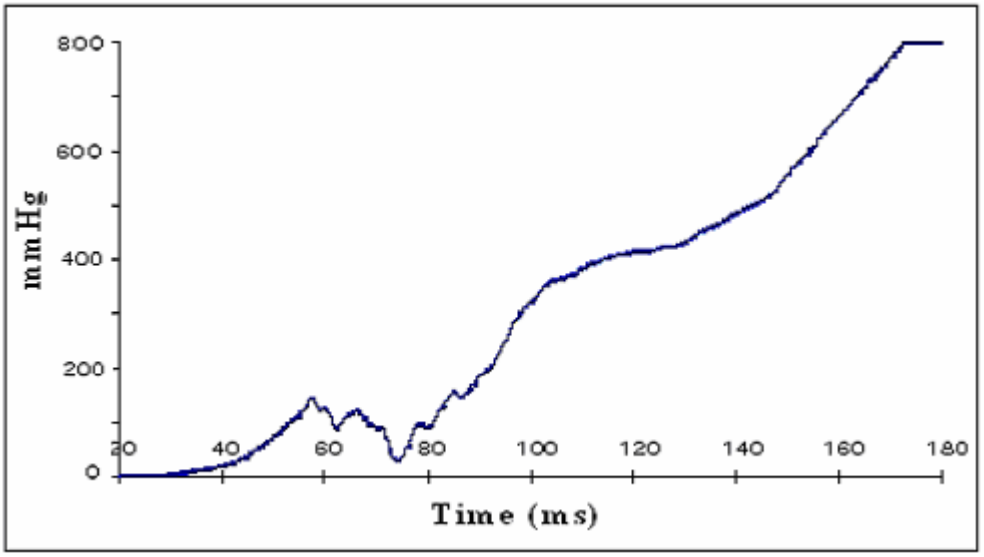

Figure 4.2 Pressure curve obtained in tests with the previous neck prototype (Olofsson and Persson, 2001)

The pressure curve shows a mild similarity to the pressure curve obtained in the animal experiment. The most important point, which is meant to be the reason of tissue injury, the pressure dip in phase 2, is recognisable. However, the pressure inside the spinal canal rises continually and is always positive. This means that no fast pressure equalisation inside the spinal canal takes place.

The pressure curves obtained in the test led by Keiser are shown in Figure 4.3. They start with a small negative pressure dip. The curve of the C6 level shows a very sharp peak at about 100 ms. The curve of C4 shows a non-negative pressure dip at about 135 ms, which can not be detected at level C2 and C6. At 160 ms all the curves have a high peak that was out of range for C2.

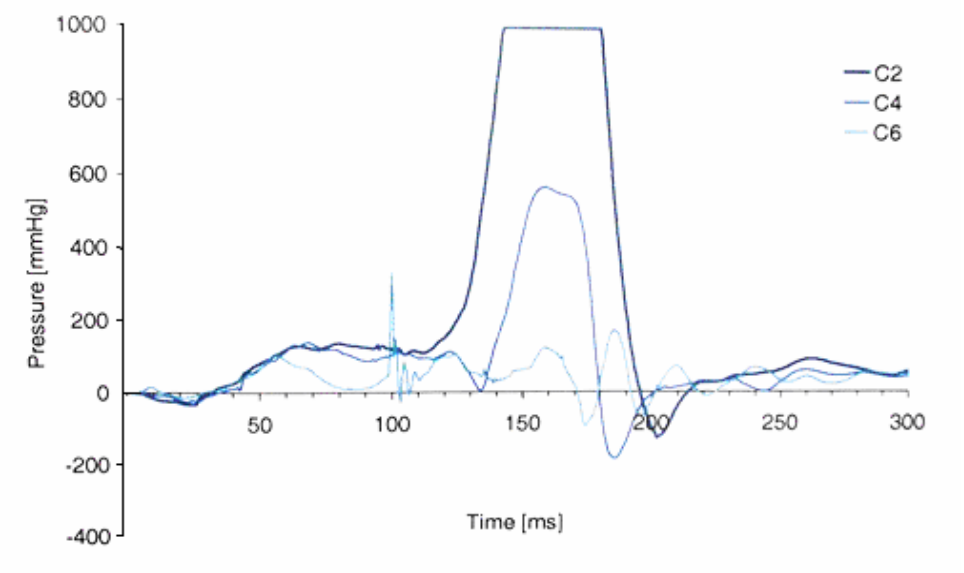

Figure 4.3 Pressure curves at C2, C4 and C6 level obtained in test executed by Keiser (2002)

After the pressure peak, significant pressure drops appear between ~170ms and ~200ms at all levels (Figure 4.3). Those drops can be explained by the fact, that the rubber cord keeps the neck in total extended position. However the discs have elastic deformation properties, hence the neck would tend to return forward in flexion motion. The flexion motion is however stopped by the rubber cord, which pulls the neck back in its fully extended position. Therefore, fast flow changes, which evoke the appearance of the negative pressures, may occur inside the spinal canal as a result of oscillations in the neck, head, rubber cord system.

4.1.3 Possible causes of failure

The same two-component silicone rubber was used for the discs and for the medulla cord. It was the CG 100 Silikongummi and it is a pourable, addition-curing that vulcanises at room temperature. This silicone turned out not to be suitable for this application as it is very difficult to glue to the acetal plastic. It got brittle after the use of the glue primer and the silicone discs survived only a few tests. The silicone

became stiff and brittle and the swift motion produced micro fractures in the discs that caused the loss of their watertighness.

The major pressure drop at level C4 obtained in these experiments at ~130ms is very small and not even negative. This can happen out for different reasons. The attach-point of the rubber cord was chosen 20 mm below the head CG (centre of gravity). This might not be enough considering the mass of the neck. Therefore, the head may have started its rotation immediately and the S-shape may not have developed. Besides, there may have remained some air bubbles in the water. However, as the silicone discs became brittle because of the glue, some air could have remained in the canal and more air could have entered through the leakages. The air bubbles expand during pressure decrease and therefore decrease the pressure dip. In case air entered the spinal canal in the early neck motion this could have caused the extensive pressure peak found at C4 and C2. The neck was in a very bad condition during the last measurement. It became very stiff by the lot of glue, which was used to mend the leakages. During the tests, the silicone discs ripped off the vertebrae at several levels of the neck and water was pouring out of the canal. This may be the reason for which there have been no significant phenomena in this pressure curve.

4.2 Different designing solutions for the new neck prototype

Several ideas about how to manufacture a monolithic spinal canal are presented in this section. The use of holed disks made of silicone glued in between the vertebrae was found as inadequate (Olofsson experiment). In fact, during the impact tests, the repeatability was low because the glue used to connect the silicone to the vertebra (acetal plastic) damaged the silicone and after few cycles micro fractures were created. These micro fractures made the water go out from the internal canal and modified the mechanical dumping properties of the disk. A constructive solution able to face the problems detected in the experiments of Olofsson is therefore investigated. Different possibilities to manufacture the intervertebral canal using a shaped pipe able to perform two main functions were analysed. These functions are:

- Containing the water and simulating the pressure of the blood and CSF within the medulla canal during the swift movements of flexion-extension.
- Simulating the resistance of the human neck through spring and dumping behaviour of the rubber pipe.

The main goal of this study is to investigate how to build a pipe flexible in axial direction but not in radial direction. In fact, it is necessary to reproduce the change of volume of the intervertebral canal, i.e. the length variation, when the neck changes its curvature. Moreover, in order to simulate the negative pressure observed in the spinal canal during the pig experiments, the pipe has not to collapse radially. Another task of this work is designing a system able to simulate the whole spinal canal and its bridges between the two plexi. Finally, the material of the pipe should be watertightness.

The pipe has to be curved in the neutral position of the neck, so eventual solutions using telescopical ones are not applicable.

In the following part of this section, different solutions for the canal are designed. For each solution, the advantages and the disadvantages about the functionality and manufacturability are briefly listed.

4.2.1 Pipe with external rubber rings

Description

In the cervical holed vertebrae, a flexible rubber pipe having the sagittal plane of the neck as symmetry plane, is installed. For each vertebra the pipe has radial connections. These connections link the internal volume of the pipe with an external volume and they represent the bridges existing between the two plexus. At its ends the pipe is fixed to the vertebrae. Rubber rings are located between two adjacent vertebrae around the pipe, having the springing and dumping functions during the swift movement of the vertebrae In Figure 4.4 is reported a drawing done by the software CAD 3D Solid Works.

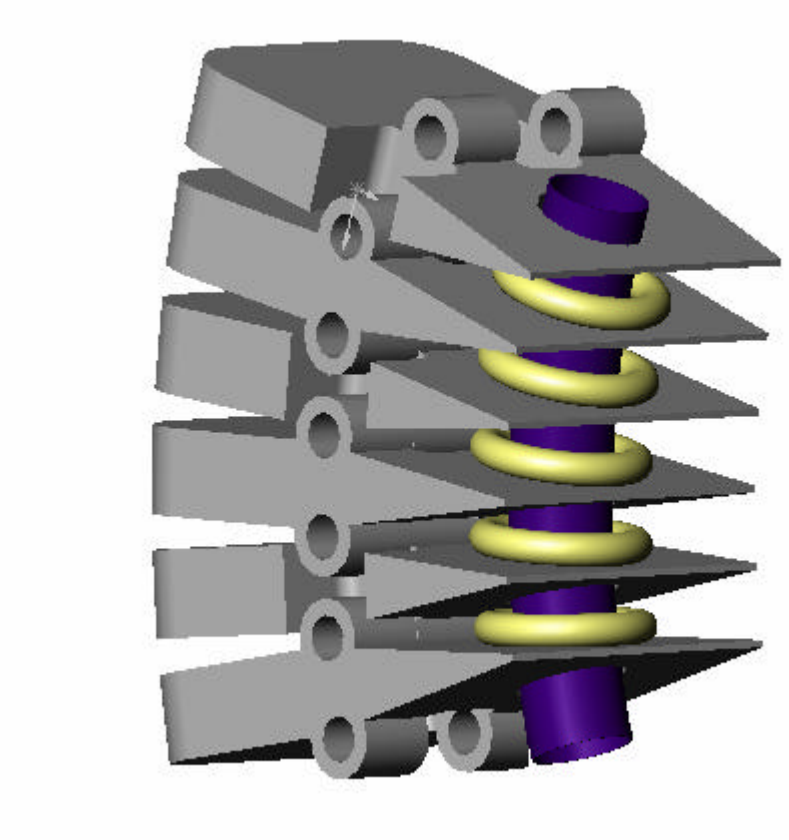

Figure 4.4 Perspective (oblique rear view) of the solution "pipe with external rubber rings"

Advantages

The pipe is simple to construct as long as a flexible straight one is used. Besides the pipe has not to be built inside the neck and it is eventually possible to adapt a commercial pipe for this application. In addition, the installation of the pipe through the holes of the vertebrae is easy, i.e. it is not necessary to cut the neck in two halves for positioning the pipe. It is possible to use different rubber rings between the vertebrae in order to obtain different stiffness among the vertebrae. Finally, the rubber rings are compressed by the vertebrae during the extension movement of the neck and their deformation gives a contribution to the reductions of internal volume of the pipe.

Disadvantages

Radial connections able to keep the waterproof capacity are difficult to be built. The movement between two adjacent vertebrae is not transmitted to the pipe, which presents a constant longitudinal deformation: this deformation is caused only by the relative rotation of the ending vertebrae, which are the only ones linked to the pipe, i.e. the pipe is not affected by the local relative movements of inner vertebrae. This last disadvantage makes the solution unacceptable.

4.2.2 "Vacuum pipe" solution

Description

A plastic pipe axially extendable and radially rigid is screwed on the sides of two adjacent vertebrae facing each other. The pipe has sagittal plane of the neck as symmetry plane. The system constituted by the pipes and the vertebrae holes forms a close volume (Figure 4.5). The Figure below shows the radial holes drilled inside the vertebrae in order to guarantee a contact of this inner volume with an external one.

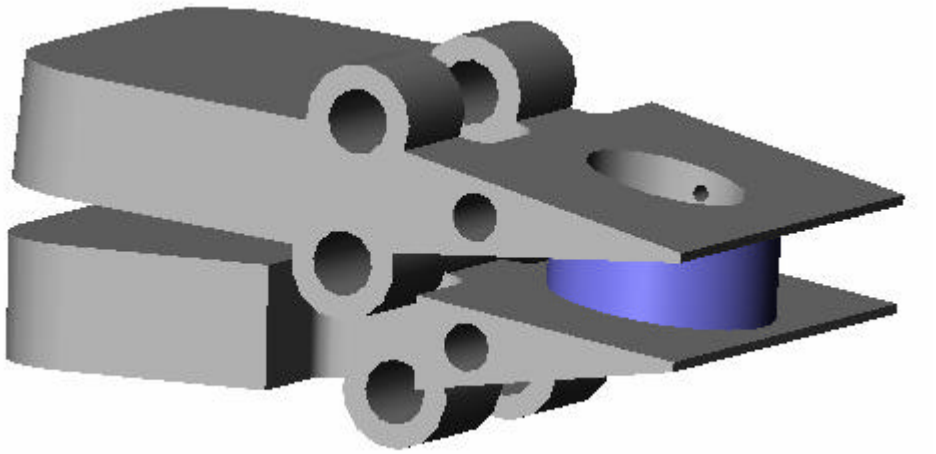

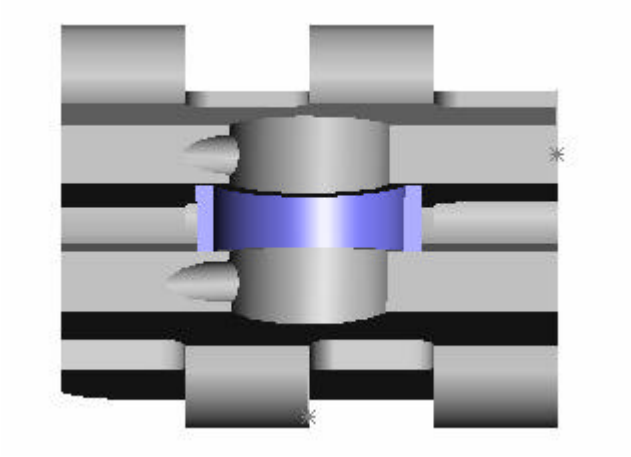

Figure 4.5 Perspective and rear view of the solution "Vacuum pipe" solution.

Advantages

With this solution, the movement of each vertebra contributes to the deformation of the pipe. That is a significant improvement in comparison with the first solution. In terms of the waterproof capacity of the structure, in this case the drawbacks of glue are avoided: the screw guarantees impermeability. The same can be said also for the inter-radial connections: the radial holes are drilled in those sections of the vertebra that are already part of the medullar canal, so no connection problem arises. Moreover, radial rigidity of the canal is guaranteed by the nature itself of the components. Finally it is not necessary to cut the neck in two halves for positioning the pipe.

Disadvantages

As a consequence of the small thickness of the vertebrae, the manufacturing of the screws ends up with affecting the resistance of the structure. Another problem is connected to the size of the intervertebral space: the screwing itself actually becomes a non trivial task. Considering those disadvantages together with the difficulties in finding a commercial plastic pipe that fit well with this problem, this solution too has been considered unacceptable.

4.2.3 Metal-ring pipe

Description

The rubber is moulded on a skeleton of opportunely designed metal rings. Each ring corresponds to a vertebra. The canal obtained is shown in the Figure 4.6, and is positioned inside the vertebral holes. Each ring presents two pins diametrically displaced whose edges protrude from the rubber. This particular design of the rings makes possible to fix the pipe to the vertebrae. Radial channels are obtained drilling one of the two pins.

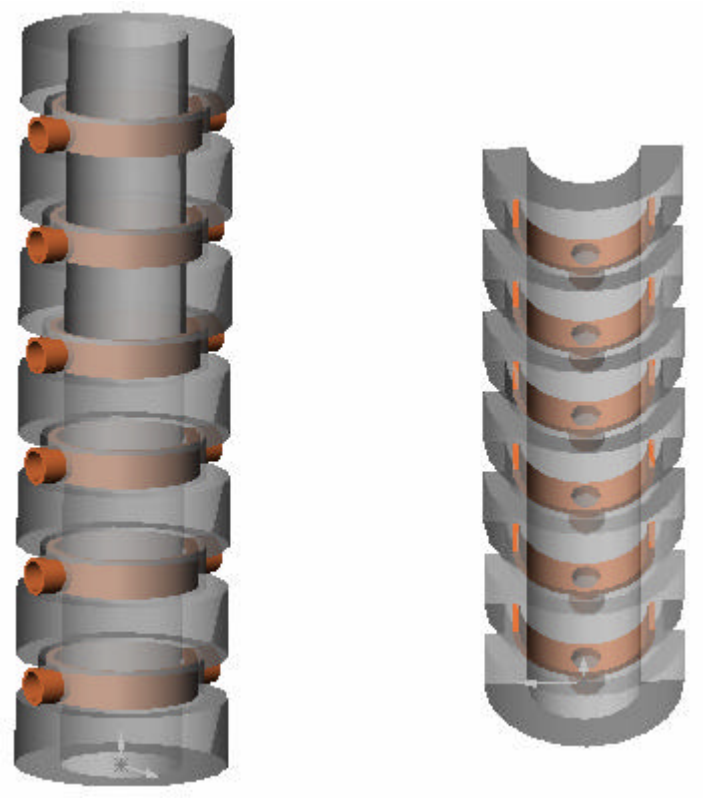

Figure 4.6 Lateral and section view of the rubber pipe with metal rings.

Advantages

Again with this solution the movement of each vertebra contributes to the deformation of the pipe. The manufacture of the mould is not complex. Waterproof capacity between the connections and the inner volume of the tube is easy to achieve. The rings provide also a good radial stability.

Disadvantages

The manufacturing of the pipe has to be done separately, and in order to position it inside the neck the latter has to be cut (either on the sagittal plane or on a diametrical plane perpendicular to the horizontal plane). During swift motions of the neck, the sharpness of the rings can damage the rubber structure: those shear stresses affect the repeatability of the process. This last drawback led to the rejection of this solution.

4.2.4 Pipe with one spring

Description

The spring is embedded in the rubber shaped pipe: it is coaxial with the pipe, it has the same length of the cervical canal and the diameter of the spring is slightly bigger than the one of the internal canal. The spring provides a higher radial stiffness but it allows a good axial elongation. If the pipe is considered as a sum of coaxial disks placed one over the other, the thickness of the disk can be chosen as the distance between the symmetry planes of two adjacent vertebrae at the point of intersection

with the axis of the cervical canal (Figure 4.7). In order to calculate the thickness of the disk, not only the geometry of the vertebrae but also the curvature of the neck in the neutral position must be taken into account. The rubber pipe is moulded outside the neck and later positioned inside after having cut the vertebrae.

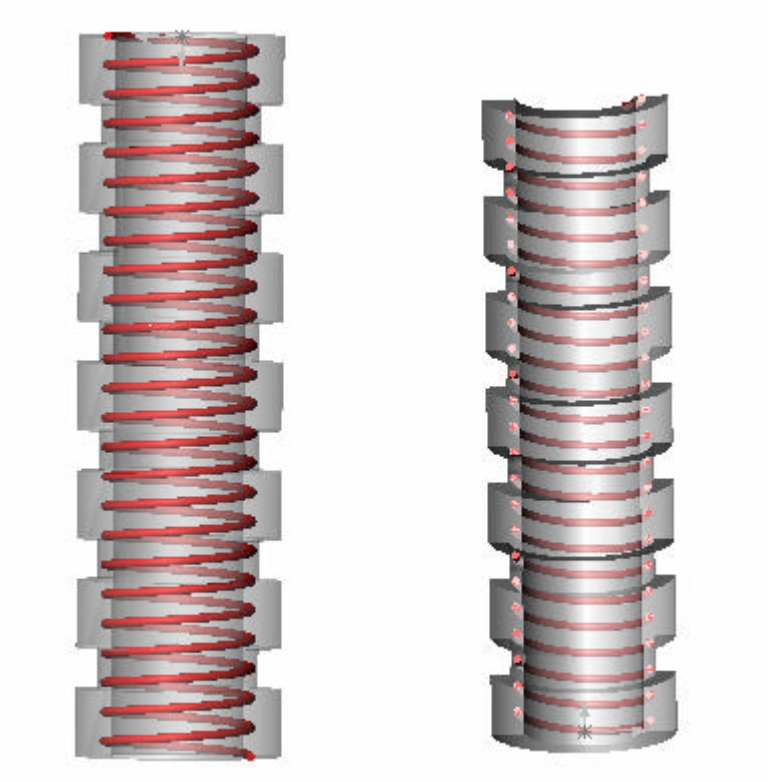

Figure 4.7 Lateral and section view of the rubber pipe with one spring.

Advantages

The shape of the pipe can assure a good transfer of the relative movements of the vertebrae to the internal volume of the canal. Then the spring provides radial stiffness and gives axial elasticity. The mould needed to make the rubber pipe is not complex: therefore its cost should not be too high.

Disadvantages

It is difficult to assure the waterproof capacity of the radial connections of the pipe.

The manufacturing of the pipe has to be done separately, and in order to position it inside the neck the latter has to be cut. Besides, the presence of the spring makes the radial connections difficult to be manufactured. Moreover, the intervertebral spaces have a vertical trapezoidal section: this means that an initial stress level is introduced into the anterior part of the disk already in the neutral position of the neck.

This last problem can be eliminated by the next solution.

4.2.5 Curved shaped pipe

Description

The rubber shaped pipe is manufactured with the same curvature of the medulla canal in the neutral position of the neck: in this case, the disks that form the pipe do not have a constant thickness. The positioning of the pipe and the radial connections are the same as the ones described in the previous solutions (Figure 4.8).

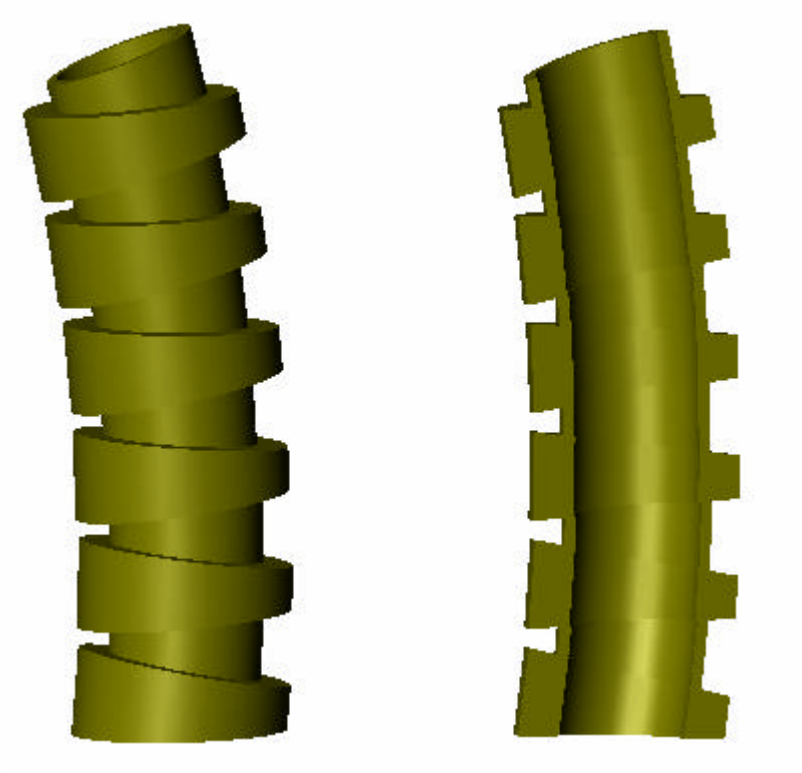

Figure 4.8 Lateral and section view of the rubber shaped pipe.

Advantages

Using this kind of geometry, the stress level introduced by the previous solution, where a pipe with cylindrical symmetry was used, is avoided. Consequently, the flat surfaces of rubber disks are entirely in contact with the vertebrae: in this way, it is simpler to obtain the adhesive connection between the disk and the vertebra.

Disadvantages

In order to install the pipe it is necessary to cut the vertebrae into two parts. The manufacturing procedure of the pipe reveals the need of an expensive mould (i.e. the mould should have two different curvatures).

For this last disadvantage, the solution is rejected.

4.2.6 Pipe moulded in loco – Final solution

Description

The rubber is moulded directly into a neck-shaped cavity. This cavity is obtained by interposing between the vertebrae properly shaped inserts, with trapezoidal cross-section (Figure 4.9). They are manufactured so that they can be easily removed after their usage: they consist of two halves kept together by a screw until the moulding process is accomplished, see Figure 4.10. The size and the shape of the inserts have been determined considering the geometry of the vertebrae and the curvature of the neck in steady state. The cavity is formed by the holes in the chain of alternate vertebrae and inserts. Using 3D Solid Works 2000, interferences between adjacent inserts have been avoided by limiting the embossment of the elements in the backward direction. The choice of using a mould in order to obtain the medullar canal instead of drilling the materials is a consequence of the difficulties in rubber perforation and by the geometry of the canal itself.

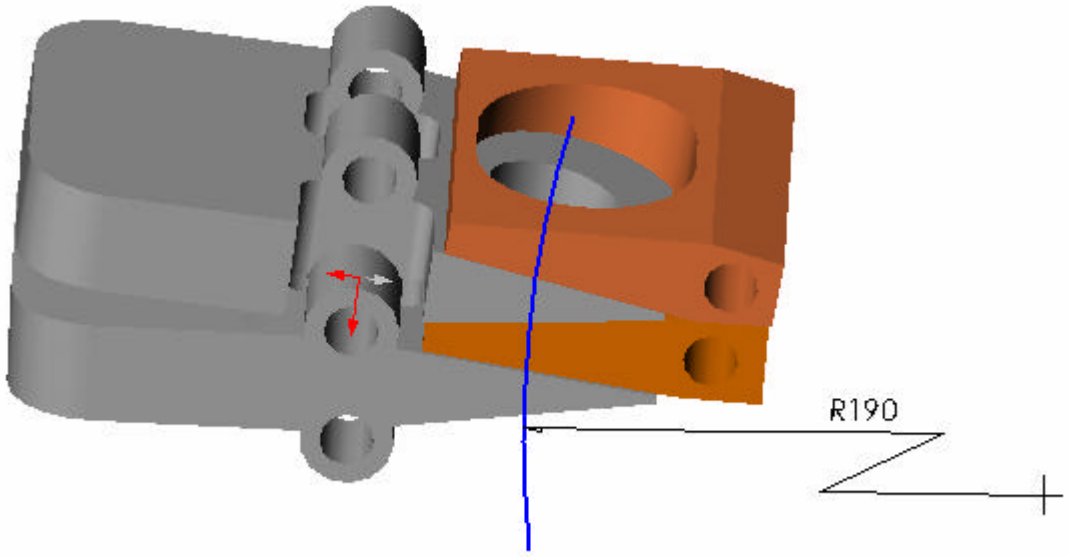

Figure 4.9 Lateral view of the final solution: the geometry of the inserts allows to obtain the curvature needed.

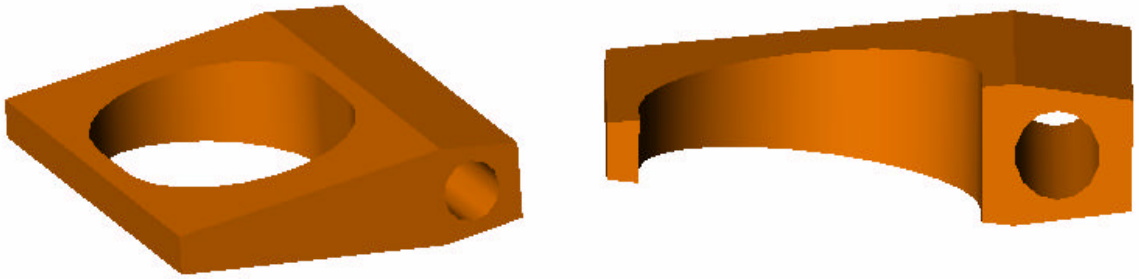

Figure 4.10 Perspective view of the mould mounted (left side) and perspective view of one half mould (right side .

Advantages

In the described way it is possible to obtain a shaped and curved pipe avoiding the manufacture of a complex and expensive mould (as required by the previously examined solution). The correct curvature is achieved without an induced stress in the rubber in steady state. Vertebrae do not need to be cut in halves in order to insert the pipe, as the canal is created directly in loco. That assures decreased costs and an improved mechanical resistance of the whole structure. Moreover, providing the material to be self-adhesive, this manufacture guarantee a good watertightness in the radial connections.

Disadvantages

It is difficult to keep the inserts in the right position during the moulding: in fact, the vertical strength applied in order to guarantee an optimal adherence between the surface causes, thanks to the geometry of the elements, an horizontal component that gives instability to the structure. In order to circumvent such a problem, another small straight vertical channel can be drilled through the whole structure: a rod inserted in such a channel and then removed after the moulding will keep the elements in the right position. Another possibility is to balance the horizontal component with rubber bands.

4.2.7 Structural modifications of the neck dummy BioRID II

In the same way used in the experience of Olofsson and Persson (2001), the neck of a dummy BIORID II is modified in order to place the apparatus that simulates the pressure.

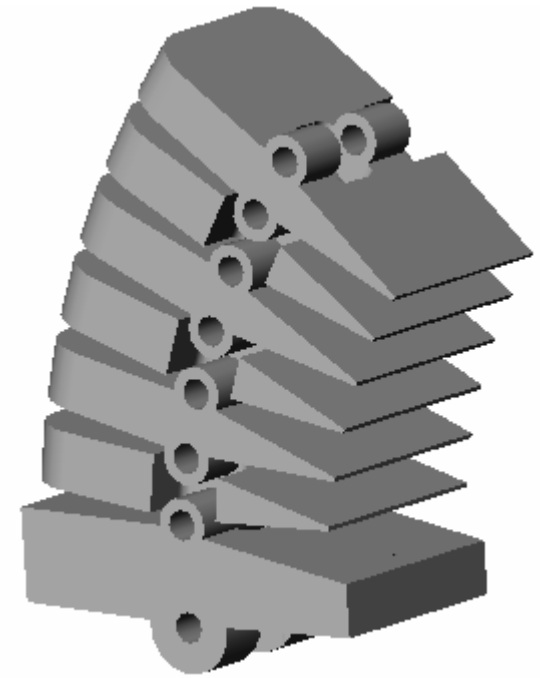

Figure 4.11 Perspective view of neck BioRID dummy: vertebrae C2-C7 (upper part) and T1 (lower part).

The basis used to start building the prototype is the neck of the mentioned dummy (made of seven cervical vertebrae, see Figure 4.11) and the first thoracic vertebra T1 used to fix the neck the test-stand.

The first of these vertebrae has a particular shape that allows it to be assembled to the head. Also the head is taken from a dummy 50percentile BIORID II.

In order to realize the prototype, the following structural modifications for each vertebrae, are performed:

- A hole with a diameter of 21 mm is drilled in the rear part of the vertebra in order to create the space for the pipe.

- A radial hole is obtained by a double drill. The first part of the hole is perpendicular to the lateral surface of the vertebra, screwed and with a diameter of 8 mm: it is needed for placing a metallic connection having a maximum internal diameter of 5 mm. To start with, it is chosen for each vertebra outlets of the diameter 5 mm, which is the maximal possible diameter. The second part of the hole presents the axis inclined of 21 degrees from the lateral surface of the vertebra and it has an internal diameter of 5 mm. This solution is imposed by the geometry of the vertebra and in particular, by the insufficient thickness of the rear part, which has a trapezoidal section, (see Figure 4.12).

- An opening with diameter of 2 mm is drilled in the vertebra, starting from the surface opposite to the one with the radial connection. This hole which is screwed in its first part, is used for the pressure sensor, see Figure 4.12.

- A circular sequence of holes with a diameter of 2.5mm is drilled around the hole of the spinal canal with the purpose of avoiding the radial collapse of the pipe.

- The bracket used to fix the neck the test-stand is different from the one used in the experience of Olofsson and Persson (2001). It is modified so that the extension of the spinal canal can pass through: therefore a hole having a diameter of 21 mm is drilled; this hole is screwed in its bottom part so that a metal L-connection (internal diameter of 13 mm) can be fixed. A flexible rubber pipe with internal diameter of 13 mm is linked to this L-connection in order to put in contact the spinal canal with the external volume. Another inclined hole is drilled in order to fill the mould with the liquid rubber during the manufacturing stage (Figure 4.13).

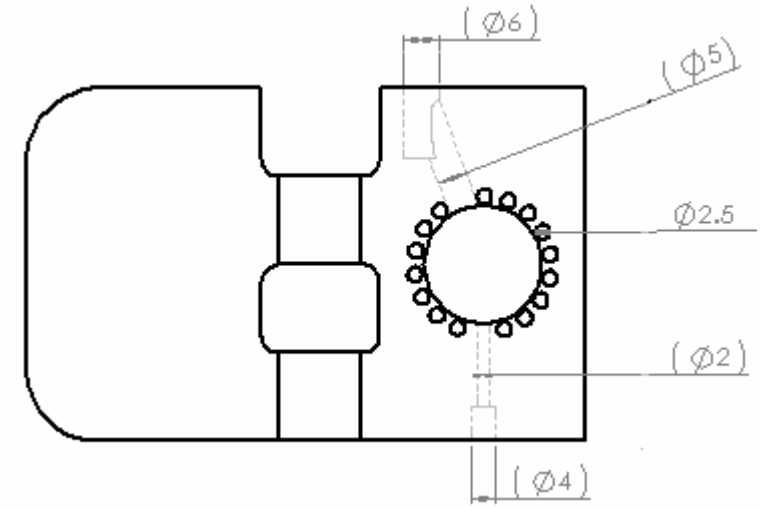

Figure 4.12 Top view of vertebrae (C2-C6) with the modification for the new prototype.

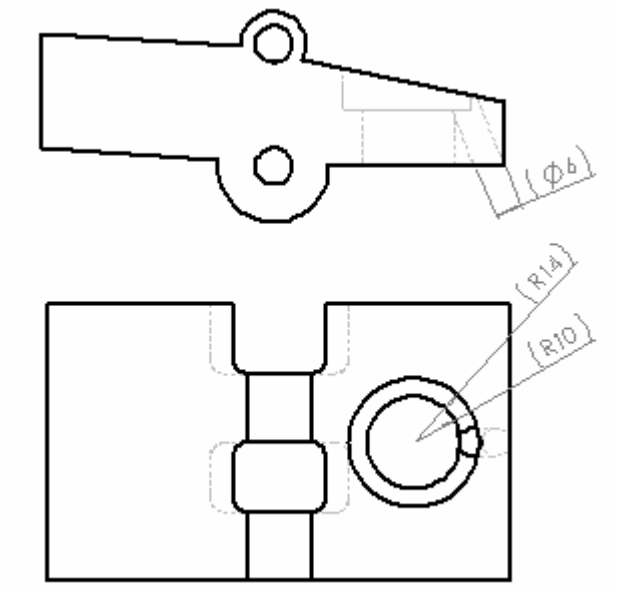

Figure 4.13 Lateral and top view of vertebra T1 with the modification for the new prototype

4.2.8 External pipe simulating the external venous plexus

The vein system of the cervical spine is very complex and it is almost impossible to rebuild it as a simple model. To obtain the same flow conditions as in a real human neck, the dimensions of this system filled with water must be adapted. The flow resistance is smaller in a blood vessel compared to a water filled tube of the same size. However, the model is very simple and a satisfactory pressure curve has to be found by changing the diameters of the outflows of the vertebrae and adding an elongation to the internal canal. To start with, it is chosen for each vertebra outlets of the diameter 5 mm, which is the maximal possible diameter.

A plastic tube with inner diameter 17 mm represented the external vein system. Along the pipe, there are six metallic outlets, on which the rubber tube can be connected in order to interlock the radial outlets of the vertebrae to the external plastic pipe. Their inner diameter is 6mm. It is the same size as the inner diameter of the rubber tubes and it is bigger than the biggest outlet of the vertebrae. Hence, the outlet of the vertebrae will be the main limiting factor of the system (see Figure 4.14).

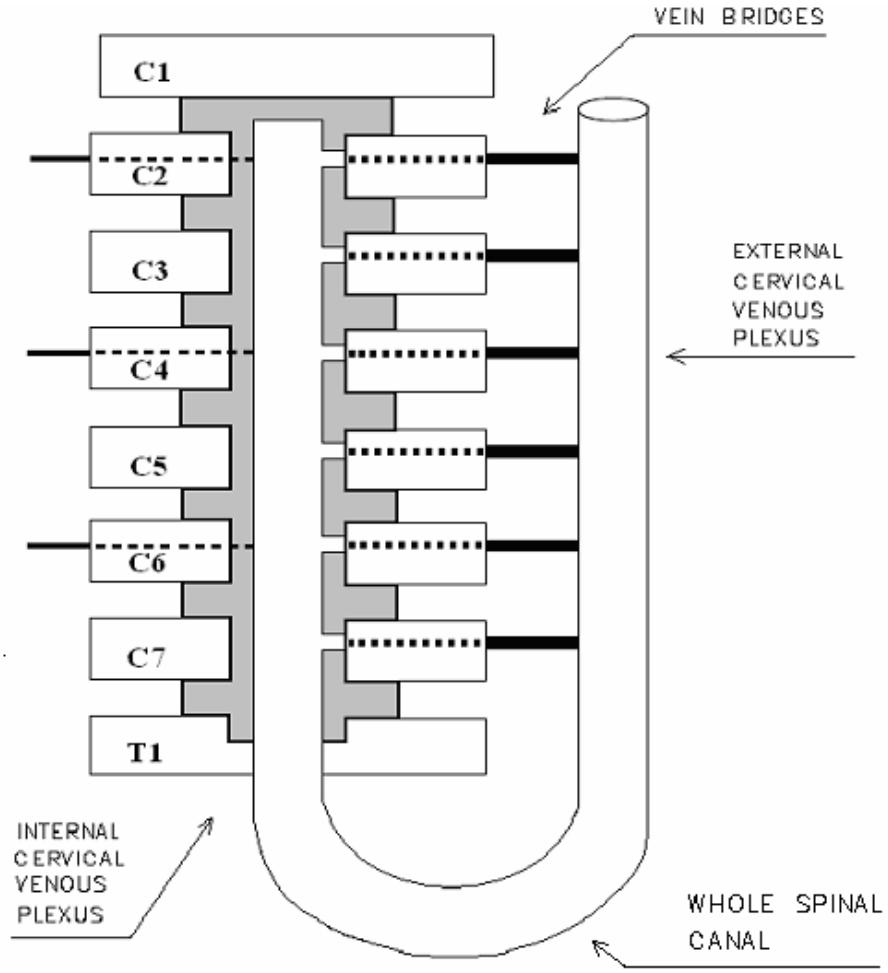

Figure 4.14 Schematic of the water system

On the upper end of the tube there is a balloon fixed, which serves as a water reservoir. In human neck, during traumatic motion, the fluids of the spinal canal are not only flowing out of the canal in radial direction, but also along the canal. Although the flow of CSF is assumed negligible, the flow of the blood is not negligible. For this reason, the bottom end is connected through a rubber flexible pipe (inner diameter 17 mm, length 500 mm) to the metal gusset screwed in the lower vertebra T1.

This rubber pipe represents the complete length of the spine and all the vein bridges between the two plexi distributed along the whole canal. This connection takes in consideration the whole spinal canal and should guarantee a faster pressure equalisation of the high positive peak observed in the Keiser's experiment. It is taken

the hypothesis that by adding this connection and increasing the diameter of the outflows, the compensation of the pressure would be faster but the pressure dip at phase 2 could still be the same.

In order to get rid of the air bubbles the water is previously boiled and then put inside the neck. The neck is let in a state of rest for about half an hour and then filled up with the rest of the water.

4.3 Choice of the materials: theoretical approach

The selection of the materials to be used for the production of the pipe is one of the main steps in the design procedure of the neck. The pipe has to be able to simulate the pressure that it is developed within the medulla canal during a quick flexo-extensional motion of the neck. Testing and indicating the stiffness properties of the structure of the neck is not aim of this thesis. Anyway, a preliminary study of the stiffness of the pipe is needed: the material should be chosen so that this property results to be in the same range of magnitude of the physiological one, in order not to perturb too much the simulation of the quick motion. In fact, in the case that this requirement was not fulfilled, the pressure phenomenon would not be properly reproduced.

The study of the proper material to be used for the pipe is based on a calculation of the stiffness, presented in the next section. These calculations are intended to give a starting point in the choice of the material, offering a limitation of the possible range.

4.3.1 Stiffness calculation

In this section, a preliminary calculation of the stiffness rate of the neck-model chosen as promising solution of this thesis. It is measured in Newton per meter [N/m].

It has to be mentioned that the following analysis is quasi static even if the behaviour of the elastomer is different when such condition is not fulfilled. The dynamic behaviour is related to rebound resilience of the material, i.e. two rubbers that have the same stiffness can behave in a different way when subjected to dynamic actions. Nevertheless, a static approach is used at this stage of modelling the prototype and further research can be performed in order to investigate and optimize the dynamic behaviour.

Equation (4.1) defines this parameter as a function of the magnitude of the force required to determine a unit deflection:

$$K = \frac{F}{d} \tag{4.1}$$

In the previous formula, F is the applied force expressed in Newton [N] and d represents the deflection in meters [m].

The rubber pieces placed in the space between two adjacent vertebrae is subjected to the action of both compression and shear forces. The compressive force is much bigger than the shear one: therefore the effect of this last internal force can be neglected. According to this simplification, the compression stiffness rate should be governed by the following formula:

$$K_c = \frac{A \cdot E_c}{t} \tag{4.2}$$

Where A is the effective loaded area expressed in square meters [m^2], E_c the compression modulus of the rubber [kPa] and t is the thickness of the undeformed elastomer [m].

The compression modulus is strongly affected by the designing geometrical conditions. The main assumption for calculating values according to the previous formula is that the operation happens in the linear range of the eleastomer modulus, which is typically smaller than 30% of the strain in case of tension and compression. This assumption does not fully agree with the test condition, so the initial value is calculated in this way but further tests are then developed in order to find the more suitable material to be used.

The effective compression modulus E_c is a function of both the material properties and the geometry of the components. Different methods are available in order to calculate the value of E_c and the one shown by the next formula is reasonably suitable to be used for simple geometry:

$$E_C = E_0 \cdot \left(1 + 2f \cdot S^2\right) \tag{4.3}$$

Formula (4.3) defines the effective compression modulus E_c for a flat sandwich block (loaded at both sides) with one dimensional strain: E_0 is the Young's modulus, f is the rubber compression coefficient and S is the shape factor. The rubber compression coefficient f is a material property empirically determined and it is included in the formula in order to correct the experimental deviation from the theoretical equations. The next table presents different values of f in relation to other coefficients.

Shear modulus G(kPa)	Young's modulus E_o(kPa)	Bulk modulus E_b(kPa)	Material compressibility coef. f
296	896	979	0.93
365	1158	979	0.89
441	1469	979	0.85
524	1765	979	0.80
621	2137	1007	0.73
793	3172	1062	0.64

1034	4344	1124	0.57
1344	5723	1179	0.54
1689	7170	1241	0.53

Table 4.1 Young modulus related to others parameters.

The shape factor S is defined as the ratio between the area of one of the loaded surfaces and the total surface area able to bulge:

$$S = \frac{A_{load}}{A_{bulge}} = \frac{A_L}{A_B} \tag{4.4}$$

It is therefore a function that describes the geometrical effects on the compression modulus.

The rubber is usually considered as an incompressible material. In some cases, the bulk compressibility contributes in a not negligible way to the deformability of a thin rubber piece and the apparent compression modulus can reach a magnitude value close to the one the bulk modulus. Therefore, in order to take into account this decrease in stiffness rate, the calculated compression modulus should be multiplied by the factor:

$$\frac{1}{1+E_o/E_b} \tag{4.5}$$

Where E_b is the modulus of bulk compression.

Moreover, a hardness measurement is a simple way of obtaining a measure of the elastic modulus of a rubber by determining its resistance to an indentation caused by a rigid indentor of a prescribed size and a prescribed shape that can be either a truncated cone or a sphere, pressed onto the surface under specified loading conditions. Indentation involves deformations in tension, shear and compression but, as in the case of a perfectly elastic rubber the moduli controlling them are closely related, it is convenient to regard hardness as depending simply on Young's modulus.

Different nonlinear scales can be used to obtain a value for the "rubber hardness" coming from those measurements. Shore hardness is on these scales and it is mainly used for flexible rubbers as the ones used in this project. It evaluates the resistance of a material to the penetration of a needle under a defined spring force. The values of this scale vary in a range between 0 and 100 and they are directly proportional to the hardness. The following table presents the correlation between the values of this scale and the modulus of elasticity.

Hardness Shore A	E (MPa)
10	0.4
20	0.7
30	1.2
40	1.7
50	2.5
60	3.8
70	6
80	10
90	23

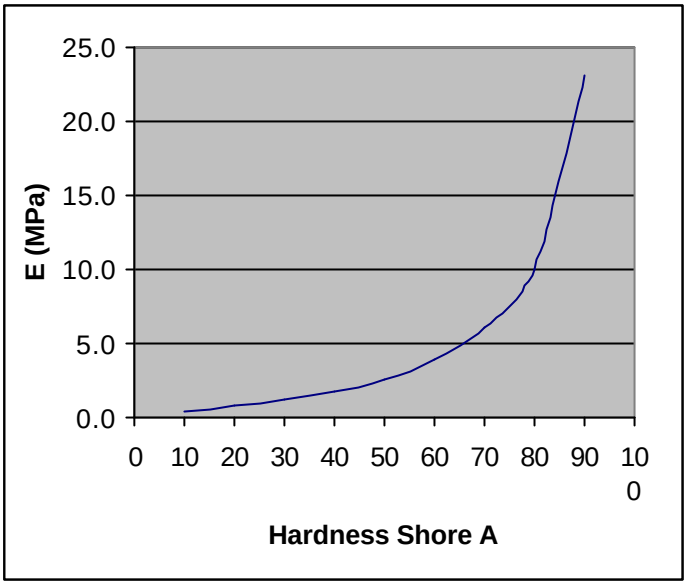

Table 4.2 Relation between Hardness Shore A and Young's modulus.

Combining formulae (4.1) and (4.2) it is possible to obtain

$$\frac{A \cdot E_c}{t} = \frac{F}{d} \tag{4.6}$$

In case of the analysed neck, F is the force that is assumed to be applied to the midpoint of the rubber disk and that corresponds to the applied moment M at the hinge between two adjacent vertebrae. The displacement of the loaded point is d. Therefore, these two parameters have to be properly set in formula (4.6) in order to get a reasonable value of E_c: the correlation between them is obtained from an experimental study on human necks. The research of Daniel Camacho et al. (1997) shows a function that, for each motion segment, correlates M (applied moment) to *?* (measured displacement):

$$q = \frac{1}{B}\ln\left(\frac{M}{A}+1\right) \tag{4.7}$$

where A and B are different parameters for each segment motion.

Object of this part of the thesis is to define an approximate global behaviour of the motion: therefore, mean values of A and B in the lower cervical spine (C2-C7) are chosen to identify the suitable M -*?* relation.

Figure 4.15 shows the graphical representation of formula (4.7) using the mentioned mean values of the lower cervical part.

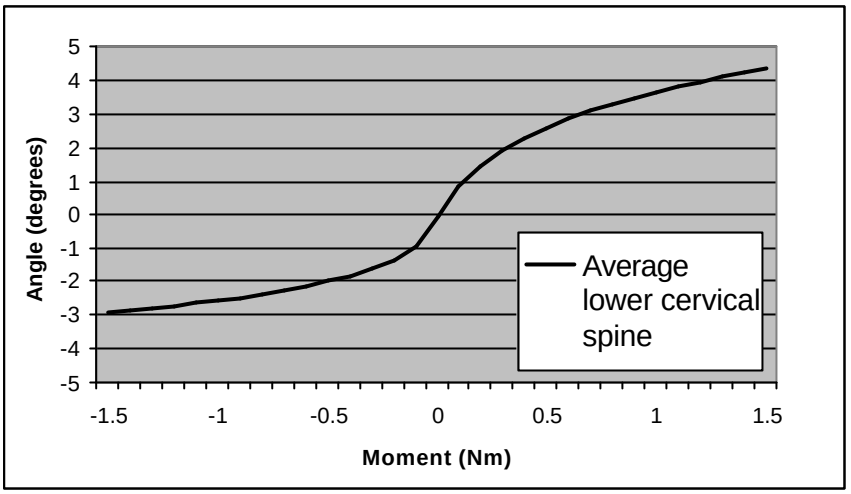

Figure 4.15 Flexibility curve for the lower cervical spine in flexion (positive moment) and extension (negative moment)

With the aid of the software Solid Work 2000, a 3-D CAD model of the neck is created and, from the value of *?*, the corresponding value of *d* can be easily found.

The higher values of the applied moment M and of the angular displacement *?* are chosen from Figure 2 and used in formula (6) in order to get an E_c of a material (i.e. for extension motion A=256mm^2; d=1.3mm; E_c ˜147000; S factor ˜ 0.375)

Then, from formula (4.3) it is possible to calculate the corresponding Young's modulus: E_0˜437000Pa. From the Table 4.2 it is possible to find the value Shore A 10 corresponding to the Young's modulus of 0.4 MPa.

Considering the several approximation made in the hypothesis, this calculus do not require to be accountable, it is only a general indication for the range in which the material has to be search.

A more accurate flexibility of the neck will be researched in the experimental way directly testing the materials.

Testing and indicating the stiffness properties of the neck are not objective of this thesis. Anyway, a test of the relation moment-angular displacement with a material (silicone) Shore A 10 is performed. Figure 4.16 shows the behaviour in flexion-extension of a segment of the neck compared to the Camacho curve average flexibility. The experimental curve has almost a linear tendency and this is due to the use of a singular and homogeneous material that cannot reproduce the physiological stiffness. The approximation can be considered acceptable and the choice of Shore A 10 is confirmed appropriate.

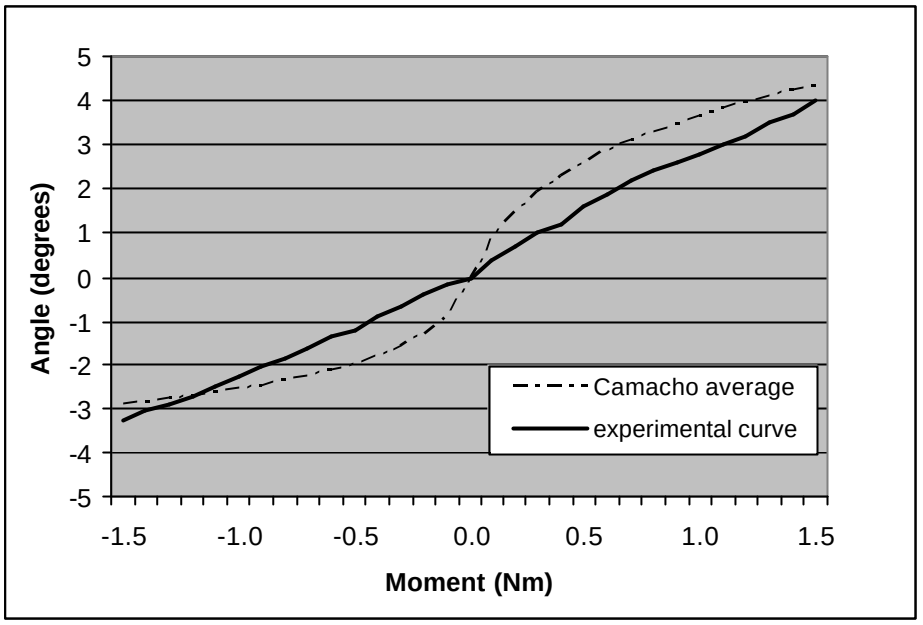

Figure 4.16 Experimental flexibility curve with Shore A 10 silicone compared with the physiological Camacho average.

The following graph (Figure 4.17) shows the relation between the modulus of elasticity and a parameter of resistance for different materials. In the specific case of the requested Young's modulus (0.1 Mpa), this parameter is the tear strength and the possible materials suitable for the design are Polymers Foams and Elastomers.

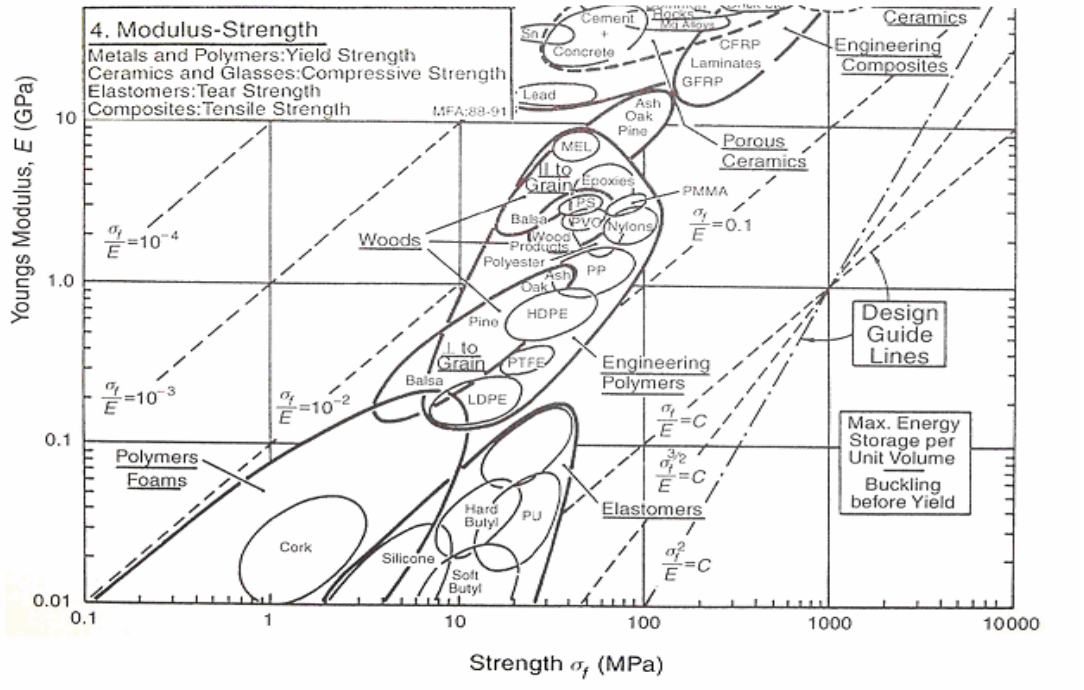

Figure 4.17 Graphic representation of the correlation between Young's Modulus and strength of several materials.

The first kind of materials is rejected because it does not fulfil the request of being waterproof and because it has a high value of rebound resilience.

Therefore, further analyses will be developed on three kinds of elastomers, in particular Butyl Rubber, Polyurethane and Silicone.

4.3.2 Other parameters

Rubber consists of long flexible molecules that are in continuous Brownian motion at normal temperatures due to thermal agitation. As a result, the molecules take up a variety of random configurations; when the molecules are straightened out by an applied force and released, they spring back to random shapes as fast as their thermal motion allows. This is the origin of the unique ability of the rubber to undergo large elastic deformations and recover completely: rubber molecules are highly extensible, but in absence of a external force they adopt rather compact, random configurations.

To give rubber a permanent shape the molecules are tied together by a few chemical bonds, in a process knows as "vulcanisation" or "crosslinking". Molecular sequences or stands between sites of interlinking still move about and change their shapes, but they are subject to the restriction caused by the crosslinks, which remain in more or less stationary positions. Before crossilinking, rubber is basically a very viscous, elastic liquid: after crosslinking, it is a soft, highly elastic solid.

4.3.2.1 Tensil stress strain

After indentation hardness, the most common type of stress/strain measurement is that made in tension. The ability of a rubber to stretch to several times its original length is one of its chief characteristics. A typical tensile stress/strain curve for rubber is shown in Figure 4.18. It can be seen that there is no linear elastic portion as is usual with, for example, metals, and in rubber technology a modulus is not measured as such but the stress at various percentage elongations is quoted, commonly 100%, 200% ecc.

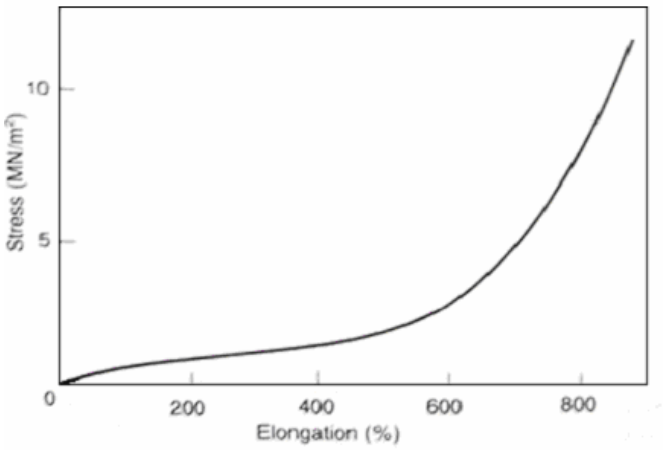

Figure 4.18 Stress/strain curve for pure gum vulcanized

In the neck application of this thesis the percentage elongation is about 70% but, considering the dynamic application and the fast application of load a choice on the safe side is to request a higher elongation at break to the material. The properties of the researched materials are: tensile strength more than 3 N/mm^2 and elongation at break more than 200%.

4.3.2.2 Dynamic stress-stain and rebound resilience

The term "dynamic mechanical properties of elastomers" refers to the behaviour of these materials when subjected to stresses or strains that change with time. An ideal linear elastic solid obeys Hooke's law: stress is proportional to strain. An ideal viscous liquid obeys Newton's law: stress is proportional to rate of change of strain with time. Many materials, elastomers in particular, have properties intermediate between these two cases. The two basic mechanical properties of any material are the modulus (stiffness) and damping (ability to dissipate energy).

Typically, some energy is lost (converted to heat) in any deformation process. Viscoelastic response is modelled with a spring (elastic component) and dashpot (viscous response). For the spring, stress is directly proportional to strain and for the dashpot, the rate of strain is proportional to the stress applied. The dashpot resistance depends on both time and viscosity.

A simple model to represent this behaviour is a spring and a dashpot in series (Maxwell model) or a spring and a dashpot in parallel (Voigt model). An oscillatory dynamic experiment differs from the simple creep and stress relation studies in two important respects. First, the time scale is determined inversely by the frequency of the sinusoidal deformation. Second, stress and strain are not in phase in a dynamic experiment, hence, in addition to the ratio of stress to strain, the phase difference or phase angle between them is measured. The phase angle depends on the dynamic viscosity and becomes zero when the viscos ity is zero. For a perfect spring, the force (stress) and the deformation (strain) are in phase (zero phase angle), but for a dashpot the force leads the deformation by p/2 radiants. A viscoelastic material has an intermediate phase angle.

The rate at which a deformed elastomer returns to its original state after release is a function of its internal friction coefficient and this value ranges over many orders of magnitude. I.e. in butyl rubber, for example, it is very high, while for dimethyl silicone, it is very low.

Several excellent reviews of experimental techniques for determining dynamic mechanical properties are available: forced resonance vibration, force nonresonance vibration, free vibration methods and rebound resilience.

Rebound resilience is defined as the ratio of the energy of the indentor after impact to its energy before impact expressed as a percentage and hence, in the case where the indentor falls under gravity, is equal to the ratio of rebound height to the drop height, which is the measure used in most instruments. Resilience is not a arbitrary parameter but, is approximately related to the loss tangent d:

$$R = \frac{E_R}{E_i} = \exp\left(-p \tan d\right) \tag{4.8}$$

$$\frac{E_A}{E_R} = p \tan d$$

where E_R is the reflected energy, E_i is the incident energy and E_A is the absorbed energy.

The results of dynamic tests are dependent on the test conditions such as test piece shape, mode of deformation, strain history frequency and temperature.

It is not possible, at this stage of the design, to calculate specifically the rebound resilience of the rubber used for the spinal canal: the resulting damping and spring constant of the neck are the sum of the properties of the rubber and of the internal water within the canal.

The damping properties of the hydrodynamic system cannot be known, as long as they depend on the size of the radial connections and on the diameter of the span of the pipe that connects the internal canal to the external volume. These sizes will be later chosen during the test stage of the prototype.

In order to guarantee a possible future set up of the model from the damping and spring point of view, a material having low rebound resilience is chosen. Eventual increases of the dumping constant of the system will be possible to be done by adding some inserts made of an appropriate material between the vertebrae. A material with a quick recovery of the deformation after a quick load is therefore needed.

This last observation confirms the rejection of the Polymers Foams from the list of the possible materials to be used.

Dynamic test are generally much more useful from a design point of view than the result of many of the simpler "static" tests; nevertheless they are even today much less used than the "static" tests principally because of the increased complexity and apparatus cost. In fact, for some tested rubbers in the technical datasheets there are not data about dynamic property.

4.4 Tested materials

During this thesis, the only one polyurethane found able to be manufactured by hand is EliChemResins ELI-FLEX FR909/N60 (see table 4.3).The common polyurethanes usually need to be processed on low-pressure casting machines equipped with gear pumps and dynamic mixers. Moreover, polyurethanes have several problems with safety: usually they are TDI (toluene diisocyanate) based, which is not a very easily handable cyanate (material safety transport ADR, classification UN 2078 and 6.1 II).Two-component polyurethane elastomer ELI-FLEX FR909 has been tested, and

the percent of its components Resin and Hardener has been varied from 21% to 24% by weight of hardener. The optimum ratio from the point of view of the shore and of mechanical resistance was 21% of hardener, even if the EliChem suggests 24%. The elastomer tried is the one with the lowest Shore A produced by the EliChem.

The material results too slow in recovering deformation (too low rebound resilience) and also the shore was too high.

Silicone Waker Elastosil RT 745 has been tested, and the percent of its components A/B has been varied from 35% to 55% of B. The optimum ratio from the point of view of the shore and of mechanical resistance was 45% of B, even if the Waker suggests 50% (see Table 4.3).

The product has been tested on different surfaces and adherence resulted to be better on rough ones. Samples of the material have been tested on rough acetal plastic, but any exaggeration in etching the vertebra results in overflows of the silicone between the mould and the vertebra itself; that phenomenon is due to the silicone low viscosity (1000 MPa).

Glue (Hermetite gul Hammerite) has been tested to fix temporarily the vertebra and the mould. Such a product allows an excellent cohesion, but the link between glue and substrate does not absorb energy, and it is easy to break. Not withstanding these advantages, the product turned out to be inadequate to the task: in fact even with no direct contact with silicone, the glue reacts with the exhalations of the polymer, melts, and at the same time it loses its adhesive property and inhibits silicone vulcanization. A treatment based on the drying of the glue before application in order to eliminate the solvent contained in it has not brought advantages.

Considering the self-adhesiveness of the silicone, different products with whom cover the walls of the mould have been tested, in order to easy the removal of the mould after the application of silicone. In particular, paraffine and vaseline have been used. Paraffine does not contaminate silicone RT 745 under a threshold of 50° C; as soon as this value is trespassed, silicone in direct contact with the material changes colour, becomes opaque and less resistant to traction. But such a limit does not represent a real problem, as the paraffine contained in the mould used to create the spinal canal already set a threshold in temperature at 50° C. A similar limit is encountered also in working with vaseline, due this time not to chemical reaction, but by the fact that increasing the temperature over 50-60° its viscosity decreases; thereafter, the layer applied to the wall of the mould does not get stuck, but it falls and forms deposits in the bottom. This is a serious drawback, as it damages the adhesion between vertebra and silicone. Vaseline is easier to apply with respect to paraffine, and it is easier to obtain a thin layer.

The self-adhesiveness of RTI 745 is directly proportional to the curing time, so that increasing the temperature adhesiveness is increased. The limit at 50° decrypted above led to the following experiment: on the plastic vertebra, in the area where silicone should adhere, a first thin layer of polymer has been applied; then the sample has been put in the oven at 95°, in order to obtain a quick vulcanization, and thereafter a strong adherence. Then the mould has been filled with silicone, so that

the new polymer could adhere to a silicone layer instead of to the acetal plastic (second vulcanization has been obtained at 50°).

Even if in former tests already vulcanized samples of silicone drenched in unvulcanized polymer have been found capable of linking with the material, in this experiment the resultant adhesiveness between the two layers of silicone turned out not to be improved.

In conclusion, samples of RTI 745 showed a good self-adhesiveness to the acetal plastic and to steel. Another positive property is that thanks to the reduced viscosity no air bubbles remain trapped in the polymer. The choice of using other materials came from the insufficient resistance to dynamic loads.

RTI 745 shows the highest mechanical properties among the other self-adhesive silicones produced by Waker. Consequently, looking for better mechanical performances, self-adhesiveness has not been required anymore to new material tested.

In order to make up for the un-self adhesiveness, plastic has been treated with primer. The first silicone to be tested has been Waker Elastosil RT 4600 (see Table 4.3). Four vertebrae, after a mechanical abrasion of their surface, have been brushed with the G790 primer by Waker. Sample number n was characterized by n layers of primer. Those different tests were necessary because instruction given with the product recommends to apply thin layers of it, more than one if substrate is porous. Experiments on more than one sample were needed as the actual porosity of Delrin was unknown. Samples have then been put in the oven for some minutes in order to dry the primer before the silicone was moulded on them.

Very smooth plastics surfaces require slight roughening before being primed but plastics such as PTFE, PE, PP, and acetal plastic should undergo special treatment (corona discharge, low pressure plasma, flame treatment, fluorination). For reasons of time and cost, in this work, the samples did not undergo these treatments.

No experiments to test standard traction have been performed. Following the guidelines chosen for the manufacture of the neck, silicone has been moulded between two vertebrae treated with primer. Samples obtained in this way have the same size of segments of spinal canal. Moreover, such a solution allows to test the material resistance to deformation it is subjected in the prototype and its adhesiveness. The third sample gave the best results: so three layers of primer were needed. In fact, this sample was the only one able to tolerate several fast cycles of traction-compression between the vertebrae with no lack in adhesiveness from the acetal plastic.

The last silicone to be tested has been the Waker Elastosil RT 402/T12 (see table 4.3) and for this product too best results has been obtained with three layers of primer. Its viscosity is high enough to avoid outflow between mould and vertebra, and at the same time low enough to fill opportunely the mould and to allow the injection of the product through a panpipe.

Another interesting property, especially in a comparison with RT 745, is its quick vulcanization (less than 2 hours at 45° against the 7 hours typical for RT 745). The lower presence of air bubbles compared to the RT 4600 and the possibility of using it following the advices of the factory in order to obtain the desired shore, made of the silicone RT402/T12 the final choice.

Material	After catalysing		Cured property		
	Pot life min at 23°C	Viscosity mPa s	Shore A	Tensile Strength Mpa	Elongation at break %
Elastosil RT 745	> 4 h	1000	15	0,3	180
Elastosil RT 4600	90	15000	20	6	700
Elastosil RT 402/T12	75	14000	10	1,2	380
Eli-FlexFR909 (polyurethane)	8	2800	55	4,5	230

Table 4.3 Summary of the datasheets of the tested materials.

4.5 Test set up

4.5.1 Components and their properties

Data storage: Brick data GMH Engineering Version 2.0. High Speed 850 - 12,800 Hz; data memory 524,218 data points; analog input channels 8 (differential input); programmable transducer excitation of 5 or 10 Vdc; independent input range (Gain) for each channel; data resolution 0.024% of full scale; data accuracy (min) 0.195% of full scale

High-speed camera: Kodak Ectapro RO imager, 1000 frames for second.

Piezoresistive pressure transducers (2): Endevco Model 8510C-50, Sensitivity 5.96 mv/psi g, Excitation 10 v_{dc}; Endveco Model 8510C-100, Sensitivity 1.61 mv/psi g, Excitation 10 v_{dc};

Accelerometer: Ental Model EGE3-73-2000, Sensitivity (x,y,z) 0.202, 0.221, 0.213, Input impedance (x,y,z) 471, 465, 488 homs, Output impedance (x,y,z) 472, 468, 488 homs, Range ±2000 g, Excitation 10 v_{dc}.

Lamps (8):220 v, 1000 W for each lamp.

Dynamometer: Max scale 25kg, resolution 0.1kg

Elastic cord: The pulling force is 125N for 100% elongation. Length cord 2m.

Personal computer equipped with softwares for data elaboration.

4.5.2 Method

The instrumentation listed in the previous section is used in the tests in order to measure the pressure at two level in the neck, the acceleration and displacement of the centre of gravity of the head. The way chosen for the set up allows knowing for each time the correspondents values of pressure, of displacement and of acceleration. (see Figure 4.19).

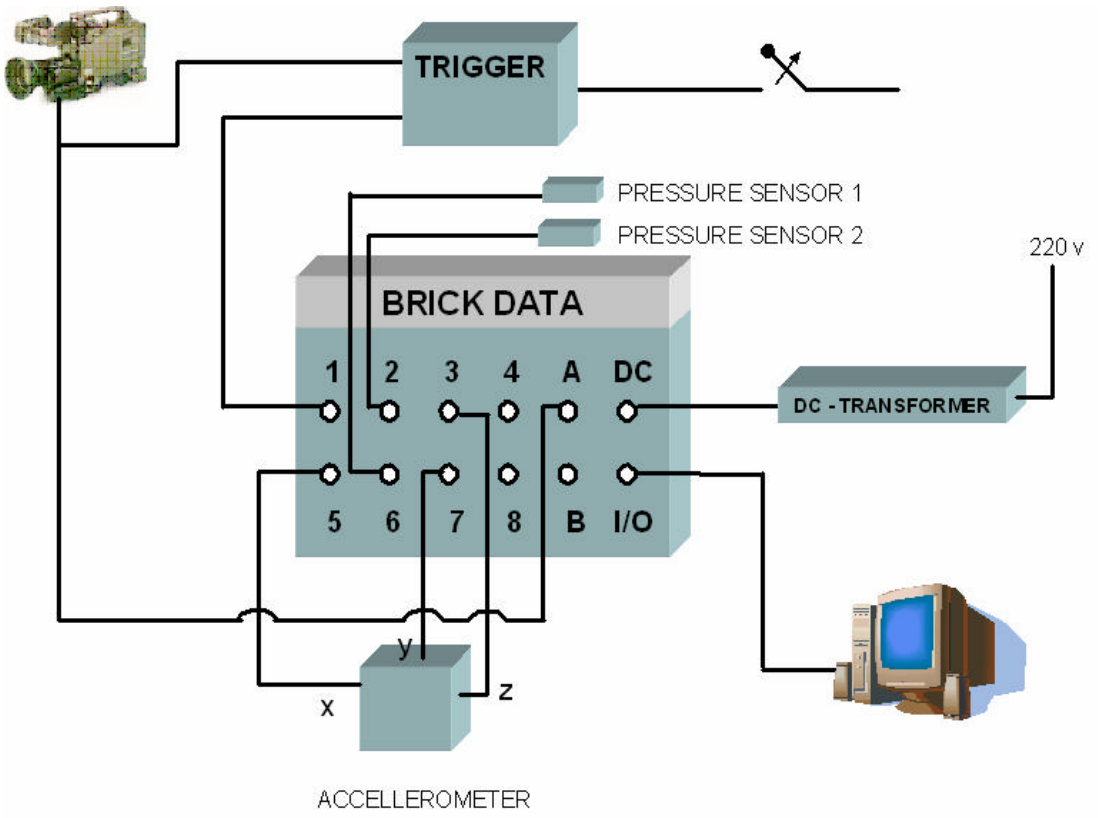

Figure 4.19 Schematic of the instrumentations used in the tests.

The neck, fixed to the ground, stands in a stable initial position thanks to two opposite forces applied on the same forward/backward direction. The backward component is caused by an elastic cord connected to a dynamometer: acting on the dynamometer it is possible to choose the strength applied (see Figure 4.21). During the experiments, the values chosen have been 150 or 200 N.

On the other side, the neck is kept firmly in its initial position by an electric wire: the reasons for such a choice will be clearer later.

The two pressure transducers are inserted in opportune positions inside the neck: they are screwed in it, in the apposite holes drilled on the left side or the vertebrae C2, C4, C6. In all tests, one of the sensors was displaced at C6: the other transducers have been fixed sometimes in C2 and some other in C4. The choice of two sensors is new for this kind of experiments: in the past only one sensor by time was used; this sensor was positioned at different points inside the neck, and the results of the different experiments were then compared. But the low repeatability that is proper of such an experiment suggests that in order to obtain more precise result and more useful comparisons more than one sensor is required.

The edge of the sensors has been covered with a layer of grease in order to avoid contacts with water that would cause corrosion. Sensors are connected to the Brick data.

The accelerometer is positioned at the centre of mass of the head; it can give acceleration at that point along three orthogonal direction x,y,z, but the task, considering the absence of lateral bending, requires only to consider two axes, z and x. Conventions used to define those axes are shown in Figure 4.20 . It is directly connected to the brick data.

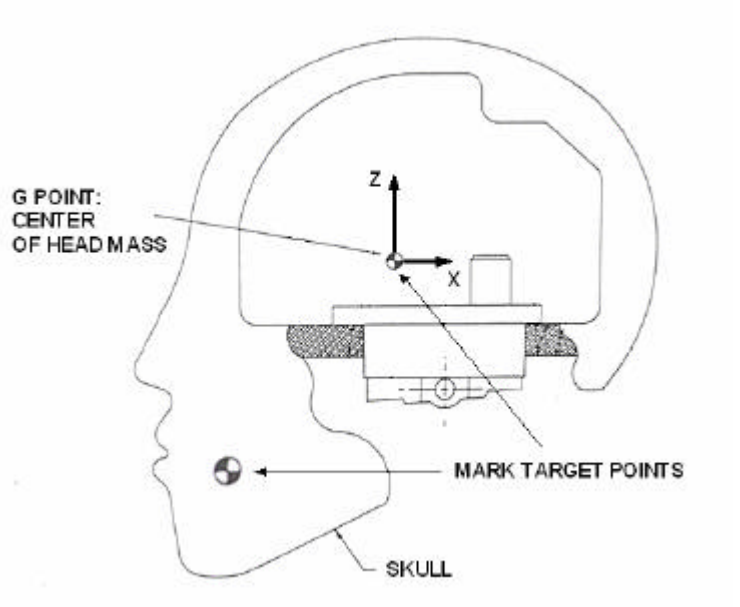

Figure 4.20 *Schematic section view of the head and the reference axis.*

The position of the camera must be set carefully, in order to avoid aberrations in the special displacement of the track points: in particular, the horizontal and vertical plane of the camera must be parallel, correspondently, to the horizontal and sagittal plane of the neck. The camera is at 1535 mm from the reference plane. The reference plane is the plane where the two main marks (fixed point needed by the software to establish a correspondence between distances in centimetres and in pixels) are situated. Distance between them is 161mm.

Track points are positioned (and fixed) in the gravitational centre of the head and on the chin, as far as possible from each other, in order to decrease as much as possible errors. Those track marks have been chosen big enough to easy the tracking with the software (see Figure 4.21). Those points lay on a plane that is 20 mm farer than the reference plane from the camera.

In order to achieve a good resolution in capturing the images, lamps have to be positioned opportunely close to the camera. Power absorbed by those lamps is around 8kW; due to the heating they produce on the neck, they cannot be left turned on for too much time.

Camera has been set as described above, and it captures images for 0.5 second: such a time is more than sufficient. In fact, the event under analysis lasts for a time certainly not longer than 300 ms. Thereafter the chosen time guarantees also an opportune margin. The brick data can store data corresponding to 0.6 s. The camera and the brick are not directly connected: they are both turned on at the right and at the same instant by a trigger.

This trigger is connected directly to the neck through the electric wire described above, used to keep the system in the right initial position. The triggering signal is obtained by cutting this electric wire: in this way the current that was flowing in it is interrupted, the circuit at the input of the trigger is open and an activation signal is sent to both brick data and camera.

The brick has eight channels, but only five of them have been used. The cut in the electric wire and the consequential signal incoming from the trigger represent the beginning of the event to be recorded; but the brick is programmed so that it also stores the values of the quantities connected to its channels in the instant immediately before the cut. This allows obtaining interesting values for setting the offsets.

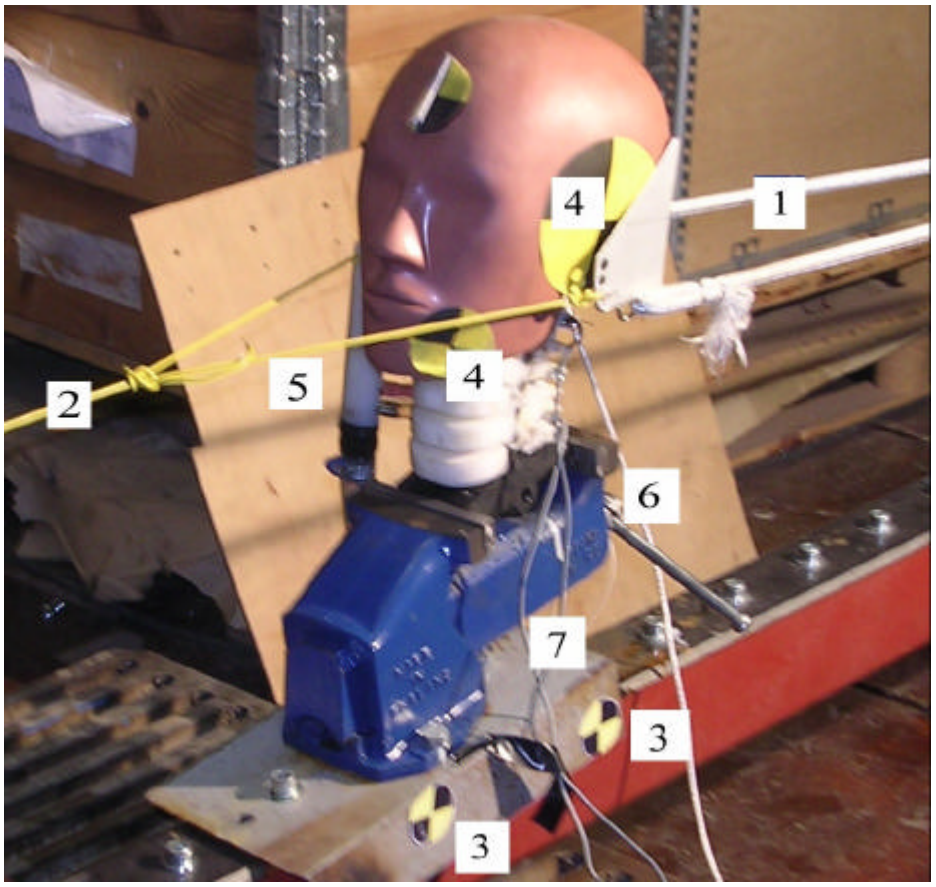

Figure 4.21 Photo of the prototype in the initial position: 1)rubber pull cord, 2)electrical wire to keep the head, 3)reference marks 4)marks, 5)external plastic pipe, 6)wire connected to the accelerometer, 7)wires connected to the pressure transducers.

5 Results and discussion of the tests

Pressure, acceleration and displacements measurement results from all the tests can be found in the appendixes A, B, C. Pressure measurement results from two particular whiplash runs are shown in Figure 5.1 and 5.4. The pull force applied in the test G11 (following figure) has a value of 150 N, which is the same used for the tests from G1 to G11 except for test G6. Test G6 and tests G12 to G17 are performed with a 200 N pull force. For the test G11 the angular displacements and linear-x displacements of the head, the x- and z- accelerations of the centre of gravity of the head are respectively shown in Figure 5.2 and Figure 5.3. The readings from the two pressure transducers at level C4 and C6 are reported in Figure 5.1 and are in the same scale time as the others measurements data. The trigger system used allows the synchronization of the data recorded by the brick and by the camera, so it is possible to compare the pressure curves with the relative accelerations and displacements data. In this way, it is easy to know the head position and accelerations corresponding to each pressure data.

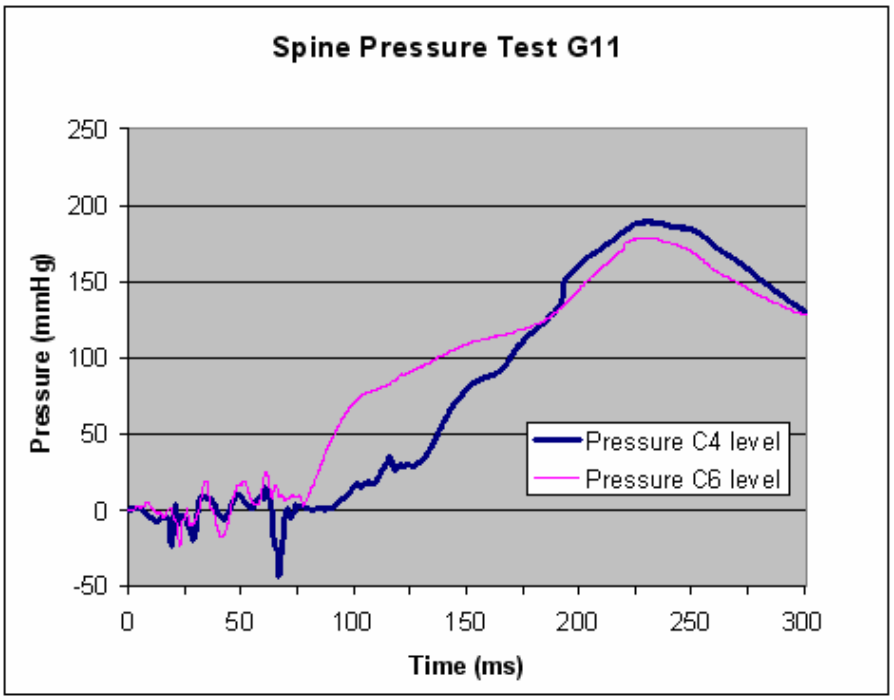

Figure 5.1 Spine pressure versus time for test G11 measured at the two level C4 and C6

In Figure 5.1 the pressure curves for the two levels C4 and C6 start with a small negative value which is slightly bigger for the upper level of the neck. After 20 ms the two curves display two negative pressure peaks; between these drops the pressure curves become positive. The C4 level curve shows a marked negative peak at 70 ms. For this run, the curve of level C6 shows a non-negative pressure dip at 75 ms. At about 80 ms, when the head has already started rotating backward, the pressure

increases for both levels. The maximum positive peaks are reached at about 220 ms (at the same time of maximum displacement) and after that the pressure decreases.

After reaching the limit of rear motion, the flexion motion is braked by the rubber cord, which pulls the neck back in its fully extended position. For this reason the pressure decreases slowly and the flow equalization takes too long time to reset the pressure level. Anyhow, the more interesting curve part is the first one, the pressure phenomena investigated takes place before the big positive peak, so in the present work is not such important what happens after the big positive peak.

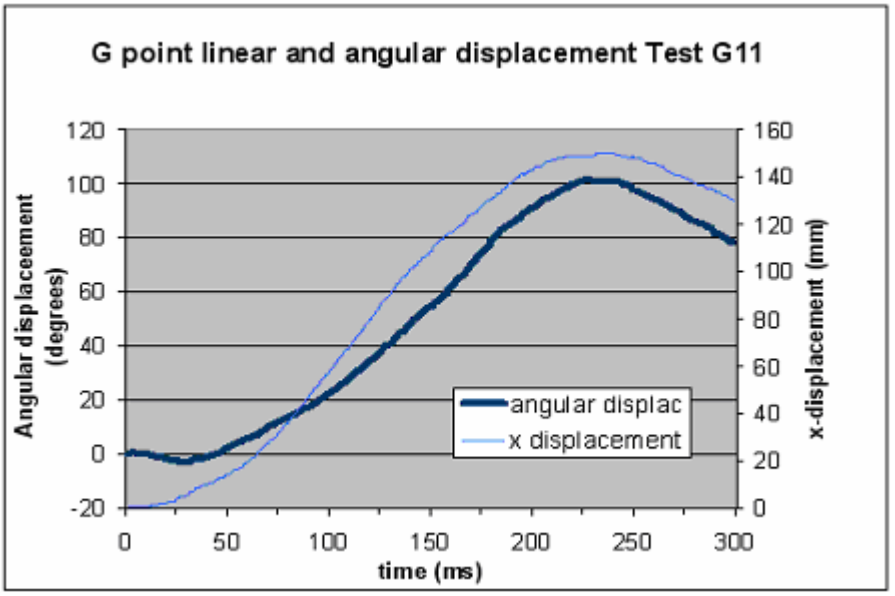

Figure 5.2 Linear and angular displacements versus time for the test G11

The swift extension motions to which the dummy neck is exposed in this study have a realistic time history when compared to other whiplash extension experiments. The interval of time from the beginning of head rearward rotation until the maximum extension angle is reached is in the range of 150 ms to 250 ms. In Figure 5.2 and approximately in all the tests, the positive angular motion of the head is delayed of about 40 ms compared to the linear x-displacement indicating that the head moves mainly translationally during the first 40 ms. In this fist phase of motion the angular negative displacement (forward rotation of the head), assures that the retraction for rearward motion takes place. This negative angular motion of the head assures that S-shape takes place completely. Obviously, the maximum x-displacement occurs at the same time as the maximum angular displacement and these maximum occur earlier with increasing pulling force. Unexpectedly, increasing the pulling force the angular displacement does not increase in magnitude. Probably this is due to the test conditions: the not constant pull force, the different initial position of the head or the motion limit already reached with 150 N.

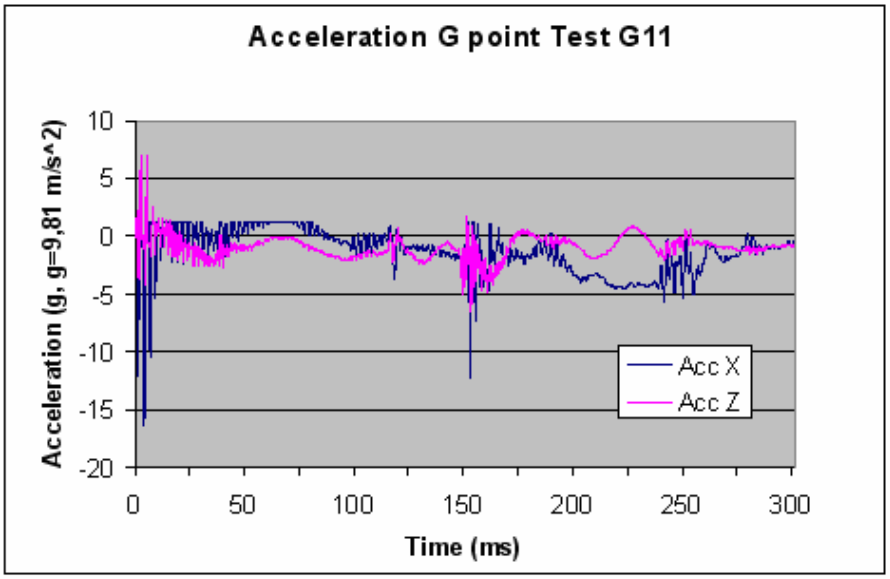

Figure 5.3 Acceleration versus time for test G11 measured at the centre of gravity of the head

The results of pressure measurement in test G6 (Figure 5.4) indicate that the pressure dip had the largest values in the lower half of the cervical spine. This agrees with the results of pig experiments where tissue damage found in the spinal ganglia was most severe at the lower half of the neck. In the previous figure at level C4 there are several slight pressure dips and a marked negative peak does not take place. After circa 100 ms the pressure increases and shows a high peak which is out of range. This overflow that saturates the cannel pressure was found also in other tests but for the present study this is not so relevant because the most important curve part is before the big positive peak. It is possible to see in Figure 5.5, in which all the pressure curves are represented at the same level C4 in tests run with the same condition, only in some tests there is the problem of pressure overflow, while other curves are in the scale range. The fact that for some tests the positive pressure peak is restricted indicates that the pressure equalization take place during the swift extension motion. This suggests that the increased dimension of the connection between internal and external volume are proper. However, the presence of pressure overflows indicates that during the test there is something of aleatory. A possible explanation of this inconvenient may be a collapse of the external rubber pipe that connects the spinal canal with the external volume. The rubber pipe in the starting position has an initial curvature and a circular area in all the cross section, but during the swift motion, the stability becomes precarious and a possible collapse may stop the flowing of the fluid and causes the big positive peak.

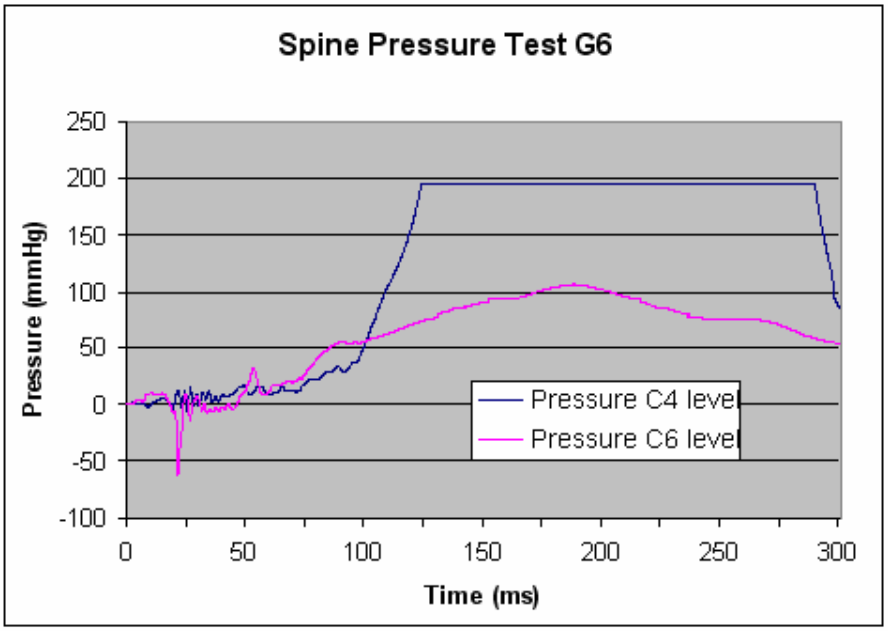

Figure 5.4 Spine pressure versus time for test G6 measured at the two level C4 and C6

A comparison of pressure profile in the spinal canal between seven different tests during simulated whiplash extension motion using 150 N pulling force is made (Figure5.5). This comparison gives an indication of the repeatability of the pressure pulses between different tests. The kinetic energy of the motion is virtually identical in the different tests but there is some difference in the distribution between angular and linear displacement. Probably, this is due to the difficulty to assure manually the same pulling force for all the tests and to the slight difference of initial position of the head (see Figures in the appendixes A and B). The electrical wire that, in the beginning of the test keeps the head in the right position is not perfectly in the same direction of the opposite pulling force, so the vertical force component gives instability to the system and makes the right head positioning difficult. The fact that the properties of the silicone canal, in particular the adhesiveness with acetal plastic, may have been affected by each whiplash extension exposure and thus gradually changed its watertightness is another possible cause of spread in the results. Nevertheless, the pressure profiles show very similar patterns and the timing of different pressure events and the magnitudes of the pressure peaks are similar. The repeatability under identical conditions in repeated test runs is acceptable and from the following graph is possible to lead some considerations.

Anyway, is not interesting to calculate an average of the curves for the tests with the same load condition because the small difference between the singular pressure curve causes a flattening of the peaks (see appendix C). The pressure average turns out with peaks less marked than the singular curves. For this reason the pressure shape obtained in the pig experiments (Figure 5.7) is directly compared with the pressure graph of Figure 5.6.

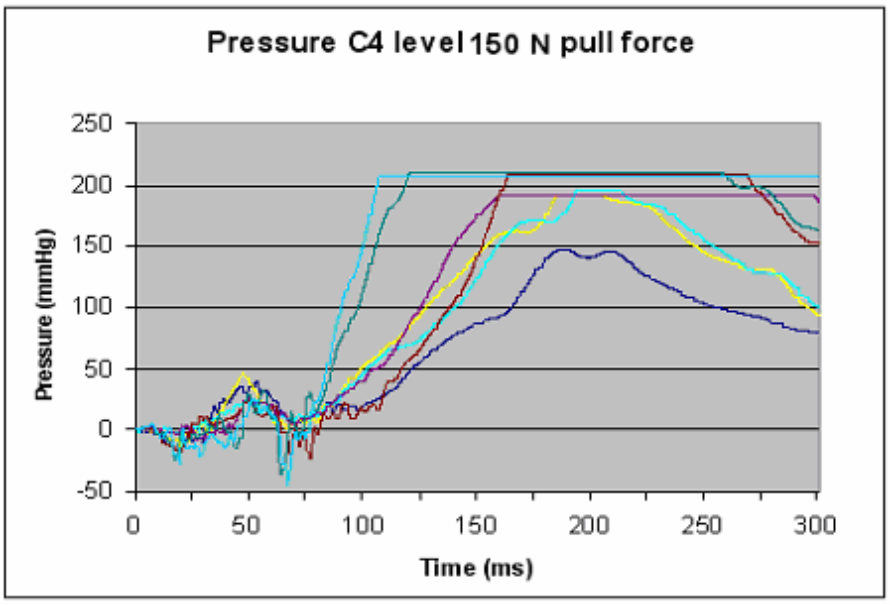

Figure 5.5 Pressure at C4 level versus time for all the test performed with a 150 N pull force

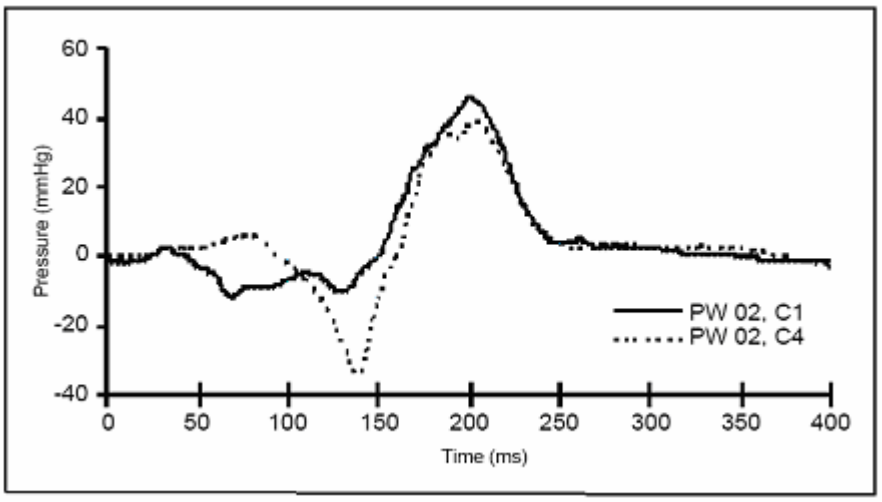

Figure 5.6 Average pressures at levels C1 and C4 versus time of six tests on the same pig at 150 N pull force

The corridor defined by the pressure curves obtained at level C4 in the neck prototype (Figure 5.5) is very similar to the average pressure of pig experiments shown in Figure 5.6 (dot line). The timing of different pressure events is not perfectly the same but this is not an important parameter because this lack of synchronisation is due to the differences of anatomy between pig and dummy neck. Comparing the acceleration values of Figure 5.3 with the acceleration curve shown in Figure 3.3 b) and considering the different pulling load is possible to explain the difference of peak magnitudes. This is not a relevant parameter either because the depression magnitude is in function of the load condition which is not the same and

in function of the anatomy. The most important result is that the pressure profiles obtained in the present work are almost identical to the profile of the pig experiments and consequently very similar to the other pressure curves obtained in the work presented in Figure 3.10.

The loading conditions on the head and spine in the experiments in these studies (pig experiments and present work) and in the real world whiplash extension motion differed to some extent. In this study, the head is pulled rearwards in one point close to the head centre of gravity while the vertebra T1 (torso) remained fixed. In a real accident, the torso is pushed forwards and the head and neck lags behind resulting in a swift extension motion of the neck. The inertial loading of the head and the neck segments go in opposite directions in the two cases. This probably means that the "s-shape" of the spine in the initial stage of the motion develops differently and that the pressure pattern during this phase may slightly differ. McConnell et al. (1993) undertook staged rear-impacts using volunteers and reported z-acceleration of the head due to the straightening of the chest-kyphosis during the acceleration of the torso. Since in this study the torso is not present, this type of head acceleration does not occur. However, the loading conditions and the head-neck motion in the experiments are considered to be close enough to a real accident situation to serve as a relevant model.

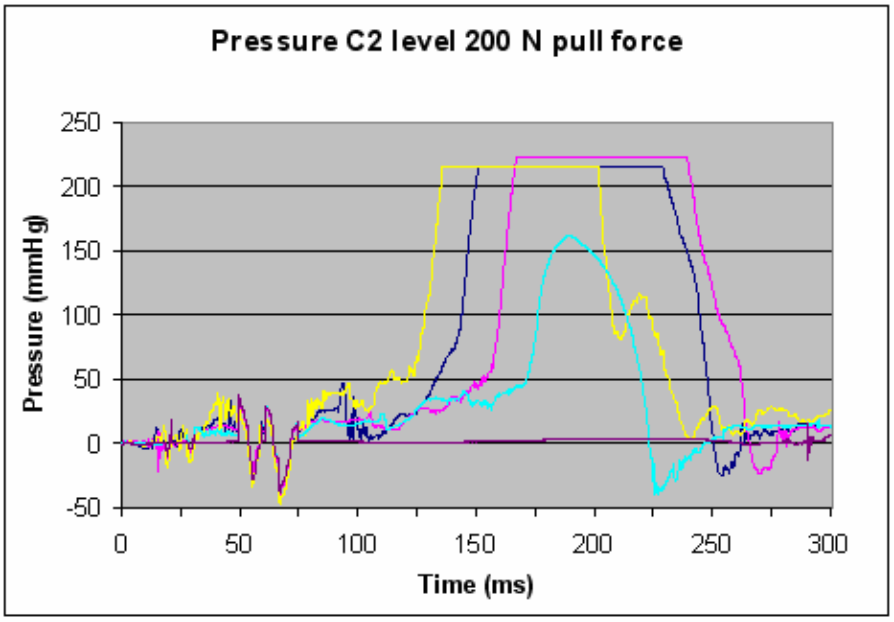

Figure 5.7 Pressure at C4 level versus time for all the test performed with a 200 N pull force

Figure 5.7 shows all the pressure curves at C2 level. In the first part the curves present the same interesting negative peaks, in particular the biggest one that occurs at circa 65ms is about -50mmHg. The positive pressure overflow after 150 ms is not a serious drawback, like explained above the cause is probably the instability of the

rubber pipe used to build the connection between internal and external volume. As for the level C4 also in this case the repeatability is acceptable.

The pressure readings have similar contours at the two levels (Figure 5.5 and 5.7) which indicates that the readings are not caused by artefacts like for instance direct mechanical loads (clamping) to the pressure transducers. The pressure transducers are insensitive to acceleration and since no correlation between the pressure readings and the acceleration readings can be found this artefact can be excluded. However, the presence of marked abrupt peaks in which there are more than 40mmHg of pressure difference during less than 5 ms which indicates that there is some artefact. In some tests, as it is possible to see in the appendix B, there are some pressure peaks in which the pressure drops almost vertically and this has a doubtful origin. It is not possible that these vertical sharp peaks are caused by hydrodynamic reasons, a change of sign so fast can be caused only by electrical problems in the piezoelectric pressure transducers.

6 Conclusions

This work has resulted in the simulating the pressure phenomena observed in the pigs during whiplash motion that could explain many of the most common neck injury symptoms caused by car collisions.

The recorded pressure pulses give support to the theoretical model presented in section 1.5 and to the experiments described in chapter 3.

With the new prototype, the expected significant negative pressure dip in the second phase of the traumatic neck motion has been presented and fast pressure equalisation after the swift extension motion has been reached

Using the monolithic spinal canal and the new connection between internal and external volume, the pressure peak obtained in this project were very similar to the previous research.

This simple model turned out to be auspicious and good result could be obtained, however in order to increase the repeatability some change could be taken into account. The silicone used results appropriated for the mechanical properties but further research could be leaded in finding a polymer with a higher adhesiveness. A possible alternative is to build the vertebrae in aluminium since the silicone adhesiveness is better with metals than with acetal plastic.

This work will contribute to more effective development and testing of new car designs for improved neck protection, primarily in rear-end collisions, but possibly also in other impact directions.

List of Firms

CG100 Silikongummi: Centri AB, Datavägen 6, S-17543 Järfälla, SE
Tel. +46 85 80 31 165

Elastosil RT: Wacker-Chemie, Hanns-Seidel-Platz 4 D-81737 Munchen, D
Tel. + 49 89 62 79 01
Fax + 49 89 62 79 17 71

P.U. ELI-FLEX 909: Eli-Chem Resins11 Sells Close,Guildford, Surrey, U.K
Tel : +44 (0) 1483 45 00 66
Fax: +44 (0) 1483 45 00 67

Primer G790: Cyncrona AB, Tomtbergavägen 2 SE-145 67 Norsborg, SE
Phone: +46 (0) 8 531 94 315
Fax: +46 (0) 8 531 94 310

7 References

Aldman, B. (1986): *An Analytical Approach to the Impact Biomechanics of Head and Neck*. Proc. 30th Annual AAAM Conf., pp. 439-454, LC 64-1965

Bathe K.-J. (1996): *Finite Element Procedures*. Prentice Hall, Englewood Cliffs, New Jersey.

Batson, O. V. (1957) : *The Vertebral Vein System*, Caldwell Lecture, 1956. The American Journal of Roengtenology, vol. 48, no.2, pp. 195-212

Boverket (1994): *Boverkets handbok om betongkonstruktioner BBK 94, Band 1, Konstruktion* (Boverket´s handbook on Concrete Structures BBK 94, Vol. 1 Design. In Swedish), Boverket, Byggavdelningen, Karlskrona, Sweden, 185 pp.

Breig, A. (1978): *Adverse Mechanical Tension in yhe Central Nervous System*. Almqvist & Wiksell Int., Stockholm, Sweden, ISBN 91-2200126-3

Carlsson, G.; Nilsson, S.; Nilsson-Ehle, A.; Norin, H.; Ysander, L.; Örtengren, R. (1985): *Neck Injuries in Rear End Car Collisions. Biomechanical considerations to improve head restraints.* Proc. Int. IRCOBI/AAAM Conf. Biomech. Of Imapcts, Göteborg, Sweden, pp. 277-289

Clemens, H.J. ; Burow, K. (1972): *Experimental Investigation on Injurt Mechanism Of Cervical Spine at Frontal and Rear-Front Vehicle Impacts.* Proc. 16th STAPP Car Crash Conf., SAE paper no. 720960, SAE Inc., New York, USA, LC 67-22372

Crocetti R. (2001): *On some Fatigue Problems Related to Steel Bridges.* Ph.D. Thesis. Department of Structural Engineering, Chalmers University of Technology, Publication no. 01:2, Göteborg, Sweden, 2001, 152 pp.

Deng, Y.-C. (1989): *Antropomorphic Dummy Neck Modelling and Injury Considerations.* Accid. Anal. & Prev. Vol. 21, No 1, pp.85-100

Foret-Bruno, J.Y.; Dauvilliers, F.; Tarriere, C.; P. Mack (1991): *Influence oh the Seat and Head Rest Stiffness on the Risk of Cervical Injuries in Rear Impact*. Proc. 13th ESV Conf. In Paris, France, paper 91-S8-W-19, NHTSA, USA, DOT HS 807 991

Hansson, H.-A.;Lövsund, P. ; Seeman, T.; Suneson, A.; Svensson, M.Y.; Säljö, A.; Örtengren, T. (1993): *Whiplash trauma and spinal ganglion dysfunction*. Manuscript in preparation

Hildingsson, C. (1991): *Soft Tissue Injury of the Cervical Spine.* Umeä University Medical Dissertations, New Series No 296, ISSN 0346-6612, ISBN 91-7174-546-7

Johansson M. (2000): *Nonlinear Finite-Element Analyses of Concrete Frame 3Corners*. ASCE Journal of Structural Engineering, Vol. 126, No. 2, February 2000, pp. 190-199.

Kapandji, I.A. (1974): *The Physiology of the Joints*, Volume Three. Churchill Livingstone, Edinbrugh, ISBN 0 443 01209 1

Lövsund, P.; Nygren, Å.; Salen, B.; Tingvall, C. (1988): *Neck Injuries in Rear End Collisions among Front and Rear Seat Occupants.* Proc. Int. IRCOBI Conference Biomech. of Impacts, Bergisch-Gladbach, F.R.G., pp. 319-325

Mc Connel, W. E.; Howard, R. P.; Guzman, H. M.; Bomar, J. B.; Raddin, J H.; Benedict, J. V.; Smith, L. H.; Hatsell, C. P. (1993): *Analysis of Human Test Subject Responded to Low Velocity Rear End Impacts.* SP-975, SAE paper no. 930889, pp. 21-30, SAE Inc., ISBN 1-56091-360-6

Mertz, H. J.; Patrick, L. M.(1967*): Investigation of the Kinematics and Kinetics oh Whiplash.* Proc. 11th STAPP Car Crash Conf., Anaheim, California, USA, pp. 267-317, SAE Inc., New York, USA, LC 67-22372

Mertz, H. J.; Patrick, L. M.(1971): *Strength and Response at the Human Neck*. Proc. Of 15th Stapp Car Crash Conf., pp. 207-255, SAE Inc., New York, LC 67-22372

Nygren, Å. (1984): *Injuries to Car Occupants – Some Aspects of the Interior Safety of Cars*. Akta Oto-Laryngologica, Supplement 395, Almqvist & Wiksell, Stockholm, Sweden, ISSN 0365-5237

O'Neill, B.; Haddon, W.; Kelley, A. B.; Sorenson, W. W. (1972): *Automobile Head Restraints: Frequency of Neck Injury Insurance Claims in Relation to the Presence of Head Restraints.* Am J Publ Health, Vol. 62, No. 3, pp. 399-406

Scott, M.W.; McConnel, W. E.; Guzman, H. M.; Howard, R. P.; Bomar, J.B.; Smith, H.L.; Benedict, J.V.; Raddin, J.H., Hatsell, C.P. (1993): *Comparison of Human and ATD Head Kinematics During Low-Speed Rearend Impacts.* SAE paper no. 930094, SAE/SP-93/945, SAE Inc., Warrendale, Phliadelphia, USA, ISBN 1-56091-330-4, LC 92-63144

Svensson, M.Y.; Örtengren, T.; Aldman, B.; Lövsund, P.; Seeman, T. (1989): *A Theoretical Model for and a Pilot Study Regarding Transient Pressure Changes in the Spinal Canal undeer Whip-lash Motion.* Dept. Of Injury Prevention, Chalmers University of Technology, Göteborg, Sweden, R 005

Svensson, (1992): *Rear-End Collisions – Development and validation of a new dummy-neck*- Thesis for the Degree of Lic. Of Eng., Dept. Of Injury Prevention, Chalmers University of Technology, S-412 96 Göteborg, Sweden.

Viano, D.C. (1992[a]): *Inluence of Seatback Angle on Occupant by the Seat in Rear-End Impacts.* SAE paper no. 922521, Proc. 36th STAPP Car Crash Conf., pp. 157-164, SAE/P-92/261, ISBN 1-56091-292-8

Viano, D.C. (1992[b]*): Restraint of a Belted or Unbelted Occupant by the Seat in Rear End Impacts.* SAE paper no. 922522, Proc. 36th STAPP Car Crash Conf., pp. 165-178, SAE/P-92/261, ISBN 1-56091-292-8

White, A.A.; Panjabi M.M. (1978): *Clinical Biomechanics of the Spine*. J.B. Lippincott Company, Philadelphia, USA, ISBN 0 397 50388 1, LC 78-15708

Appendix A

In this appendix there are the graphs for each tests performed with 150N. Pressure at level C4 and C6 are reported versus time, angular and linear displacements of centre of gravity of the head versus time and acceleration measured at level of centre of gravity versus time. In the first tests, due to some problems to the trigger system, some data were lost.

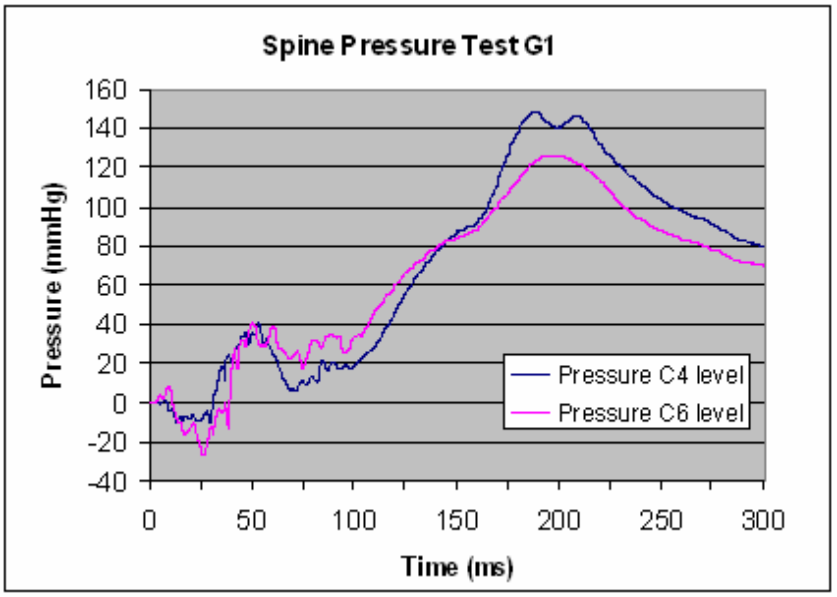

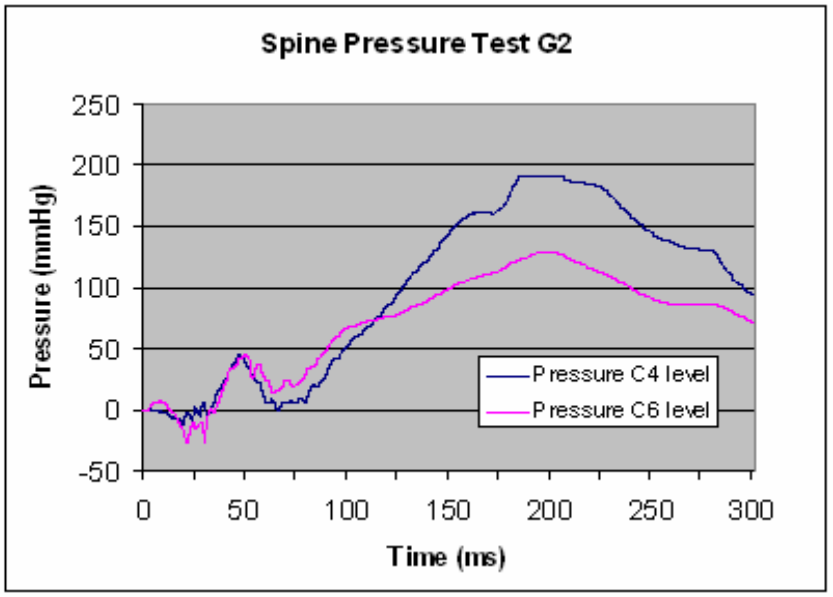

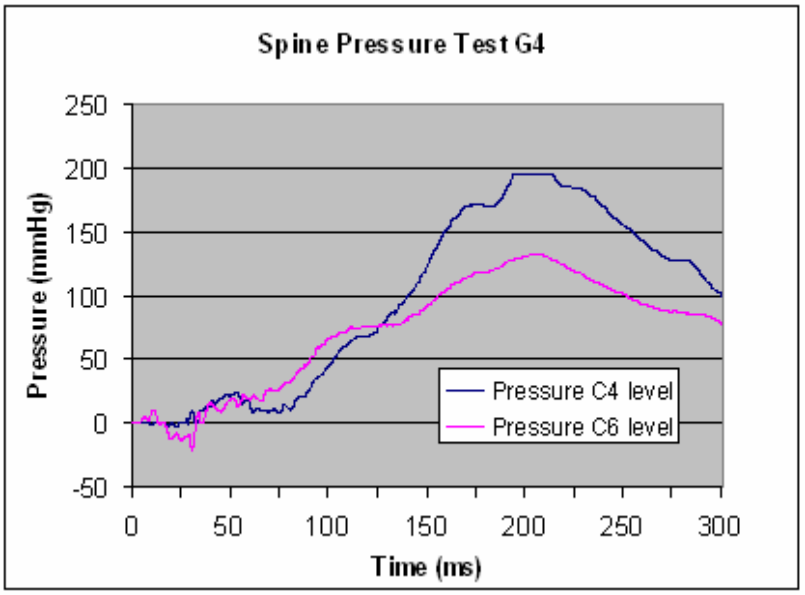
Spine Pressure Test G4
Pressure (mmHg)
250
200
150
100
50
0
-50
0
50
100
150
200
250
300
Time (ms)
Pressure C4 level
Pressure C6 level

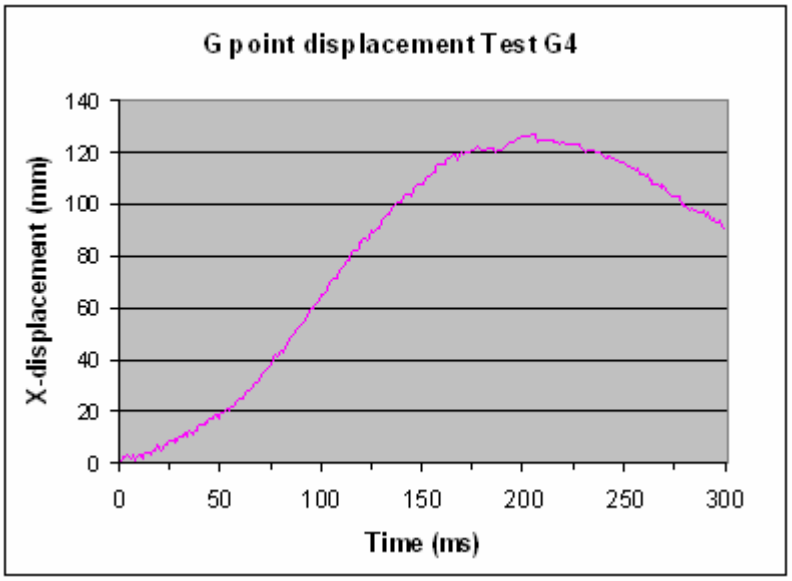
G point displacement Test G4
X-displacement (mm)
140
120
100
80
60
40
20
0
0
50
100
150
200
250
300
Time (ms)

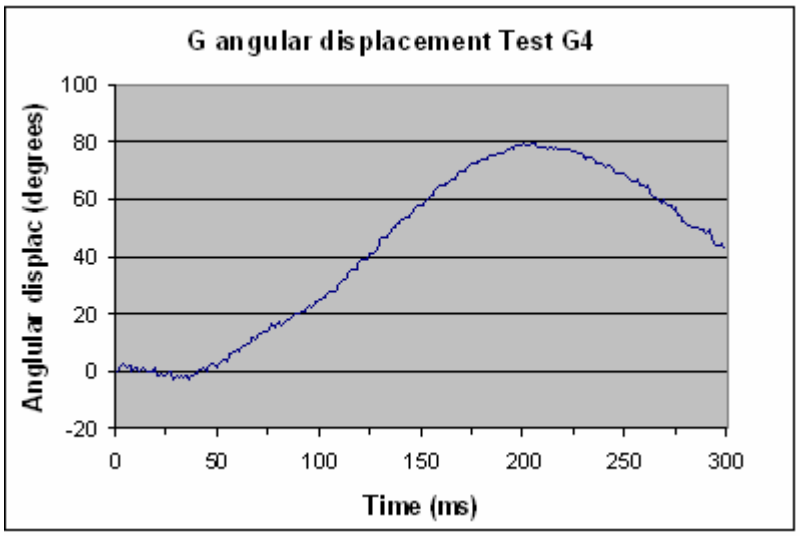
G angular displacement Test G4
Angular displac (degrees)
100
80
60
40
20
0
-20
0
50
100
150
200
250
300
Time (ms)

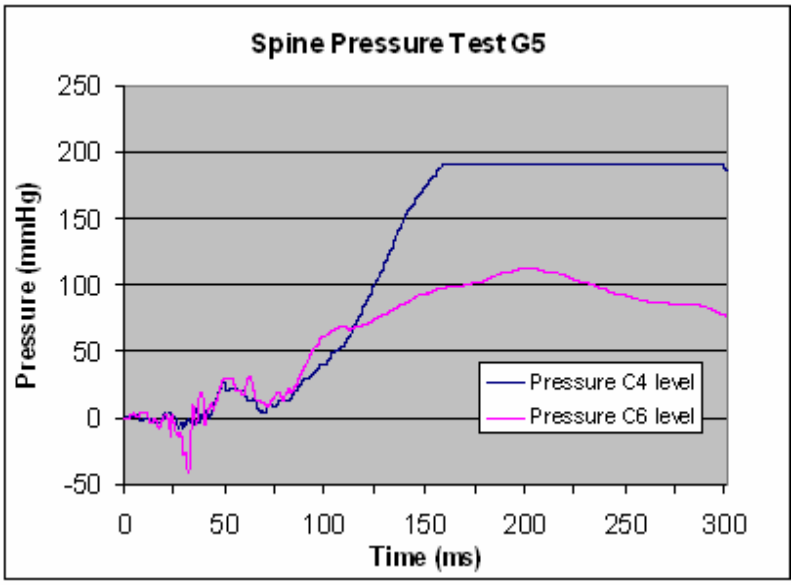
Spine Pressure Test G5
Pressure (mmHg)
250
200
150
100
50
0
-50
0
50
100
150
200
250
300
Time (ms)
Pressure C4 level
Pressure C6 level

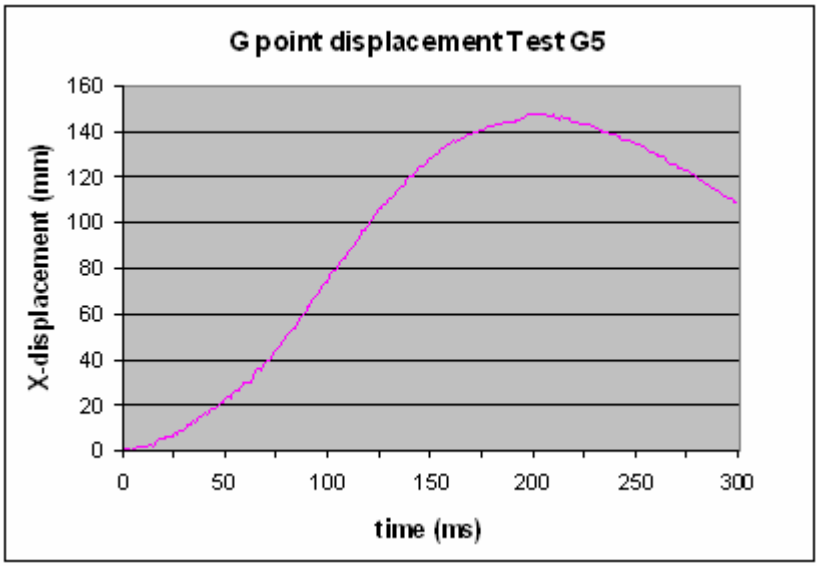
G point displacement Test G5
X-displacement (mm)
160
140
120
100
80
60
40
20
0
0
50
100
150
200
250
300
time (ms)

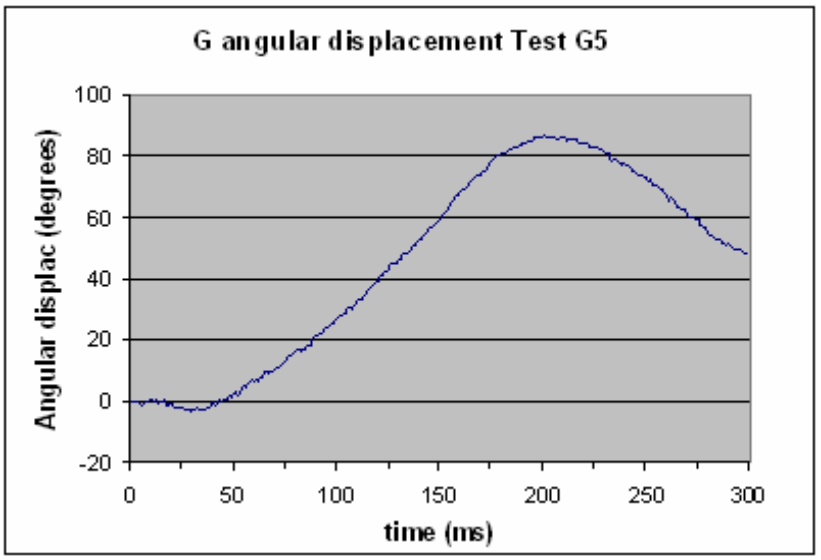
G angular displacement Test G5
Angular displac (degrees)
100
80
60
40
20
0
-20
0
50
100
150
200
250
300
time (ms)

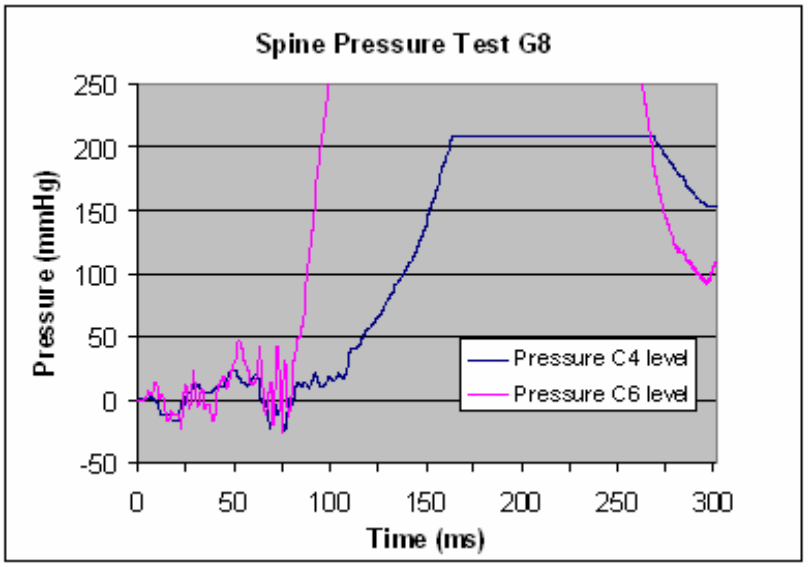
Spine Pressure Test G8
Pressure (mmHg)
250
200
150
100
50
0
-50
0
50
100
150
200
250
300
Time (ms)
Pressure C4 level
Pressure C6 level

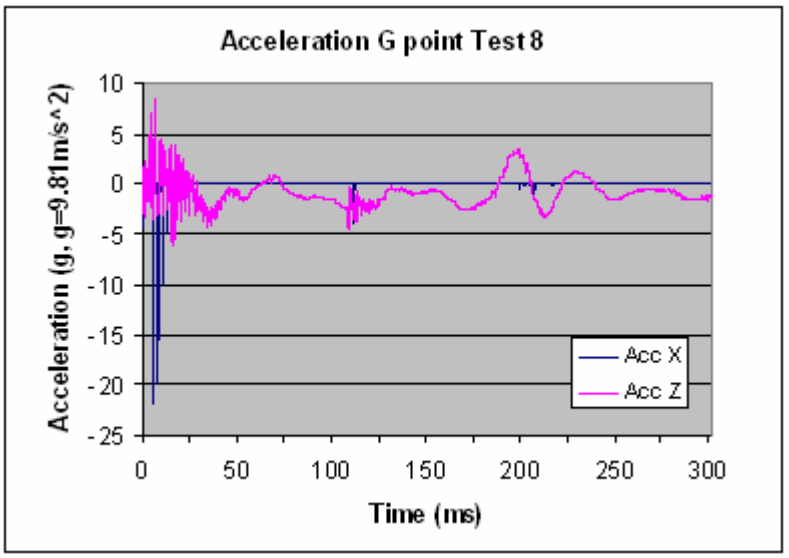
Acceleration G point Test 8
Acceleration (g, g=9.81m/s^2)
10
5
0
-5
-10
-15
-20
-25
0
50
100
150
200
250
300
Time (ms)
Acc X
Acc Z

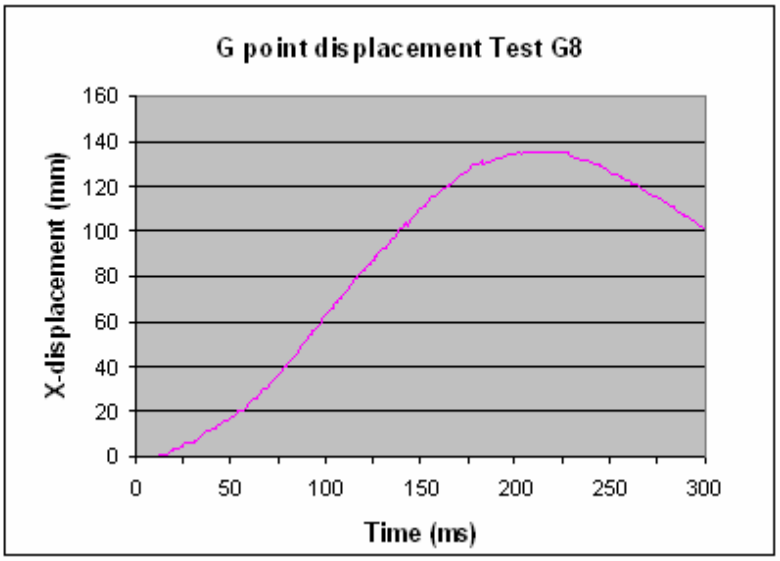
G point displacement Test G8
X-displacement (mm)
160
140
120
100
80
60
40
20
0
0
50
100
150
200
250
300
Time (ms)

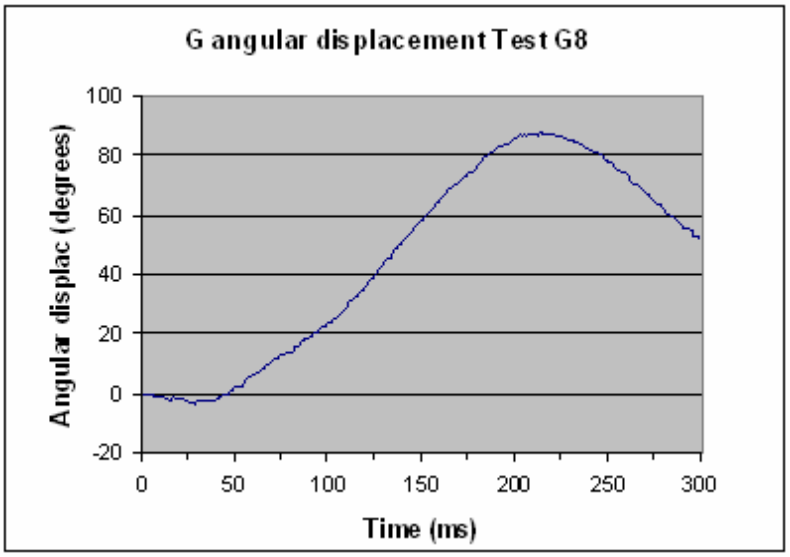
G angular displacement Test G8
Angular displac (degrees)
100
80
60
40
20
0
-20
0
50
100
150
200
250
300
Time (ms)

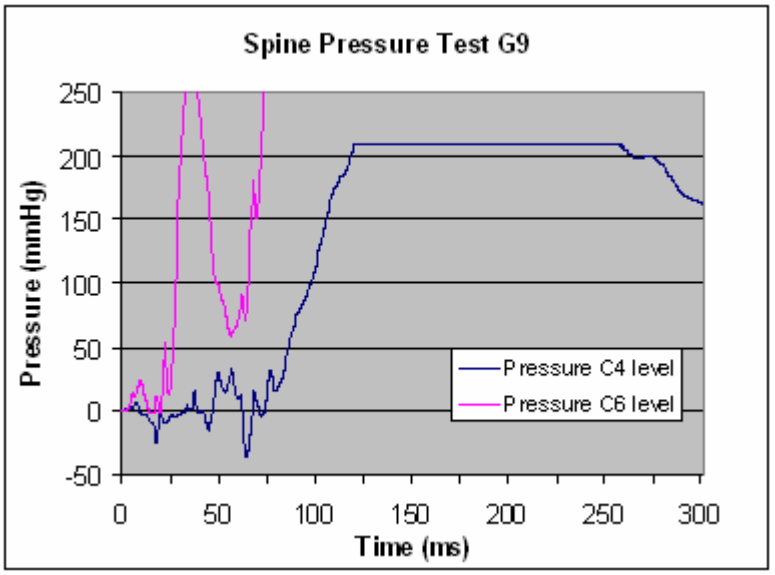
Spine Pressure Test G9
Pressure (mmHg)
250
200
150
100
50
0
-50
0
50
100
150
200
250
300
Time (ms)
Pressure C4 level
Pressure C6 level

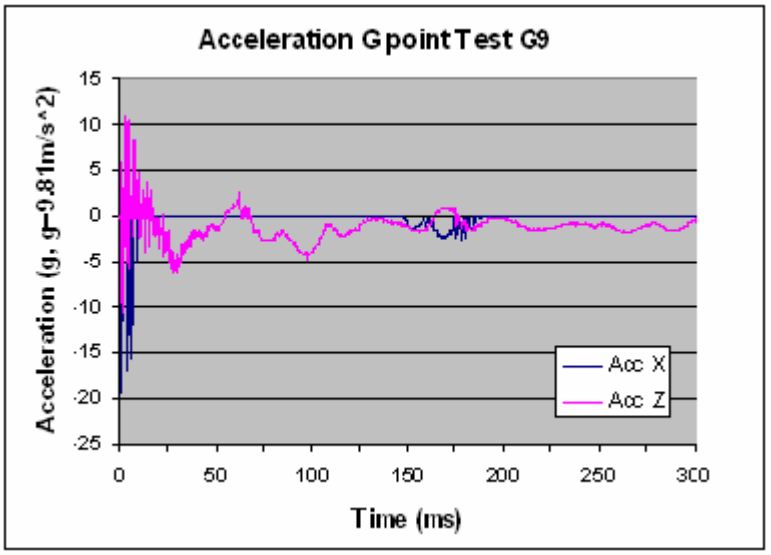
Acceleration G point Test G9
Acceleration (g, g=9.81m/s^2)
15
10
5
0
-5
-10
-15
-20
-25
0
50
100
150
200
250
300
Time (ms)
Acc X
Acc Z

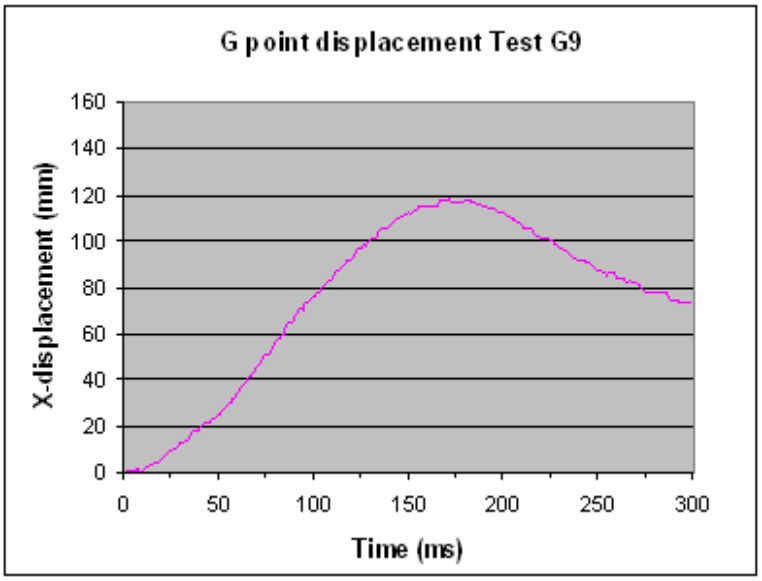
G point displacement Test G9
X-displacement (mm)
160
140
120
100
80
60
40
20
0
0
50
100
150
200
250
300
Time (ms)

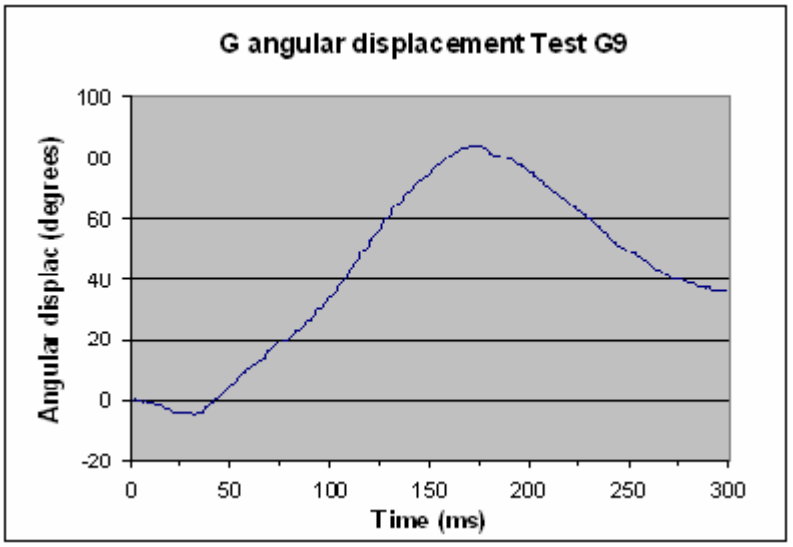
G angular displacement Test G9
Angular displac (degrees)
100
00
60
40
20
0
-20
0
50
100
150
200
250
300
Time (ms)

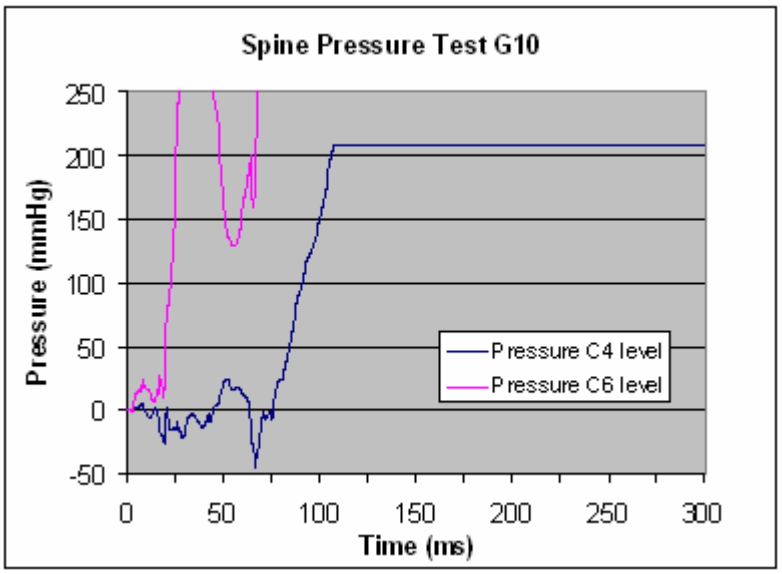
Spine Pressure Test G10
Pressure (mmHg)
250
200
150
100
50
0
-50
0
50
100
150
200
250
300
Time (ms)
Pressure C4 level
Pressure C6 level

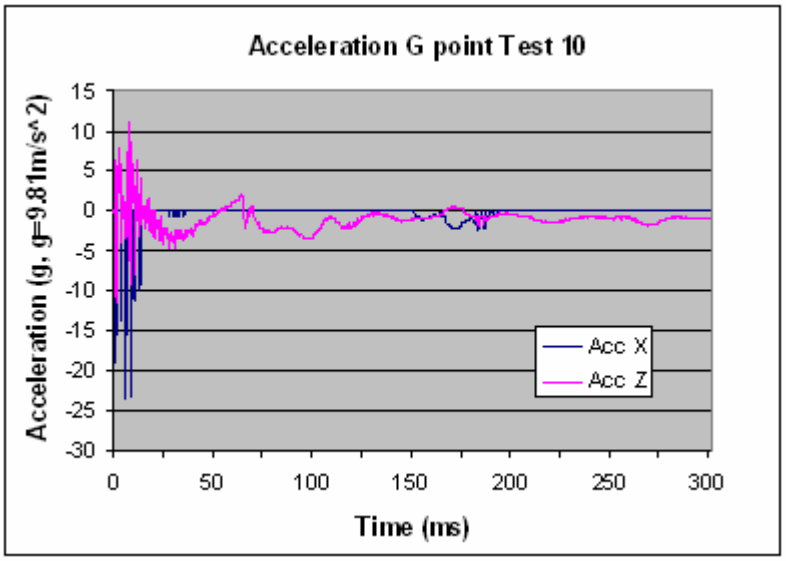
Acceleration G point Test 10
Acceleration (g, g=9.81m/s^2)
15
10
5
0
-5
-10
-15
-20
-25
-30
0
50
100
150
200
250
300
Time (ms)
Acc X
Acc Z

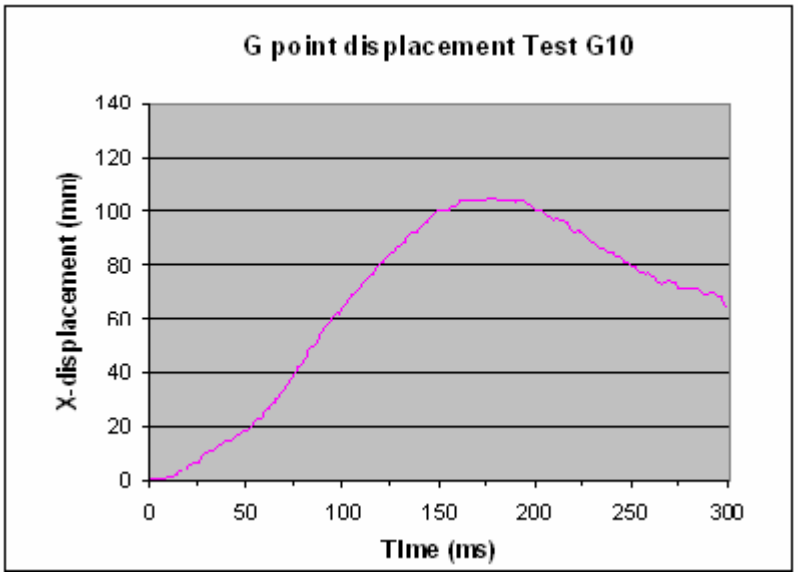
G point displacement Test G10
X-displacement (mm)
140
120
100
80
60
40
20
0
0
50
100
150
200
250
300
Time (ms)

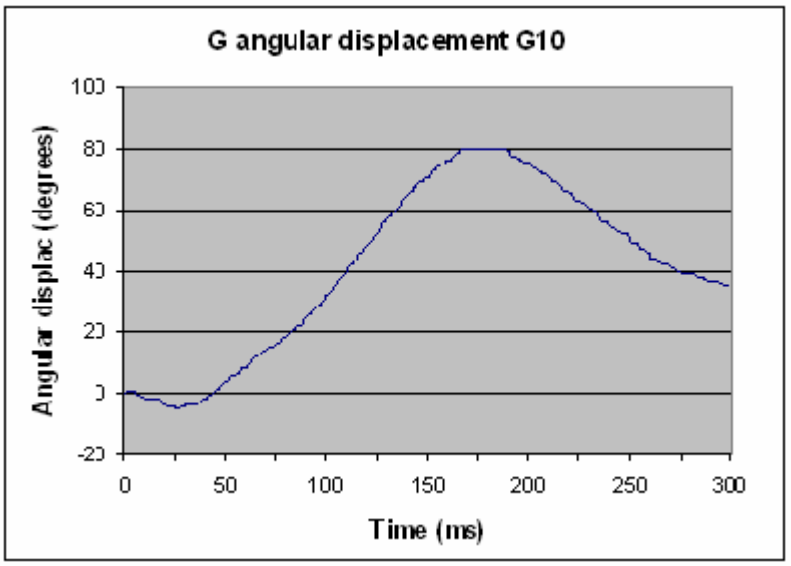
G angular displacement G10
Angular displac (degrees)
100
80
60
40
20
0
-20
0
50
100
150
200
250
300
Time (ms)

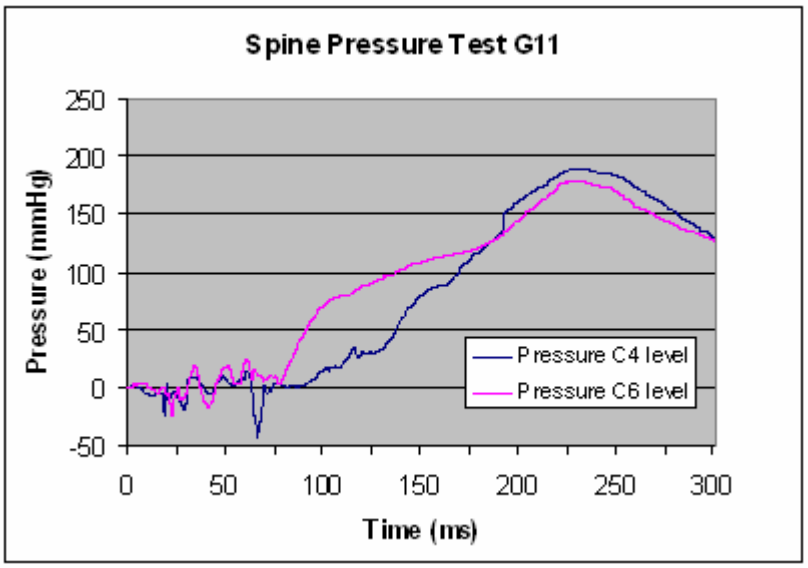
Spine Pressure Test G11
Pressure (mmHg)
250
200
150
100
50
0
-50
0
50
100
150
200
250
300
Time (ms)
Pressure C4 level
Pressure C6 level

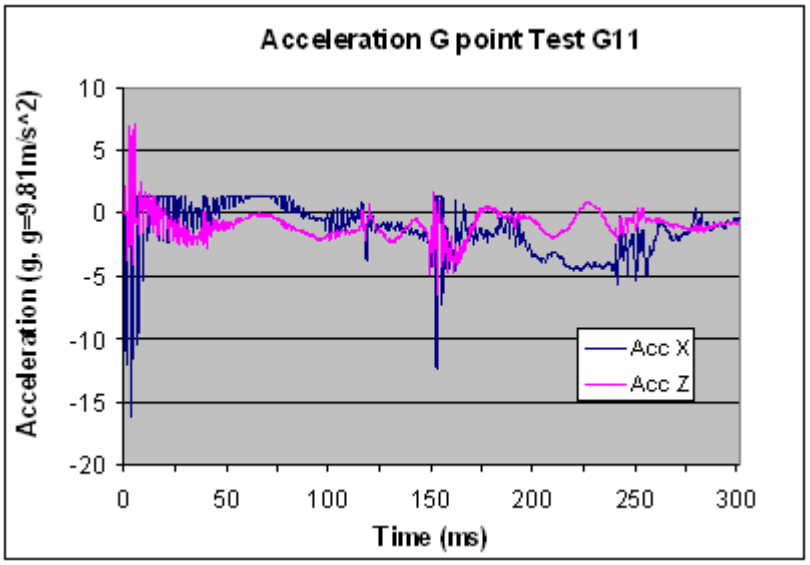
Acceleration G point Test G11
Acceleration (g, g=9.81m/s^2)
10
5
0
-5
-10
-15
-20
0
50
100
150
200
250
300
Time (ms)
Acc X
Acc Z

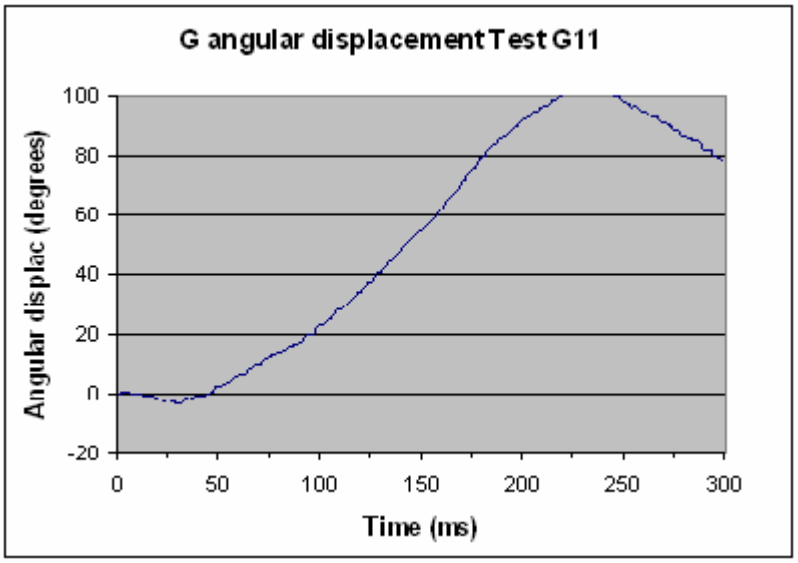
G angular displacement Test G11
Angular displac (degrees)
100
80
60
40
20
0
-20
0
50
100
150
200
250
300
Time (ms)

Appendix B

In this appendix there are the graphs for each tests performed with 200N. Pressure at level C2, C4 and C6 are reported versus time, angular and linear displacements of centre of gravity of the head versus time and acceleration measured at level of centre of gravity versus time.

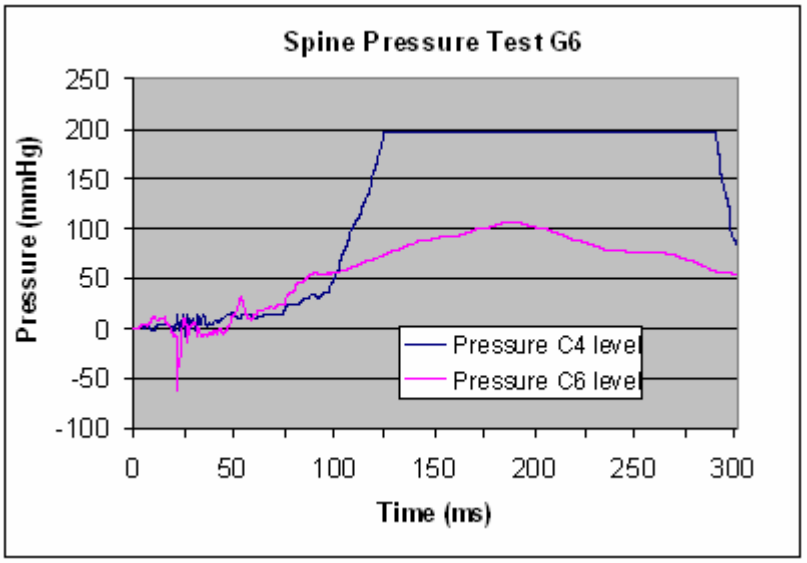

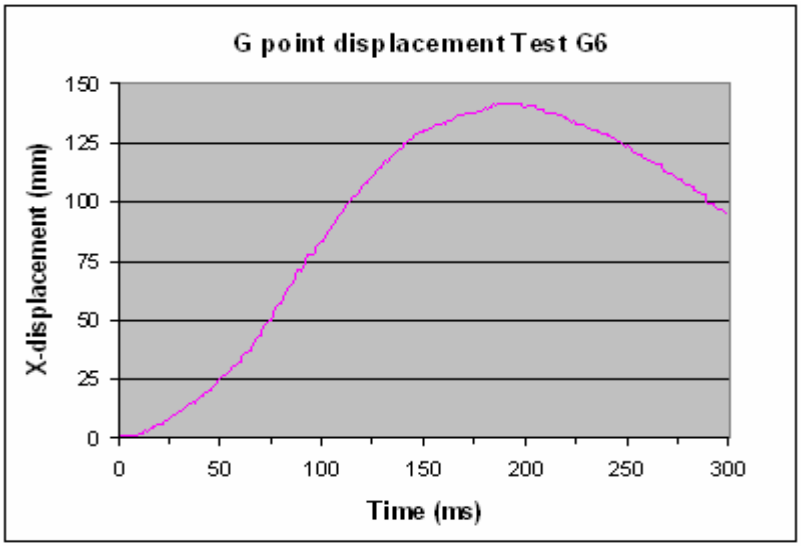

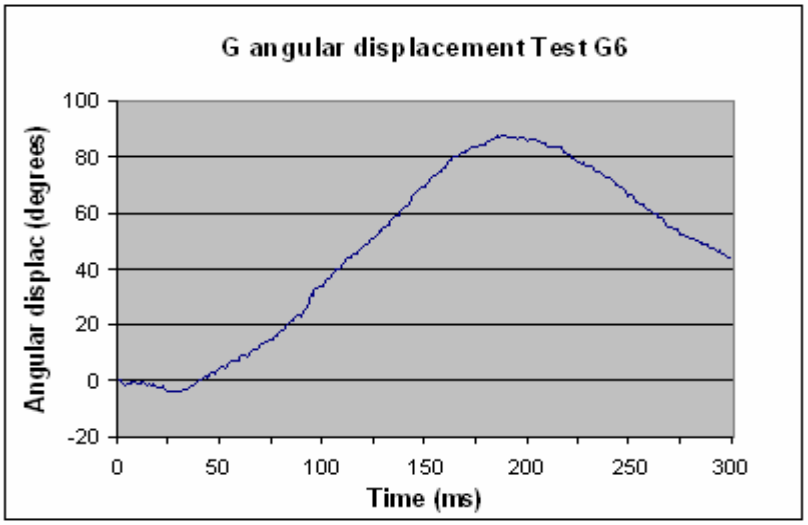
G angular displacement Test G6
Angular displac (degrees)
100
80
60
40
20
0
-20
0
50
100
150
200
250
300
Time (ms)

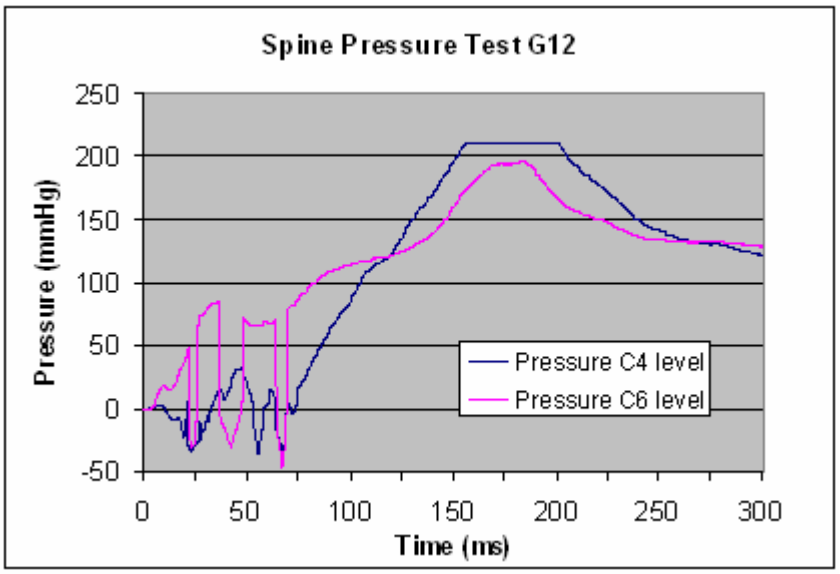
Spine Pressure Test G12
Pressure (mmHg)
250
200
150
100
50
0
-50
0
50
100
150
200
250
300
Time (ms)
Pressure C4 level
Pressure C6 level

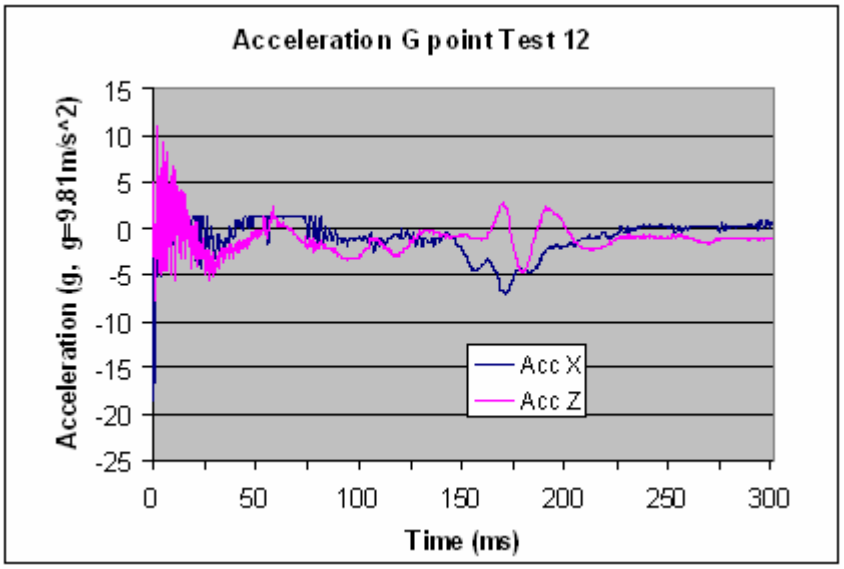
Acceleration G point Test 12
Acceleration (g, g=9.81m/s^2)
15
10
5
0
-5
-10
-15
-20
-25
0
50
100
150
200
250
300
Time (ms)
Acc X
Acc Z

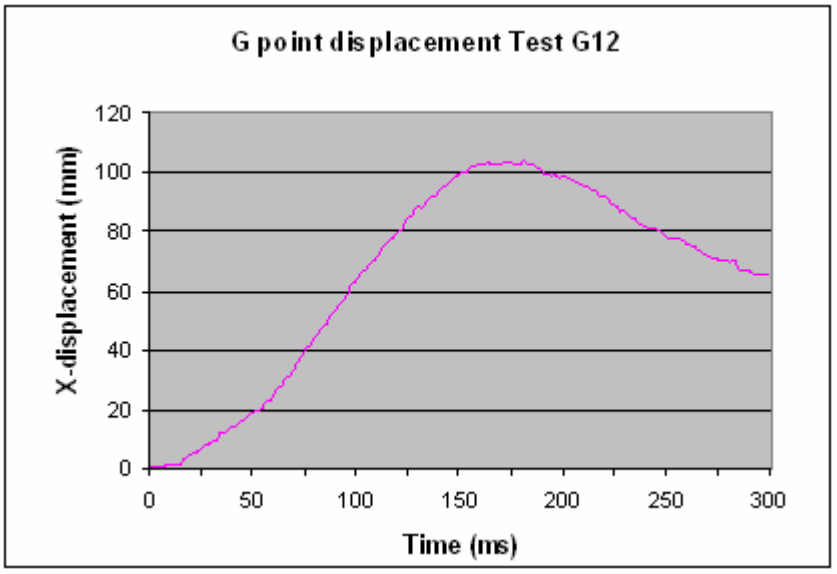
G point displacement Test G12
X-displacement (mm)
120
100
80
60
40
20
0
0
50
100
150
200
250
300
Time (ms)

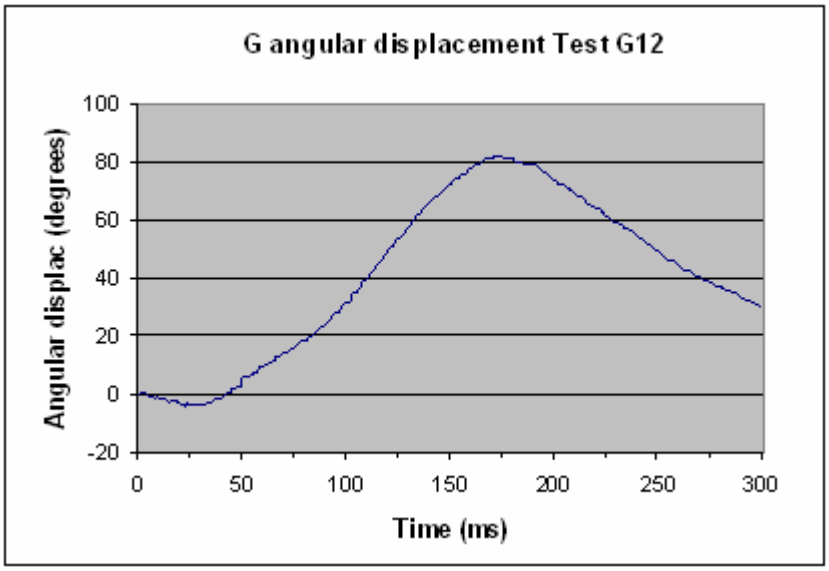
G angular displacement Test G12
Angular displac (degrees)
100
80
60
40
20
0
-20
0
50
100
150
200
250
300
Time (ms)

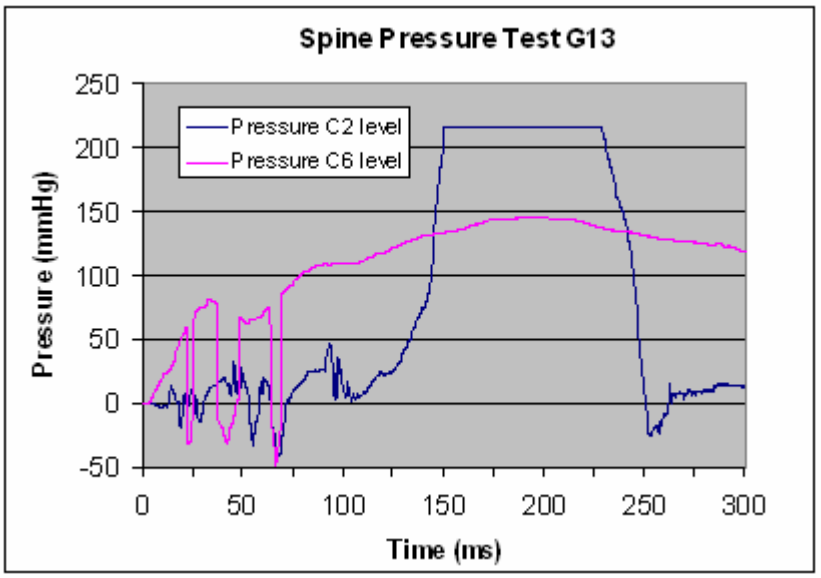
Spine Pressure Test G13
Pressure (mmHg)
250
200
150
100
50
0
-50
Pressure C2 level
Pressure C6 level
0
50
100
150
200
250
300
Time (ms)

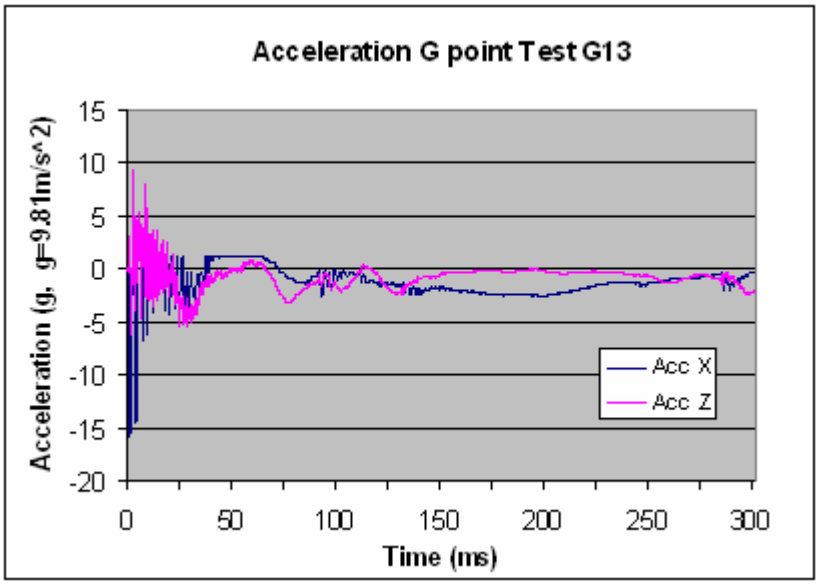
Acceleration G point Test G13
Acceleration (g, g=9.81m/s^2)
15
10
5
0
-5
-10
-15
-20
0
50
100
150
200
250
300
Time (ms)
Acc X
Acc Z

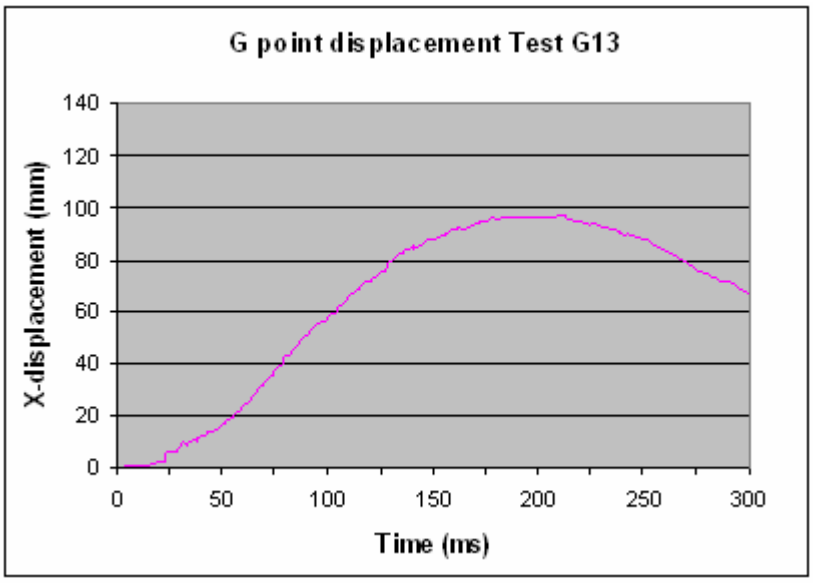
G point displacement Test G13
X-displacement (mm)
140
120
100
80
60
40
20
0
0
50
100
150
200
250
300
Time (ms)

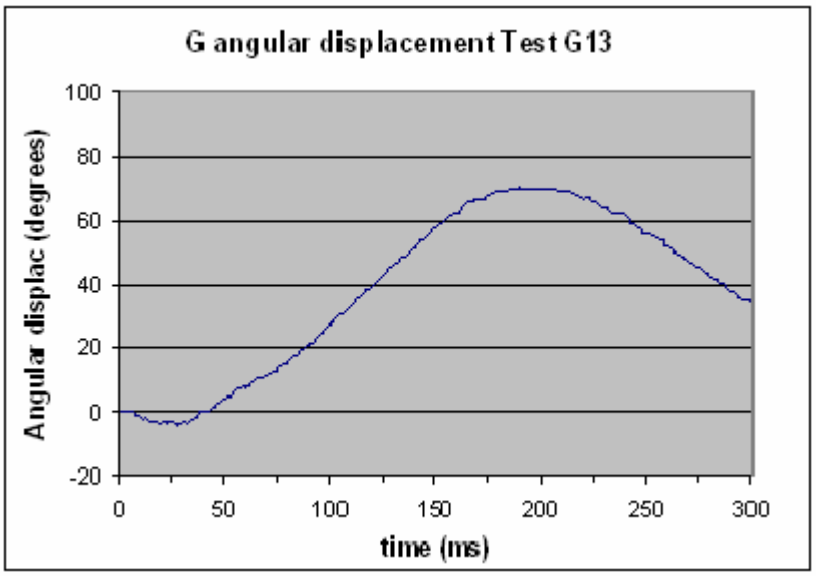
G angular displacement Test G13
Angular displac (degrees)
100
80
60
40
20
0
-20
0
50
100
150
200
250
300
time (ms)

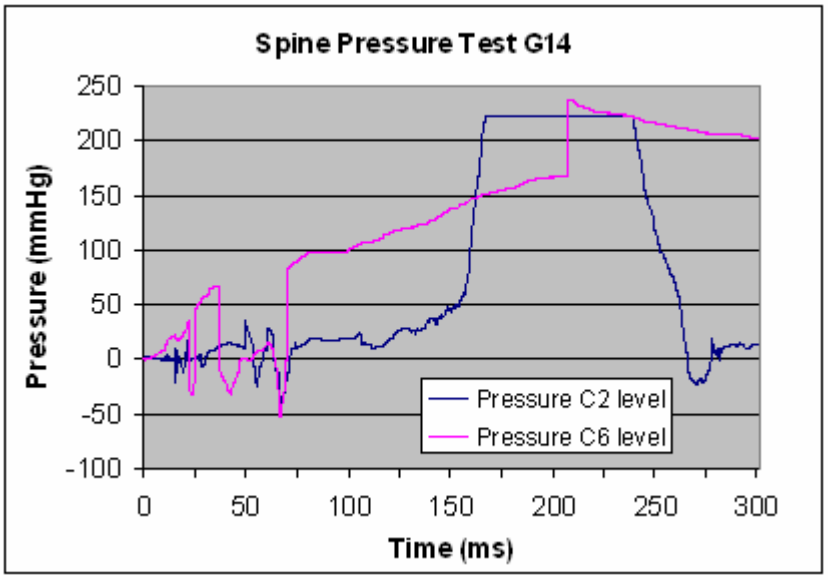
Spine Pressure Test G14
Pressure (mmHg)
250
200
150
100
50
0
-50
-100
0
50
100
150
200
250
300
Time (ms)
Pressure C2 level
Pressure C6 level

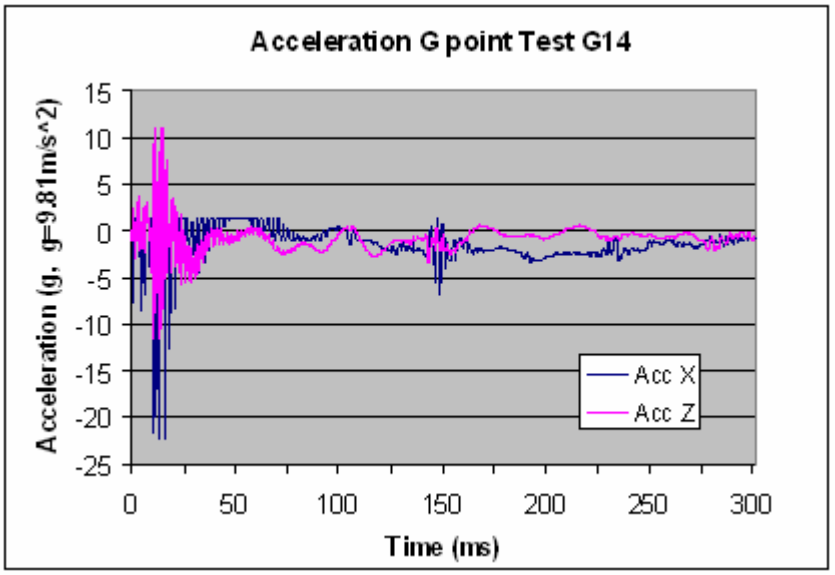
Acceleration G point Test G14
Acceleration (g, g=9.81m/s^2)
15
10
5
0
-5
-10
-15
-20
-25
0
50
100
150
200
250
300
Time (ms)
Acc X
Acc Z

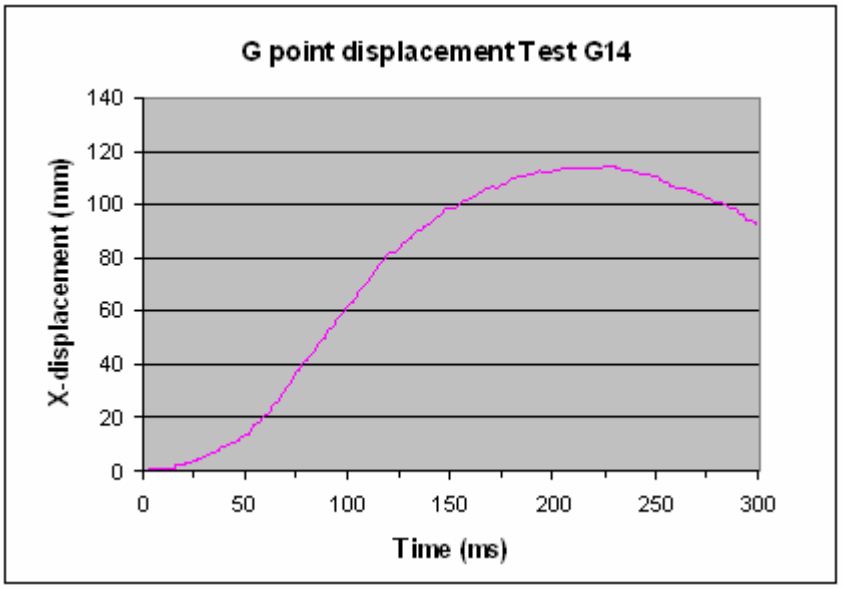
G point displacement Test G14
X-displacement (mm)
140
120
100
80
60
40
20
0
0
50
100
150
200
250
300
Time (ms)

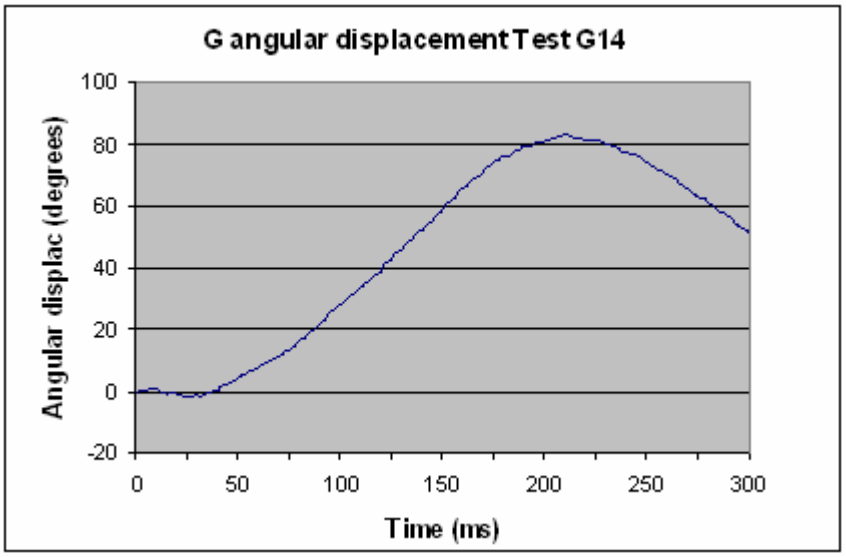
G angular displacement Test G14
Angular displac (degrees)
100
80
60
40
20
0
-20
0
50
100
150
200
250
300
Time (ms)

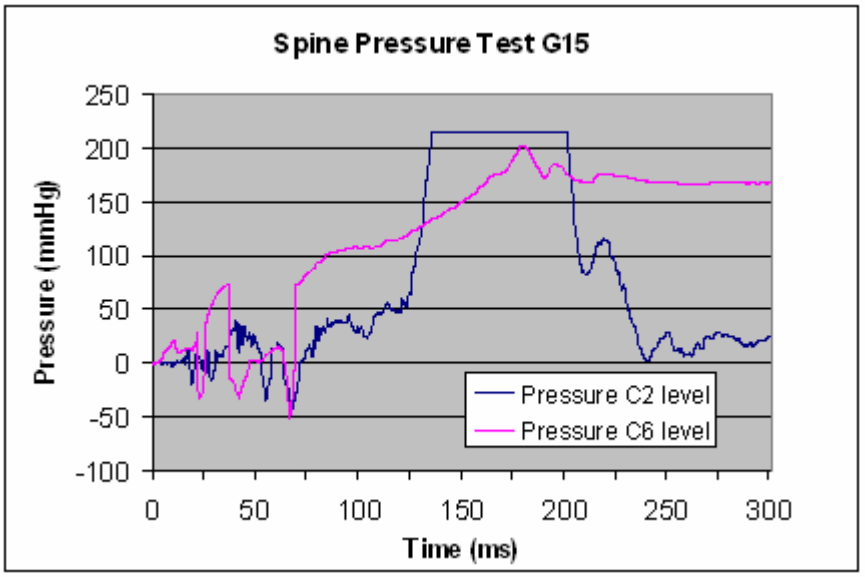
Spine Pressure Test G15
Pressure (mmHg)
250
200
150
100
50
0
-50
-100
0
50
100
150
200
250
300
Time (ms)
Pressure C2 level
Pressure C6 level

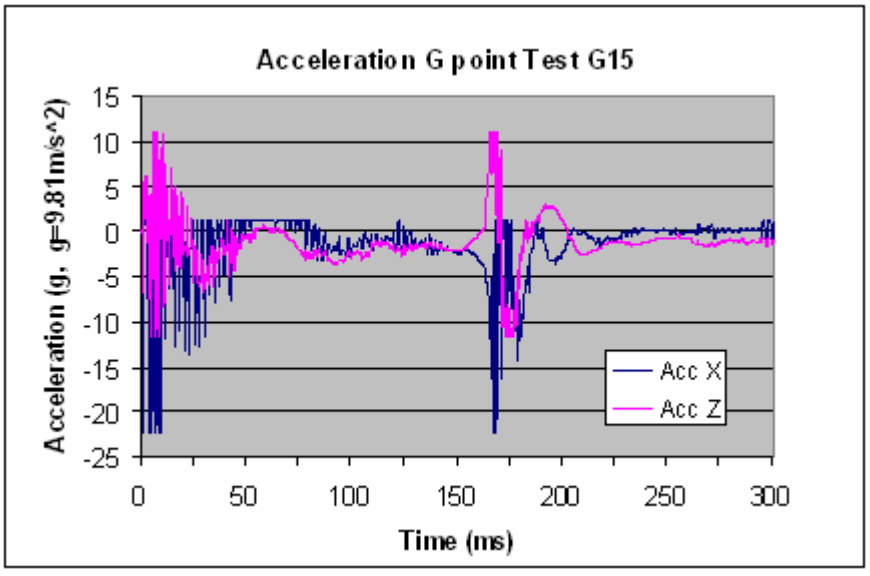
Acceleration G point Test G15
Acceleration (g, g=9.81m/s^2)
15
10
5
0
-5
-10
-15
-20
-25
0
50
100
150
200
250
300
Time (ms)
Acc X
Acc Z

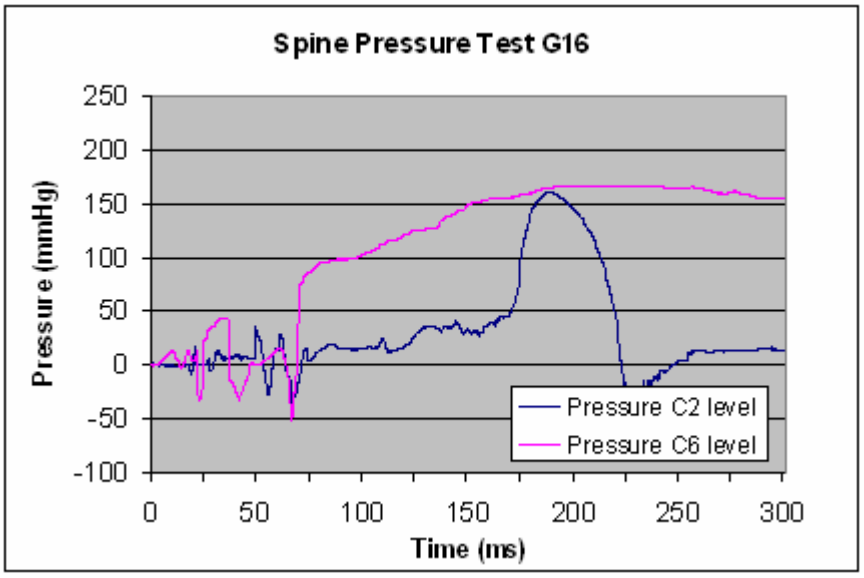
Spine Pressure Test G16
Pressure (mmHg)
250
200
150
100
50
0
-50
-100
0
50
100
150
200
250
300
Time (ms)
Pressure C2 level
Pressure C6 level

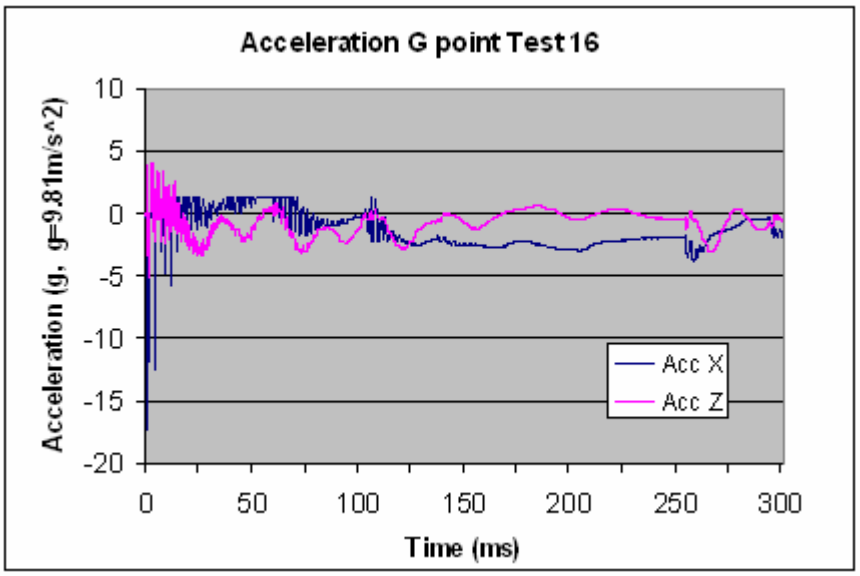
Acceleration G point Test 16
Acceleration (g, g=9.81m/s^2)
10
5
0
-5
-10
-15
-20
0
50
100
150
200
250
300
Time (ms)
Acc X
Acc Z

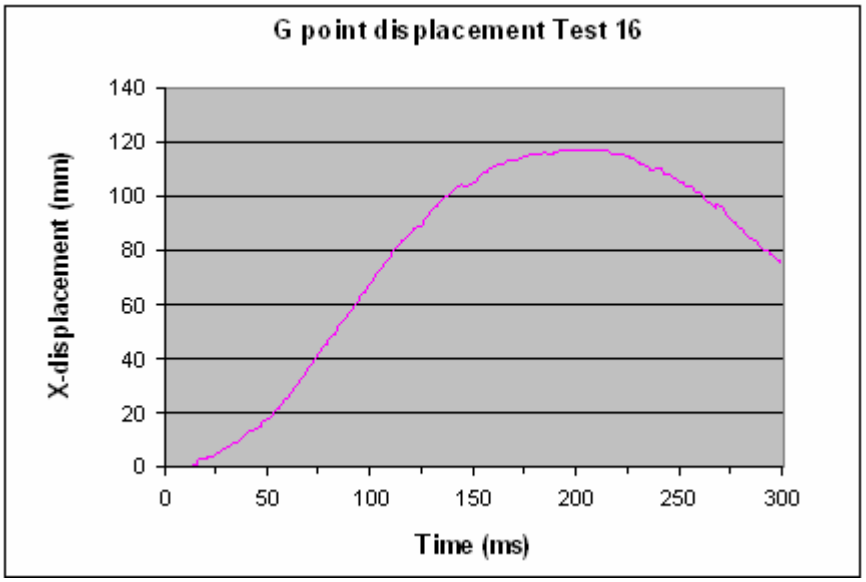
G point displacement Test 16
X-displacement (mm)
140
120
100
80
60
40
20
0
0
50
100
150
200
250
300
Time (ms)

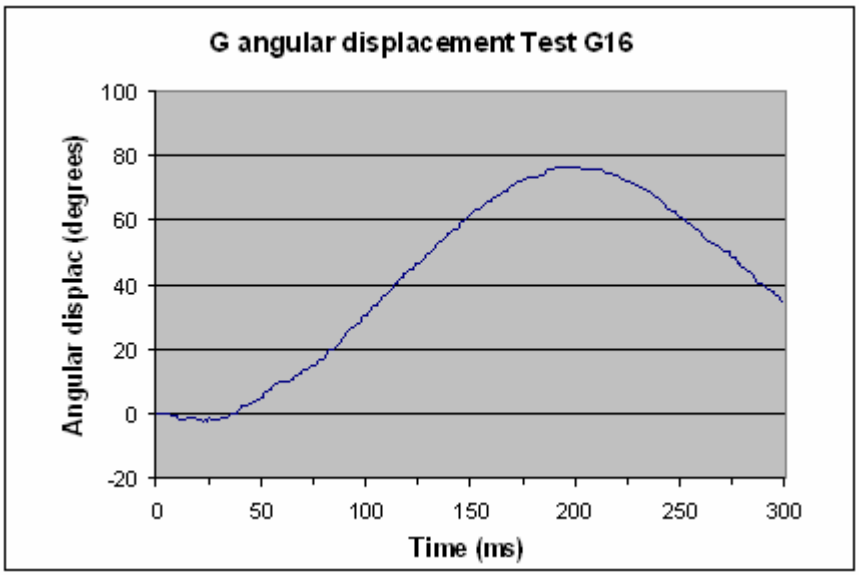
G angular displacement Test G16
Angular displac (degrees)
100
80
60
40
20
0
-20
0
50
100
150
200
250
300
Time (ms)

Appendix C

In this appendix pressure and displacements of the tests performed in the some conditions are shown on the some graphs. A pressure average is plotted at all the three level and for the average at C6 level test G9 and test G10 were excluded.

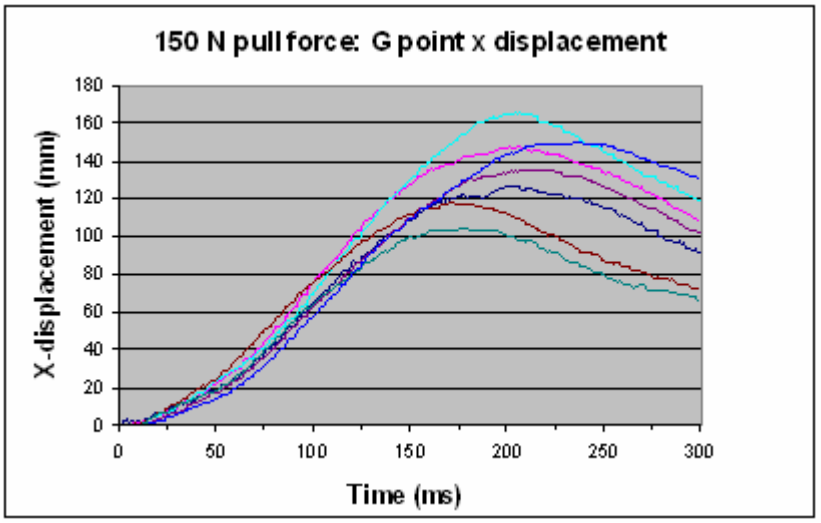

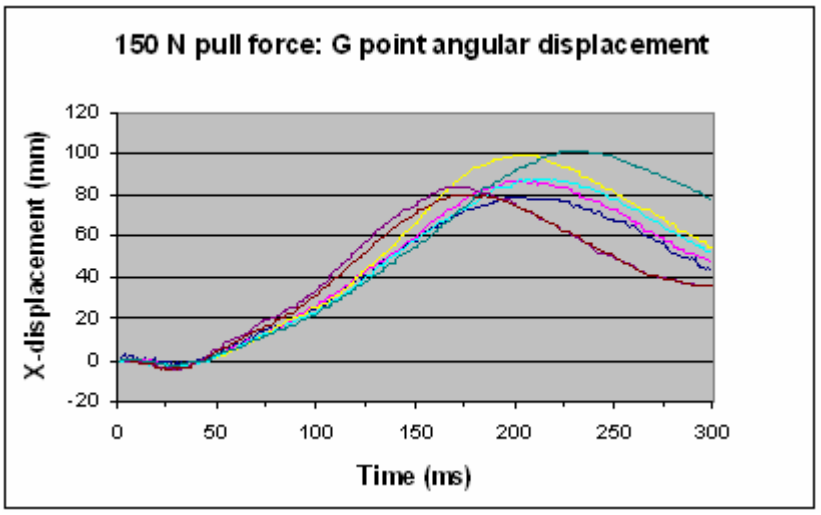

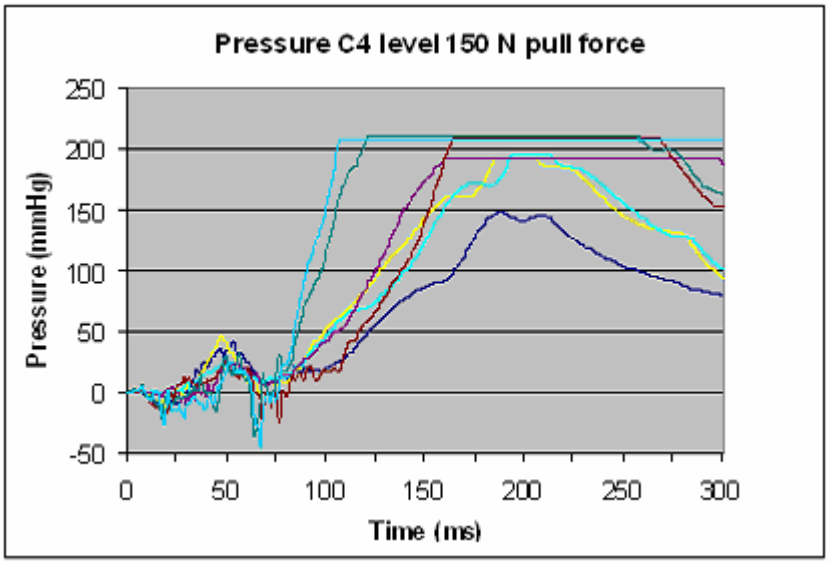
Pressure C4 level 150 N pull force
Pressure (mmHg)
250
200
150
100
50
0
-50
0
50
100
150
200
250
300
Time (ms)

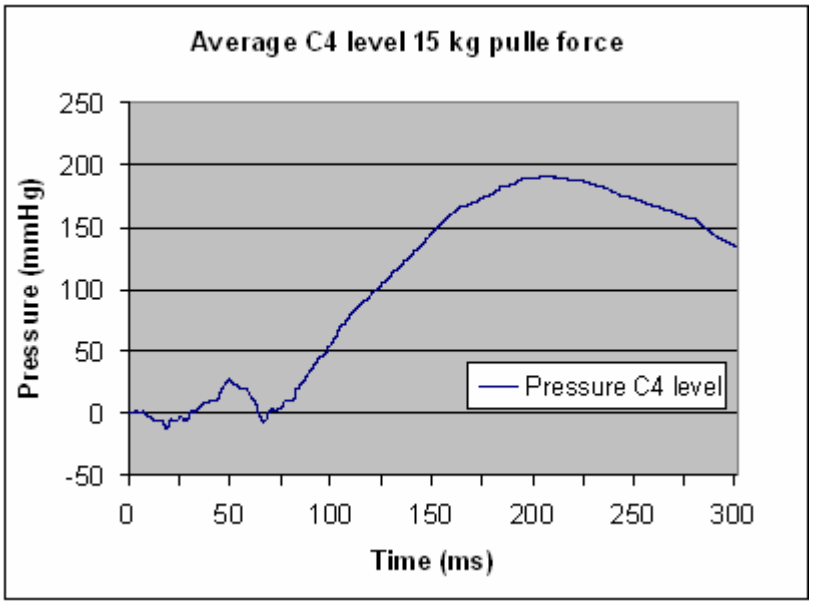
Average C4 level 15 kg pulle force
Pressure (mmHg)
250
200
150
100
50
0
-50
Pressure C4 level
0
50
100
150
200
250
300
Time (ms)

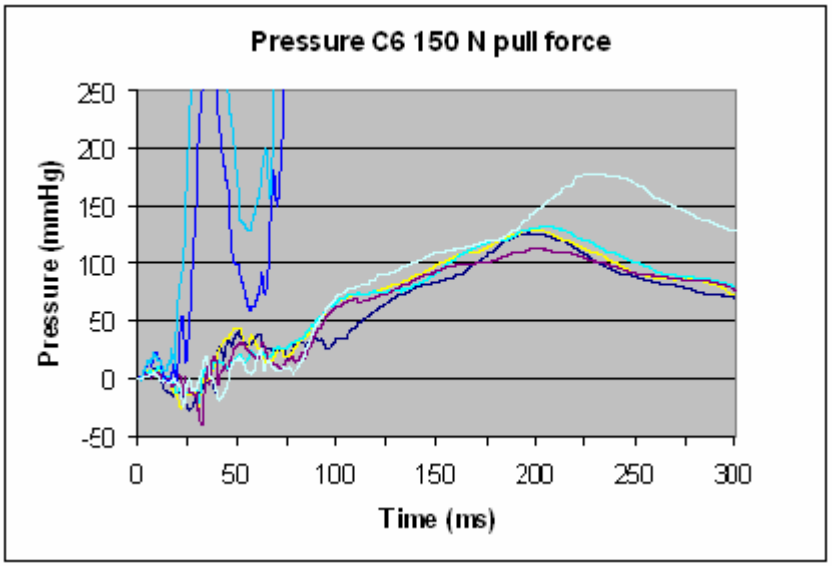
Pressure C6 150 N pull force
Pressure (mmHg)
250
200
150
100
50
0
-50
0
50
100
150
200
250
300
Time (ms)

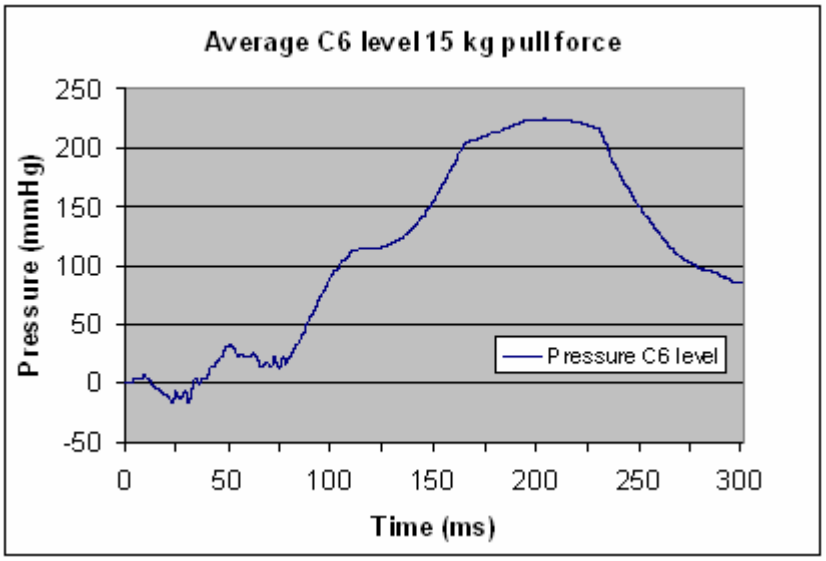
Average C6 level 15 kg pull force
Pressure (mmHg)
250
200
150
100
50
0
-50
0
50
100
150
200
250
300
Time (ms)
Pressure C6 level

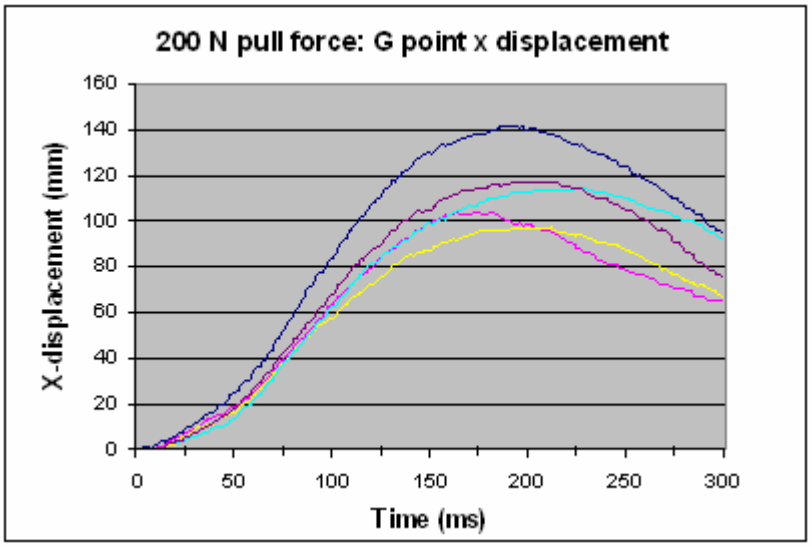
200 N pull force: G point x displacement
X-displacement (mm)
160
140
120
100
80
60
40
20
0
0
50
100
150
200
250
300
Time (ms)

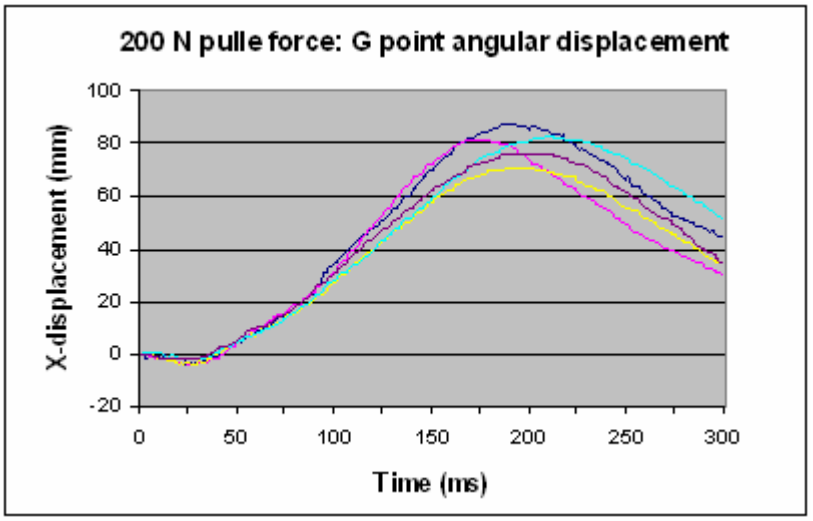
200 N pulle force: G point angular displacement
X-displacement (mm)
100
80
60
40
20
0
-20
0
50
100
150
200
250
300
Time (ms)

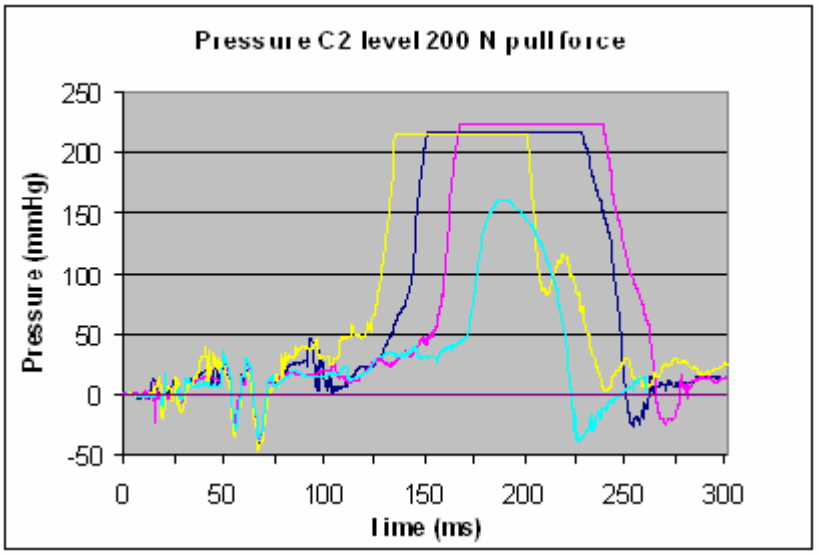
Pressure C2 level 200 N pull force
Pressure (mmHg)
250
200
150
100
50
0
-50
0
50
100
150
200
250
300
Time (ms)

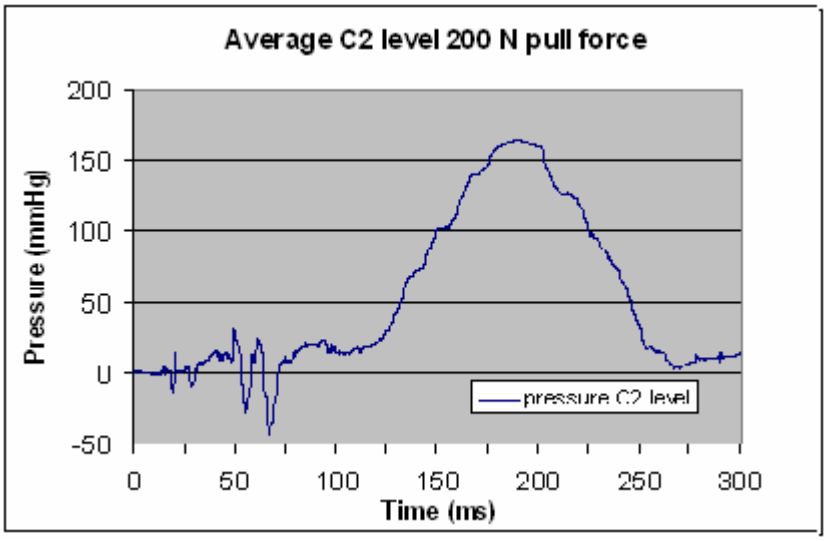
Average C2 level 200 N pull force
Pressure (mmHg)
200
150
100
50
0
-50
0
50
100
150
200
250
300
Time (ms)
pressure C2 level

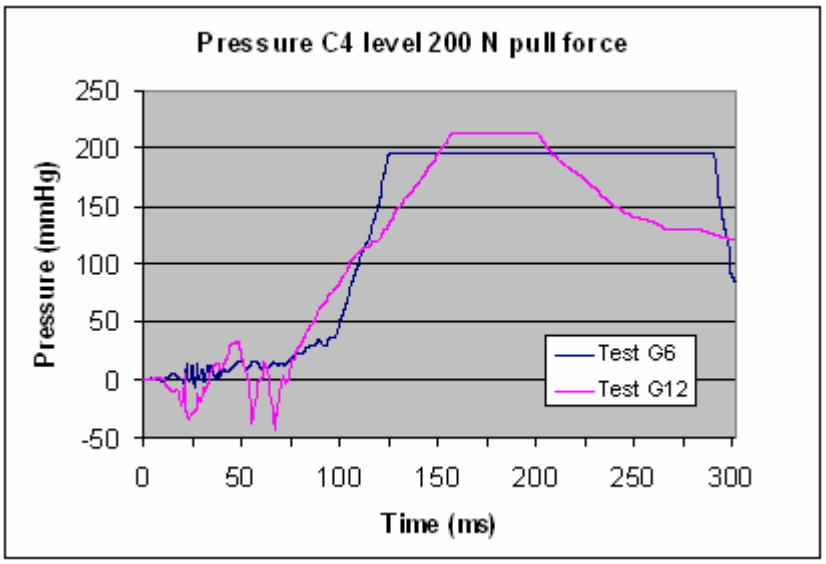
Pressure C4 level 200 N pull force
Pressure (mmHg)
250
200
150
100
50
0
-50
0
50
100
150
200
250
300
Time (ms)
Test G6
Test G12

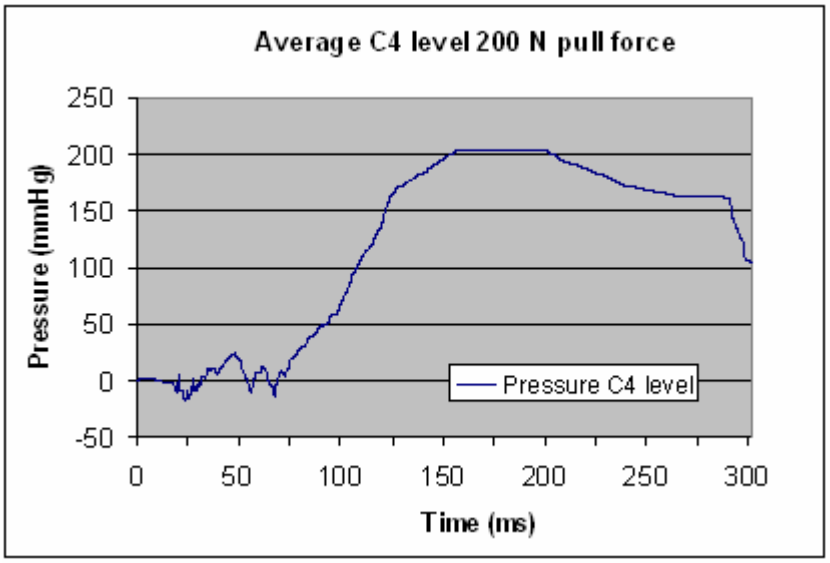
Average C4 level 200 N pull force
Pressure (mmHg)
250
200
150
100
50
0
-50
0
50
100
150
200
250
300
Time (ms)
Pressure C4 level

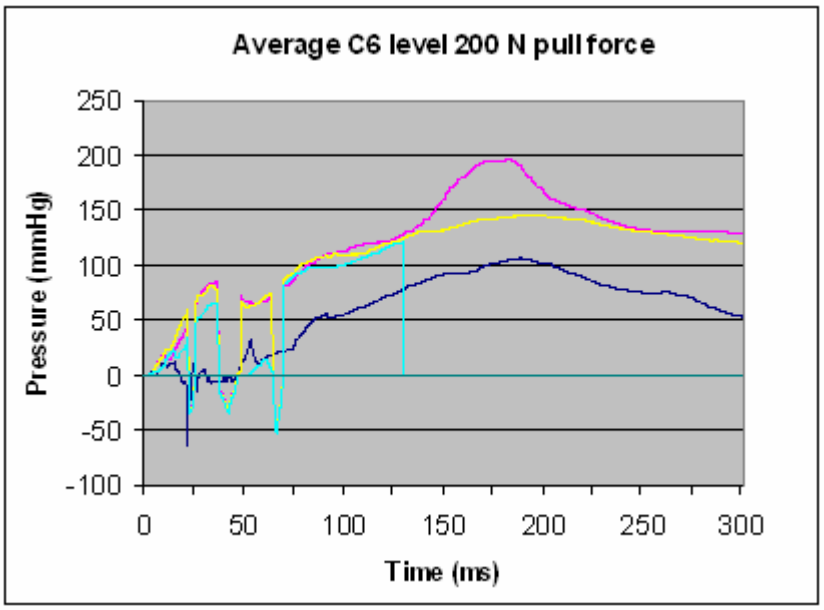
Average C6 level 200 N pull force
Pressure (mmHg)
250
200
150
100
50
0
-50
-100
0
50
100
150
200
250
300
Time (ms)

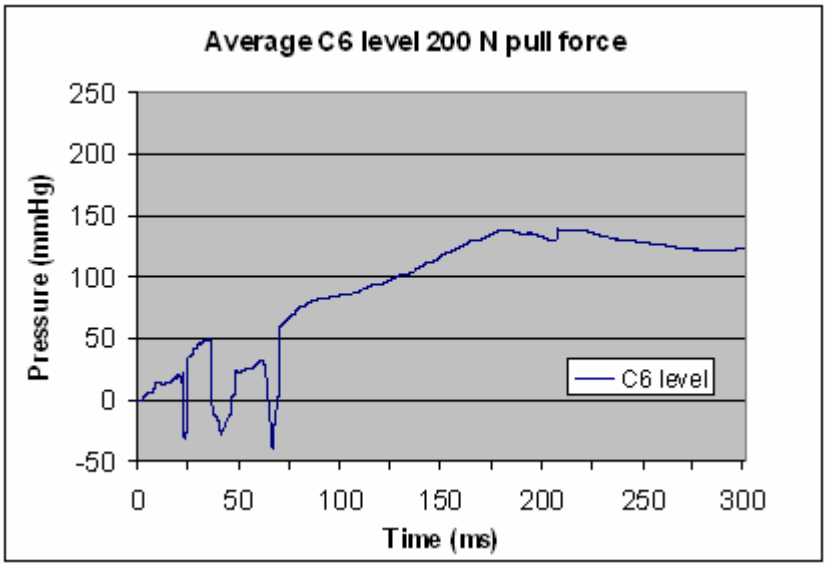
Average C6 level 200 N pull force
Pressure (mmHg)
250
200
150
100
50
0
-50
0
50
100
150
200
250
300
Time (ms)
C6 level